PROBABILISTIC ESTIMATION OF SHALE-OIL RESOURCES IN 93 GLOBAL FORMATIONS IN 36 COUNTRIES

A Thesis

by

DEEPTHI SEN

Submitted to the Office of Graduate and Professional Studies of
Texas A&M University
in partial fulfillment of the requirements for the degree of

MASTER OF SCIENCE

Chair of Committee,	Duane A. McVay
Co-Chair of Committee,	Stephen A. Holditch
Committee Members,	Walter B. Ayers
	Yuefeng Sun
Head of Department,	Dan Hill

August 2017

Major Subject: Petroleum Engineering

ABSTRACT

An in-depth probabilistic study of global shale-oil resources is presently absent in literature. In 2013, the Energy Information Agency (EIA) reported the total volumes of shale oil available in 36 countries to be 388 billion barrels of oil (BBO) following a volumetric assessment of several potentially shale-oil-rich global formations. However, their study did not take into consideration the inherent heterogeneity of shale formations and the resulting uncertainties in reservoir parameters used in the assessment.

I employed a probabilistic approach to the volumetric estimation of the original-in-place shale oil ($OOIP_{sh\_oil}$) in 93 formations from these 36 countries (and the US) belonging to seven geographical regions. This was followed by reservoir-simulation studies of five US formations whereby generalized-recovery-factor (*RF*) distributions were established for three values of hydraulic-fracture stage spacing. These generalized-*RF* distributions were used to compute the technically-recoverable resources of shale oil (TRR_{sh_oil}) from the 93 formations considered. The results were aggregated to regional and global levels assuming 100% dependence (arithmetic aggregation) as well as 100% independence (statistical aggregation) between summand formation-wise resource distributions.

The arithmetically-aggregated volumes (P10-P50-P90) of $OOIP_{sh\_oil}$ in the assessed global formations are 900-8,700-67,700 BBO (P90/P10 = 75), whereas the arithmetically-aggregated volumes of TRR_{sh_oil}, using 50-ft stage spacing, are computed to be 25-374-3,906 BBO (P90/P10 = 159). Using statistical aggregation, the total

volumes (P10-P50-P90) of $OOIP_{sh\_oil}$ in the assessed global formations are 15,000-23,600-43,900 BBO (P90/P10 = 3), whereas the aggregated volumes of TRR_{sh_oil}, using 50-ft stage spacing, are computed to be 250-1,300-3,100 BBO (P90/P10 = 12). The high values of P90/P10 highlight the large uncertainty in both arithmetically- and statistically-aggregated estimates. Since true dependency between the resource distributions of aggregated formations is unknown, the actual resource estimates are expected to fall between the statistically- and arithmetically-aggregated estimates. Because this study does not consider the uncertainties in, and possible correlations between, all variables, the wider resources distributions from arithmetic aggregation may be deemed more appropriate than from statistical aggregation.

This study accounts for only 41% of all global petroleum basins. Thus, actual world resources are likely to be considerably larger.

DEDICATION

This thesis is dedicated to the loving memories of my grandmothers Indira and Sathyabhama, who valued education and independence above all.

ACKNOWLEDGEMENTS

I would like to thank Prof. Duane A. McVay and Prof. Stephen A. Holditch for serving as the chair and co-chair of my graduate committee and for their guidance and support without which this project would not have come to fruition. I am also indebted to Prof. Walter B. Ayers for his valuable inputs on hydrocarbon generation modeling. I thank both Prof. Ayers and Prof. Yuefeng Sun for being part of my committee.

I am grateful to all my colleagues and staff at the Department of Petroleum Engineering at Texas A&M, especially Simin Sadeghi, Dahiyana Cristancho and Tanya Kar for their selfless support and encouragement.

This list will never be complete without mentioning Joshiba and Dilshad, who have been my closest companions for the past eight years and who will continue to be in the years to come.

Finally, I thank my parents, Beena and Sen, for their love and guidance and my ever-so-patient fiancé Aditya for his empathy and sacrifice.

CONTRIBUTORS AND FUNDING SOURCES

Contributors

This work was supervised by a thesis committee consisting of Professors Duane A. McVay [advisor], Stephen A. Holditch [co-advisor] and Walter B. Ayers of the Department of Petroleum Engineering and Professor Yuefeng Sun of the Department of Geology at Texas A&M University.

All other work conducted for the thesis was completed by the student independently.

Funding Sources

There are no outside funding contributions to acknowledge related to the research and compilation of this document.

NOMENCLATURE

$\gamma_{o,API}$	Specific gravity of oil (^{o}API)
γ_g	Specific gravity of gas (air=1)
A	Prospective area (sq miles)
BBO	Billion barrels of oil
B_{ob}	Bubble-point pressure (psia)
B_{oi}	Initial oil formation volume factor (psia)
$Cc(\%)$	Percentage of convertible carbon (no unit)
c_o	Oil compressibility (psi)
D	Depth (ft)
d_f	Hydraulic-fracture spacing (ft)
d_s	Stage spacing (ft)
d_{well}	Well spacing (ft)
F_{cD}	Dimensionless fracture conductivity (no unit)
GOR	Gas-oil-ratio (scf/bbl)
g_{press}	Subsurface pressure gradient (psi/ft)
g_{therm}	Geothermal gradient (^{o}F/ft)
h_{avg}	Average net pay (ft)
h_f	Hydraulic-fracture height (ft)
HI	Hydrogen index (mg HC/g TOC)

HI_i	Initial hydrogen index (mg HC/g TOC)
high	Upper limit of published ranges
$k_{conduit}$	Conduit permeability (md)
k_{matrix}	Matrix permeability (md)
k_{rg}	Relative permeability to gas (no unit)
L	Well length (ft)
low	Lower limit of published ranges
m	Bernoulli random variable (no units)
MBO	Million barrels of oil
N_g	Corey exponent for oil (no unit)
N_o	Corey exponent for gas (no unit)
$N_{p,stage}$	Cumulative oil produced from one stage (STB)
n_r	Number of published ranges considered
n_s	Number of stages (no unit)
O_{gen}	Volume of oil generated in oil window in formation (bbl/ac.ft)
$O_{gen,tot}$	Total volume of oil generated in oil window in formation from entire prospective area (BBO)
$OOIP_{sh\_oil}$	Shale original oil in place (BBO)
$OOIP_{sh\_oil\_well}$	Original oil in place in well drainage area (STB)
P_{atm}	Atmospheric pressure (psia)
P_b	Bubble-point pressure (psia)

$p_{playsuccess}$	Play-success-modifier distribution
P_{res}	Initial reservoir pressure (psia)
PV_{max}	Maximum pore volume available (BBO)
Px	x^{th} percentile
RF	Recovery factor (no unit)
$R_o\%$	Vitrinite reflectance (no unit)
s	Play success factor
S2	Hydrocarbon generative capacity of source rock (mg HC/ g rock)
S_{gi}	Initial gas saturation (no unit)
S_{oirr}	Irreducible oil saturation (no unit)
SRV	Stimulated reservoir volume
S_w	Water saturation (no unit)
$S_{w,avg}$	Average water saturation (no unit)
$TOC_{avg,i}$	Initial total organic carbon (wt%)
$TOC_{avg,pd}$	Present day total organic carbon (wt%)
TR	Transformation ratio (no unit)
T_{res}	Reservoir temperature (^oF)
TRR_{sh_oil}	Technically-recoverable resources of shale oil (BBO)
$TRR_{sh\_oil\_well}$	Technically-recoverable resources of shale oil in well drainage area (BBO)
T_{surf}	Surface temperature (^oF)

$w_{conduit}$	Width of conduit (ft)
x_f	Fracture half-length (ft)
ρ_b	Bulk density of rock (g/cc)
ρ_{ker}	Kerogen density (g/cc)
ϕ	Total porosity (no unit)
ϕ_{ker}	Kerogen porosity (no unit)

TABLE OF CONTENTS

Page

LIST OF FIGURES

Page

LIST OF TABLES

Page

1. INTRODUCTION

The large-scale implementation of hydraulic fracturing and horizontal drilling in North America has proved to be a game changer in the global energy market in recent years. As the US moves towards achieving total energy independence, other nations are expected to invest in the development of their unconventional oil and gas resources.

The collapse of natural-gas prices in 2008 resulting from the global recession and increased domestic production, coupled with the comparatively quicker rebound of oil prices drove operators into exploring unconventional-oil plays in the US. This resulted in a number of increasingly profitable new plays such as the Eagle Ford and the Bakken coming into the limelight (EIA and IHS 2016). Since then, production from these new unconventional-oil plays has been on the rise, owing to the use of increasingly longer laterals as well as more intensive fracture techniques.

In 2015, production from tight-oil resources (4.9 million BOPD) accounted for 52% of US crude-oil output (9.6 million BOPD) (EIA 2016). Despite the recent dip in oil prices, which may bring down tight-oil production to 4.2 million BOPD in 2017, technological advances in oil recovery and further exploration and development are expected to drive the figure up to 7.1 million BOPD by 2040. The Lower 48 states are expected to lead the increase in crude-oil output with increased production from tight-oil plays in the Williston, Western Gulf and Permian basins (EIA 2016).

1.1 Unconventional, Tight and Shale Oil and Oil Shale

Currently, there is no consensus on the formal definition of unconventional resources. These have been characterized by a variety of criteria such as matrix permeability, requirement for specialized extraction methods, or even difficulty of access. Holditch and Ayers (2009) illustrated the relationship between various hydrocarbon resource types and their relative abundance, reservoir quality and complexity of exploration technology required using a 'resource triangle' **(Fig. 1.1)**, modelled after Masters (1979) and Gray (1977).

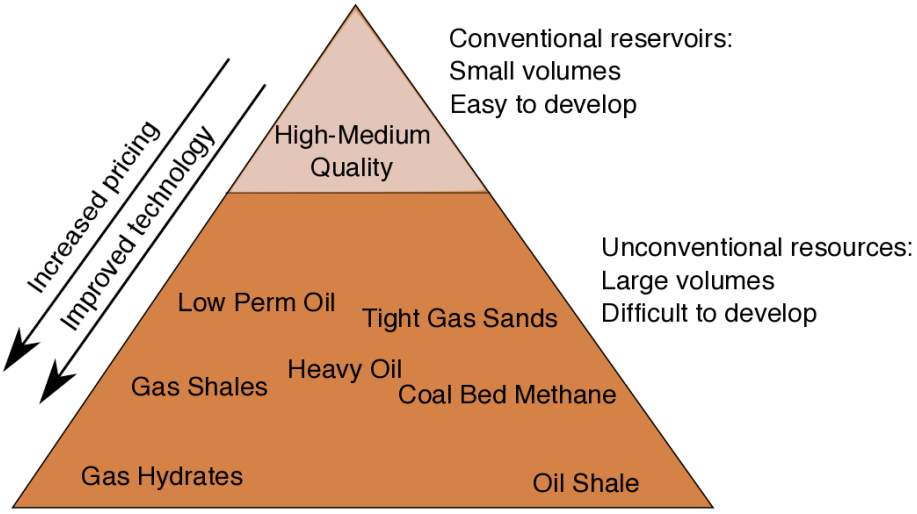

Fig. 1.1—Resource triangle (Adapted from Holditch et al. (2009))

Cander (2012) used the ratio of permeability to viscosity in order to demarcate unconventional resources from conventional resources **(Fig. 1.2)**. By this definition, tight oil, shale oil and oil shale are categorized under 'unconventional oil.' Tight-oil formations are characterized by rocks that are not sufficiently porous or

permeable to allow spontaneous production from a conventional vertical well (Madden and Vossoughi 2013). Therefore, shale oil forms a subset of tight oil wherein production happens from self-sourced shale formations, rather than from low-permeability sandstone or carbonate formations (EIA and ARI 2013).

Shale oil is to be distinguished from oil shale: the former refers to crude oil that is trapped within shaly formations whereas the latter is described as a type of kerogen-rich sedimentary rock from which oil may be generated by heating (retorting) (Colorado Oil & Gas Association 2013). This study focuses exclusively on shale-oil formations.

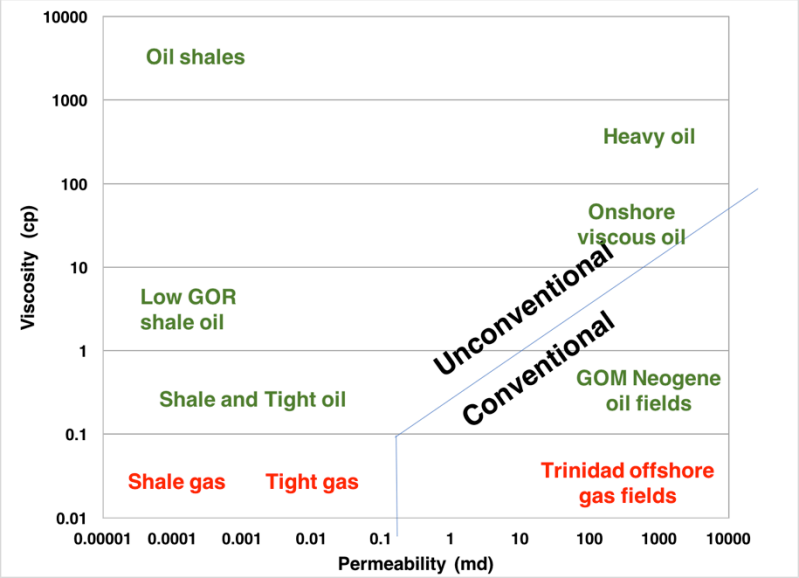

Fig. 1.2—Demarcation between conventional and unconventional resources based on viscosity and permeability (Adapted from Cander (2012))

Unconventional-play resource estimates entail large uncertainties due to high spatial variability in reservoir characteristics. Given the high volatility in product prices and the relatively higher production costs associated with unconventional resources, a

comprehensive evaluation of uncertainty is crucial to the assessment of technical and economic recoverability of unconventional resources. An in-depth probabilistic study of unconventional-oil resources that quantifies uncertainty is lacking in literature to date.

1.2 Status of the Question

Rogner (1997) conducted a pioneering assessment of global resources in place for many categories of conventional and unconventional hydrocarbons, by means of a regional study based on comparisons with analogous US resources. Deterministic estimates for various types of unconventional gas resources were provided for eleven geographical regions. Nevertheless, an assessment of global shale-oil resources was not incorporated into this work.

McGlade (2012) reported the first publicly-available 'global' assessment of 'light tight-oil' (LTO) resources. In this paper, LTO refers to "the oil found in low permeability shale formations requiring stimulation (such as hydraulic fracturing) in order to flow" (McGlade 2012). Therefore, LTO will be termed 'shale oil' henceforth to avoid confusion. McGlade adopted Rogner's (1997) methodology of computing the ratio of technically-recoverable shale-oil to shale-gas resources (TRR_{sh_oil}: TRR_{sh_gas}) wherever information was available. These ratios were applied to regions with pre-existing estimates of shale gas (but not shale oil) in order to compute the TRR_{sh_oil} in these regions. In McGlade's analysis, the ratio between the volumes of technically-recoverable shale oil and gas was chosen (as opposed to in-place volumes) since information on technically-recoverable volumes was more readily available and inclusive of considerations such as mineralogy, reservoir properties and recovery efficiency. The

'high,' 'low' and 'central' values for TRR_{sh_oil}: TRR_{sh_gas} were computed using shale-oil and shale-gas resource estimates from four regions—Alaska, Poland, Uruguay and the US (except Alaska). The 'high,' 'low' and 'central' values for TRR_{sh_gas} in 12 regions were assigned based on the author's judgment of best estimates from previously published literature (McGlade, Speirs, and Sorrell 2012). Subsequently, the 'high,' low' and 'central' estimates for TRR_{sh_oil} for each of the 12 regions were determined by multiplying the computed TRR_{sh_oil}: TRR_{sh_gas} by TRR_{sh_gas} assuming perfect correlation between the ratio and TRR_{sh_gas}. McGlade's 'central' estimate for the global TRR_{sh_oil} was 278 BBO, with 'low' and 'high' values of 151 BBO and 508 BBO, respectively. However, the range of TRR_{sh_oil}: TRR_{sh_gas} was established based on just four sources. Thus, it is likely that the uncertainty in this parameter has been underestimated. In addition, the TRR_{sh_oil} estimates for six of the 12 regions considered were based on single-value estimates of TRR_{sh_gas}. Furthermore, the assumed perfect correlation, which suggests that a 'high' (or 'low') value of TRR_{sh_gas} necessarily implies a 'high' (or 'low') value of TRR_{sh_oil}: TRR_{sh_gas}, is unfounded. It is worth mentioning that the estimates for each region were not inclusive of potential resources within all countries in the region. For instance, TRR_{sh_gas} for 'Eastern Europe' is based only on published estimates for Poland (McGlade, Speirs, and Sorrell 2012). Therefore, the term 'global resource' estimate, applied to the sum of the 12 region-wise estimates, is misleading.

In 2013, Energy Information Agency (EIA) published a report prepared by Advanced Resources International (ARI) wherein $OOIP_{sh\_oil}$ in 31 countries (excluding the US) was estimated to be 5799 BBO out of which 289.6 BBO were expected to be

technically recoverable (EIA and ARI 2013). These figures were updated to 6867 BBO and 340.6 BBO, respectively, after the inclusion of four countries—Chad, Kazakhstan, Oman and United Arab Emirates, in 2014 (EIA 2015b). In the Annual Energy Outlook 2015 Assumptions report, EIA independently estimated TRR_{sh_oil} in the US to be 78.2 BBO (EIA 2015a). Combining these estimates, EIA placed the TRR_{sh_oil} in 36 countries at 419 BBO (EIA 2015c). However, an assessment of remaining shale-oil resources in eight US basins conducted by ARI estimated 47.7 BBO of TRR_{sh_oil} and 954 BBO of $OOIP_{sh\_oil}$, assuming an average RF of 5% (EIA and ARI 2013). Aggregating these values with the updated EIA estimates of non-US $OOIP_{sh\_oil}$ and TRR_{sh_oil}, the $OOIP_{sh\_oil}$ estimate for the 36 countries stands at 7821 BBO, out of which 388 BBO are expected to be technically recoverable. However, EIA and ARI (2013) have included oil as well as condensate volumes under the 'shale-oil' resource estimates mentioned above, even though the prospective areas for oil and condensates for each formation have been treated separately in the full report (EIA and ARI 2013). A summary of the methodology adopted by EIA and ARI (2013) is given in **Fig. 1.3**.

The report (EIA and ARI 2013) assumed single representative values for petrophysical parameters for each of the non-US shale plays, even though these are known to vary greatly over short distances. Moreover, the values of certain key parameters, such as porosity (ϕ) and water saturation (S_w), that were used in the assessment of a number of formations, were not made available publicly. In addition, even though the report recognized the presence of considerable uncertainty in parameters including, but not limited to, prospective area (A) and expected well lives, EIA and ARI

(2013) did not quantify these uncertainties while computing the resource estimates. The investigators further scaled down the volumetrically computed $OOIP_{sh\_oil}$ by assigning 'composite success factors' to each play to account for risks due to structural complexities and lack of reservoir/geological data and prior development. The 'composite success factor' was computed as the product of the 'play success factor' and the 'prospective area success factor.'

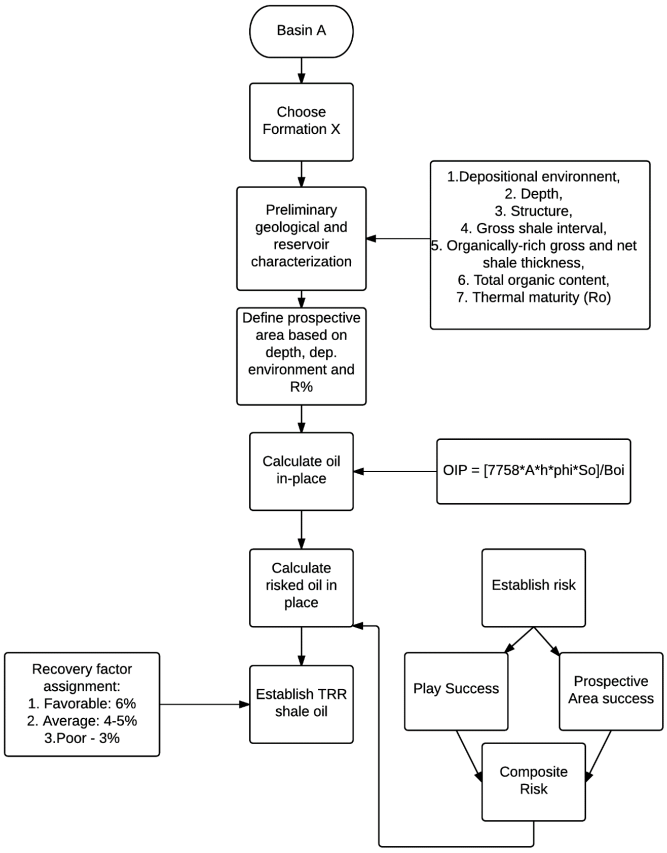

Fig. 1.3—Methodology employed by EIA and ARI (2013)

The ‘play success factor’ was assigned based on the existence of prior developmental activity in the play in question and the level of speculativeness of the play. The ‘prospective area success factor’ downgraded a portion of the prospective area as unproductive due to various criteria that were not considered in assigning the prospective area. Both factors comprising the ‘composite success factor’ were single values, assigned based on expert judgment. Hence, they have not analyzed the variance in their estimation of $OOIP_{sh\_oil}$. Furthermore, the assignment of risk factors based on judgment alone may lead to underestimation of uncertainty, as demonstrated by Capen (1976).

In 1999, the United States Geological Survey (USGS) developed a methodology called the ‘FORSPAN model’ for probabilistic resource estimation of continuous accumulations (Schmoker 1999). The USGS defines continuous accumulations as spatially expansive hydrocarbon accumulations that may exist downdip of water-saturated rocks. In addition to the aforementioned features, these accumulations are characterized by the lack of traps/seals, low matrix permeability and abnormal pressures (Schmoker, Crovelli, and Balay 1995). As per the FORSPAN model, the continuous accumulation being assessed was divided into fairly homogenous subunits called ‘assessment units.’ The assessment units were assumed to consist of petroleum-charged ‘cells’ having areal dimensions equal to the well drainage area and extending vertically through the assessed strata. Schmoker assigned values to the expected ultimate recovery from each cell by sampling from a lognormal distribution of expected ultimate recovery per cell, specific to the assessment unit under study. These distributions were based on

available production data from the assessment unit or other analogous units. The final deliverable was the 'potential additions to reserves' over a span of 30 years solely from sweet spots (cells with expected ultimate recoveries greater than or equal to a specified value). Charpentier and Cook (2010) extended this idea to calculate the TRR from both sweet spots and non-sweet spots in an assessment unit. The USGS has assessed continuous oil accumulations in 15 international regions, as of March 2017. However, the calculation of TRR using Charpentier's methodology requires production history from the assessed area or sufficient geologic information in order to assign a realistic analog. This limits the application of this methodology to understudied formations where production trends and sufficient geologic information are not available.

Dong (2012) presented a probabilistic assessment of the original-in-place and technically-recoverable unconventional gas resources (shale gas, tight gas and coal-bed methane) in seven geographical regions. She generated PDFs of region-wise conventional original-in-place gas and original-in-place oil volumes using publicly available estimates of conventional oil and gas TRRs and an *RF* distribution determined from statistics on recovery factors in conventional oil and gas plays provided by (Laherrere 2006). Statistical relationships between conventional petroleum (and coal) and unconventional gas were established based on North American data (Dong, Holditch, and McVay 2012). These relationships were used along with the region-wise conventional original-in-place resource distributions to generate a PDF for original-in-place unconventional gas volumes in each global region. In doing so, it was assumed that there was perfect similarity between the distribution of basin types in North America

and that in each of the seven global regions. Dong developed a workflow that combines probabilistic resource estimation using Monte Carlo simulation with an analytical reservoir simulator. This method was used to generate TRR and *RF* distributions in well-studied North American unconventional gas plays where sufficient geologic and reservoir data were available (Dong, Holditch, and McVay 2013). A resulting generalized-*RF* distribution was multiplied by region-wise unconventional original-in-place gas distributions to calculate the region-wise unconventional TRR distributions for each region (Dong et al. 2014). However, the study was not extended to include global shale-oil resources.

This section may be summarized as follows: Rogner (1997) and Dong (2012) did not extend their assessment of global resources to shale oil. McGlade (2012) computed probabilistic estimates of global recoverable shale oil assuming perfect correlation between recoverable shale-gas resources and recoverable shale-oil resources. Moreover, McGlade's estimates are based on data from just four sources and, thus, the uncertainty is likely to have been underestimated. EIA and ARI (2013) conducted an in-depth deterministic assessment of 88 international shale-oil formations but did not quantify the uncertainty in their estimates.

1.3 Research Objective

The objective of this project is to estimate $OOIP_{sh\_oil}$ and TRR_{sh_oil} in 93 formations from 36 countries belonging to seven geographical regions to quantify the uncertainties in these estimates. Of the 93 formations, 88 have been studied by EIA and ARI (2013) and the remaining five are US formations.

1.4 Resource Estimation and Classification

Resource estimation may be performed by various entities for various purposes at any stage of resource development. The estimates may be deterministic or probabilistic, based on suitability to each specific case or existing guidelines on reporting of reserves/resources.

Deterministic estimates are computed as the 'best estimates' of volumes of various classes of resources using single-value estimates of input parameters. On the other hand, probabilistic estimates refer to a range of values for hydrocarbon quantities distributed according to a PDF, computed taking the entire range of input parameters into consideration. The resource estimates computed using the probabilistic method are specified by the 10^{th}, 50^{th} and 90^{th} percentiles of the cumulative distribution function (CDF). These percentiles are referred to as the P10, P50 and P90 estimates for the resource under consideration. This terminology is followed throughout this report.

Resource classification delineates and quantifies various 'classes' of resources based primarily on the degree of uncertainty in the production and/or commerciality of the resource. Several organizations have developed their own frameworks for resource classification, such as the USGS McKelvey box (Cronquist 2001), SPE/AAPG/WPC/SPEE PRMS (henceforth referred to as 'SPE-PRMS') (SPE et al. 2007), EIA resource categorization (Budzik and Ford 2014) and the United Nations Framework Classification for Fossil Energy and Mineral Resources (United Nations 2009). In this study, EIA resource categorization was adopted for simplicity. However, it

is worthwhile to draw a comparison between this and the more widely-accepted SPE-PRMS resource classification.

1.4.1 *EIA Oil and Natural Gas Resource Categorization*

EIA **(Fig. 1.4)** classifies the total petroleum initially in place ('original oil and natural gas in-place') into two broad categories: cumulative production to date and the remaining oil and natural gas in place (Budzik and Ford 2014). 'Technically recoverable resources' (TRR) are a subset of 'remaining oil and natural gas in place' that includes all petroleum that can be produced based on current technology and industry practices. 'Economically recoverable resources' (ERR) form a subset of TRR which include all petroleum that may be commercially produced subject to prevalent oil and gas prices, and capital and operating costs.

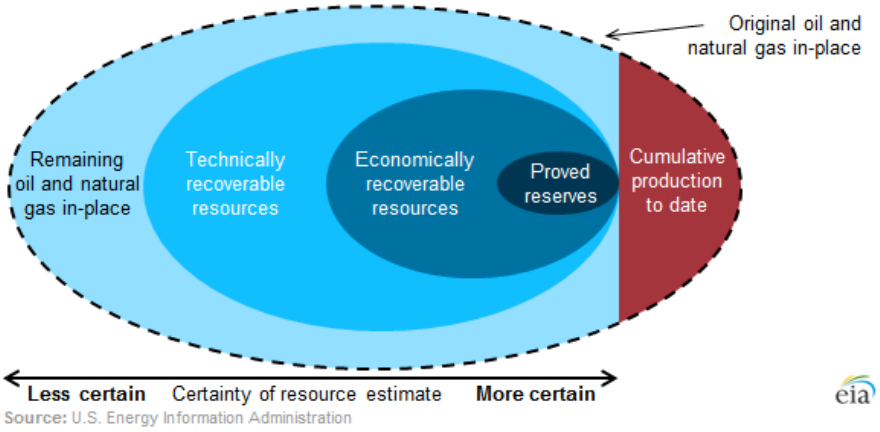

Fig. 1.4—EIA oil and natural gas resource categories (Reprinted from Budzik and Ford (2014))

1.4.2 *SPE-PRMS Resource Classification*

The SPE-PRMS **(Fig. 1.5)** allocates the total petroleum initially in place into two broad categories: discovered and undiscovered, conditional on evidence suggesting the presence/absence of significant quantities of moveable hydrocarbons through the results of one or more exploratory wells (SPE et al. 2007).

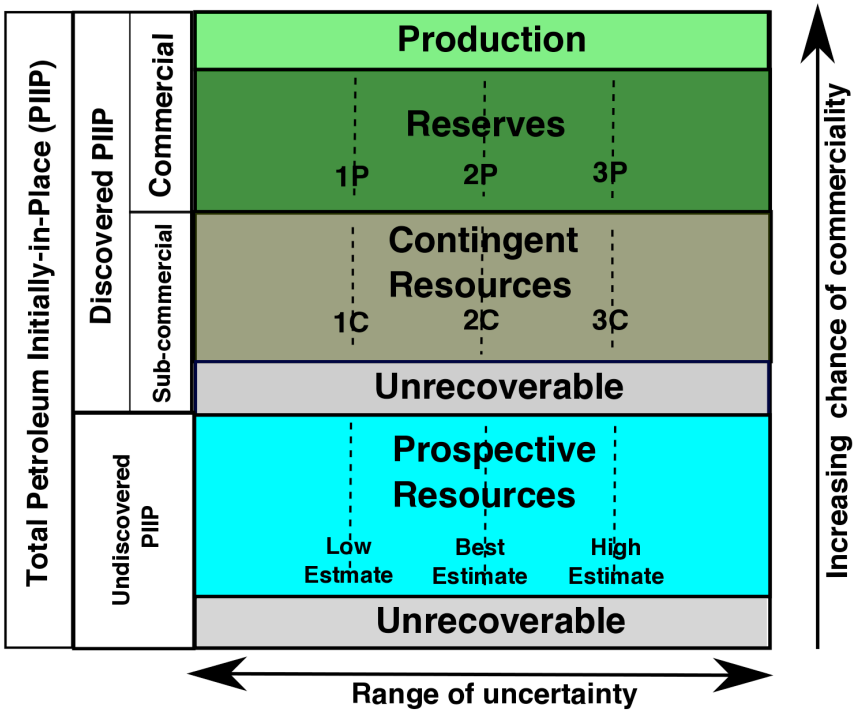

Fig. 1.5—SPE-PRMS Resource classification framework (Adapted from SPE et al. (2007))

The discovered petroleum initially in place may be further subdivided as:

a. **Produced**: The volumes of hydrocarbons that have already been produced to date

b. **Reserves**: The volumes of hydrocarbons expected to be commercially producible from a given date forward. In order to be commercially producible, the development project to be applied on the petroleum accumulation should be sufficiently defined, with a high degree of confidence in its commerciality, supported by production data or formation tests. The development projects should also be viable enough to be initiated within a reasonable period of time.
c. **Contingent resources**: The volumes of hydrocarbons that are potentially producible but currently unfeasible due to reasons such as non-commerciality or under-assessed commerciality.
d. **Unrecoverable resources**: The volumes of hydrocarbons that not expected to be recoverable due to insufficient technology or physical/chemical constraints.

The undiscovered petroleum initially in place may be further classified as:

a. **Prospective resources**: The volumes of hydrocarbons anticipated to be potentially recoverable. Since these have not been discovered yet, prospective resources are associated with a probability of discovery as well as a probability of development.
b. **Unrecoverable resources**: The volumes of hydrocarbons that are not currently expected to be recoverable due to insufficient technology or physical/chemical constraints.

Dong (2012) approximately mapped the EIA classification scheme to the SPE-PRMS scheme (SPE et al. 2007) **(Fig. 1.6)**. It is to be noted that, according to Dong's mapping, the cumulative production is categorized under the 'technically recoverable' resource base. This description of cumulative production was adopted in this study.

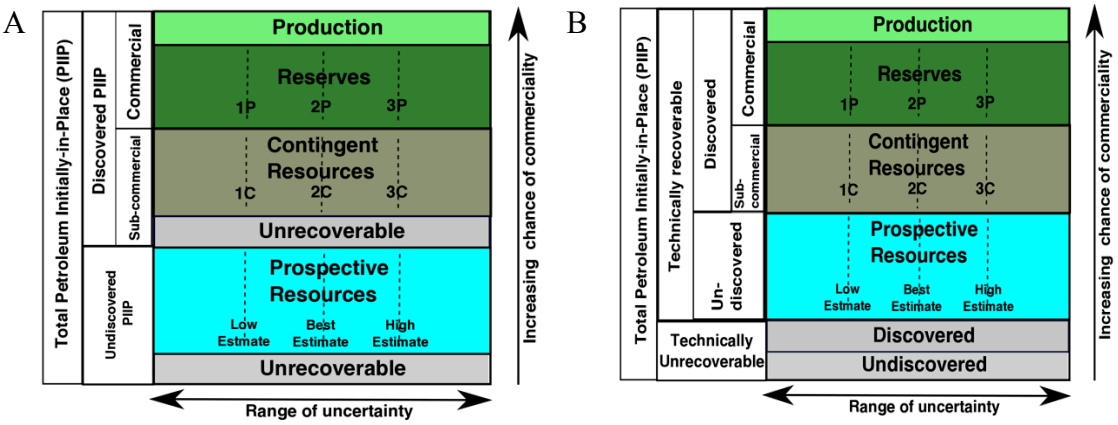

Fig. 1.6—Comparison of (A) SPE-PRMS and (B) EIA oil and natural gas resource categories (Adapted from Dong (2012))

1.5 Overview of Methodology

Even though a deterministic study of shale-oil resources in international formations was conducted by EIA and ARI (2013), the problem warrants a probabilistic approach owing to the lack of high-quality data for key parameters. In this study, I covered 36 countries, belonging to seven geographical regions, which are potentially shale-oil-rich, as identified by EIA and ARI (2013) **(Table 1.1)**. It has to be stressed that this is not a comprehensive study of all formations in any geographical region or on a global scale.

A few notable exclusions made in this study were Saudi Arabia, Iraq and Iran in the Middle East, which are highly likely to hold substantial volumes of shale-oil resources. Yet, the unavailability of the required data on shale-oil formations in these countries led to their exclusion from the study.

A further caveat is the absence of any Central American country in this assessment even though the term 'Latin America' includes both Central and South America. I used 'Latin America' in place of merely 'South America' in order to adhere to descriptions of geographical regions given in previously published literature (Rogner 1997; Dong, Holditch, and McVay 2012; Dong et al. 2014).

Table 1.1—Potentially shale-oil-rich countries and the number of formations assessed in this study

Region	Abbreviation	Country	Number of assessed formations
North America	NAM	Canada	5
		Mexico	5
		US	5
Latin America (Central and South America)	LAM	Northern South America (Colombia, Venezuela)	3
		Argentina	4
		Brazil	2
		Other South America (Paraguay, Uruguay, Bolivia, Chile)	4

Table 1.1 Continued

Region	Abbreviation	Country	Number of assessed formations
Commonwealth of Independent States (Former USSR)	CIS	Russia	2
		Ukraine	1
		Kazakhstan	6
Europe	EUR	Poland	2
		Lithuania	1
		United Kingdom	1
		Germany	2
		Netherlands	2
		France	2
Africa	AFR	Western Sahara	1
		Algeria	1
		Tunisia	1
		Libya	4
		Egypt	4
		Chad	5
Australasia (Asia, Australia and Oceania)	AAO	China	6
		Mongolia	2
		Indonesia	4
		India	2
		Pakistan	2
		Australia	8
Middle East	MEA	Jordan	1
		Turkey	2
		UAE	1
		Oman	2
		Total number of formations	93

The $OOIP_{sh\_oil}$ and TRR_{sh_oil} distributions for each formation were computed from several geological parameters that were input as PDFs. Subsequently, a bottom-up approach was adopted to aggregate the resources in each formation to country-level and subsequently to region-level **(Fig. 1.7)**. The volumetric method is the most appropriate approach to resource assessment of undeveloped accumulations with meager production

data, as opposed to the computation of TRR through the extrapolation of production trends (McGlade, Speirs, and Sorrell 2013).

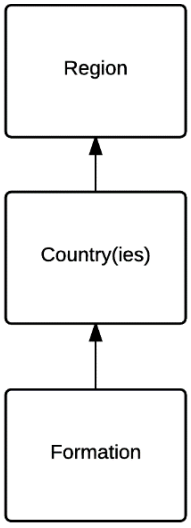

Fig. 1.7—Bottom-up approach to resource estimation

The methodology employed in this study **(Fig. 1.8)** for probabilistic assessment of shale-oil resources is summarized below:

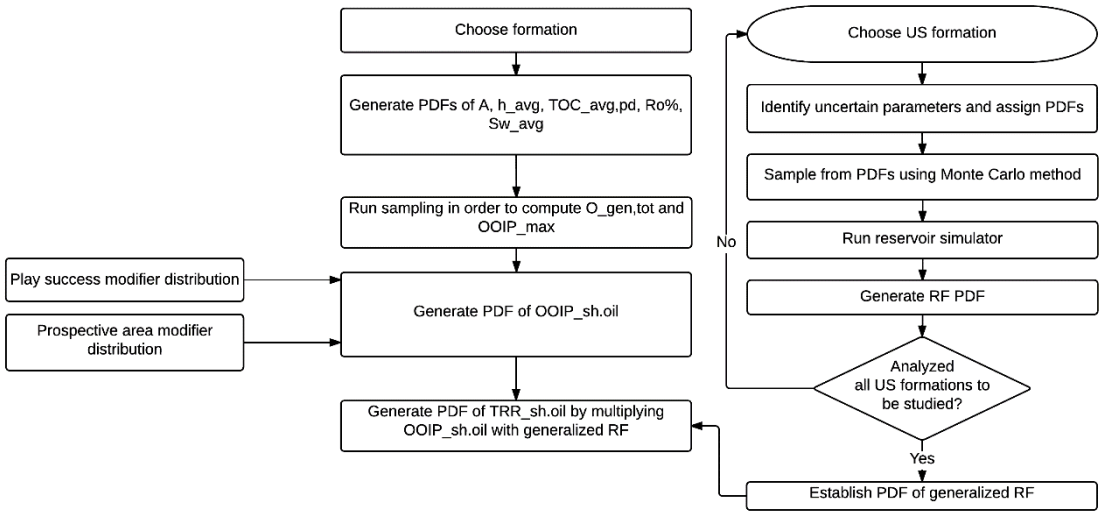

Fig. 1.8—Proposed methodology for probabilistically estimating $OOIP_{sh\_oil}$ and TRR_{sh_oil} of a formation

1. Major formations with sufficient available data on key parameters were selected from each region. A total of 93 shale-oil formations were studied out of which 88 are international formations that were assessed deterministically by EIA and ARI (2013). The remaining five are US formations.

2. Uncertain parameters were identified and PDFs assigned to each of these parameters. The parameters considered and the PDF forms assigned are given in **Table 1.2**. All normal and lognormal distributions were defined by specifying the median and the 95th percentile values, whereas triangular distributions were defined by specifying the minimum, maximum and modal values. Porosity (ϕ) was modeled as the sum of shale matrix porosity (ϕ_{mat}) and kerogen porosity (ϕ_{ker}) generated due to decomposition of organic matter in kerogen. ϕ_{mat} was assigned a constant value of 5% (Li 2015). The evolution of ϕ_{ker} was modeled based on the approach proposed by Modica and Lapierre

(2012) wherein ϕ_{ker} is computed from $R_o\%$ and present-day TOC using Type-2 kerogen decomposition kinetics. I extended the applicability of the approach to Type-1 and Type-3 kerogens as well.

3. $OOIP_{sh\_oil}$ distributions were generated for each formation using a volumetric approach wherein the total volumes of oil generated in the oil window to date ($O_{gen,tot}$) were computed using the carbon transformation ratio (TR), $R_o\%$ and $TOC_{avg,pd}$ (Modica and Lapierre 2012). However, the total pore volume (PV_{max}) in the formation, that can be used to store the generated oil, was computed from simple volumetrics.

Table 1.2—List of uncertain parameters for original-in-place shale-oil estimation and the respective probability distribution forms and central tendencies used to model the uncertainty

Uncertain parameter (Abbreviation)	Unit	PDF form
Average present day total organic carbon content by weight ($TOC_{avg,pd}$)	%	Normal
Vitrinite reflectance ($R_o\%$)	%	Triangular
Prospective area (A)	sq miles	Lognormal
Average net pay (h_{avg})	ft	Normal
Average water saturation ($S_{w,avg}$)	%	Normal

4. The risk of having a portion of the prospective area rendered unproductive due to additional constraints, which was indicated by the 'prospective area success factor' in the EIA and ARI (2013) report, was accounted for by multiplying the minimum of $O_{gen,tot}$ and PV_{max} by a 'prospective-area modifier.'

5. The degree of speculation in the potentiality of production from the formation, which was indicated by the 'play success factor' in the EIA and ARI (2013) report, was accounted for by multiplying the minimum of $O_{gen,tot}$ and PV_{max} by a 'play-success-

modifier' modeled as a Bernoulli variable. This would set $OOIP_{sh\_oil}$ to zero, with the probability specified by EIA and ARI (2013) as the 'play success factor.'

6. Following Dong's (2012) methodology, production from five US shale-oil formations (Bakken, Eagle Ford, Wolfcamp, Niobrara and Avalon) were simulated using a reservoir simulator in order to arrive at a generalized-*RF* distribution. I used the IMEX reservoir simulator (Computer Modelling Group Ltd. 2013b). CMOST software (Computer Modelling Group Ltd. 2013a) was used to run reservoir simulations using Monte Carlo sampling from input distributions of uncertain parameters and to establish the *RF* distributions for each formation. The uncertain parameters that were considered in this step are net pay, porosity, water saturation, and matrix permeability (k_{mat}). The PDFs for these parameters were modeled by setting the 5th and 95th percentiles equal to the average lower and average upper limits based on published ranges for each formation. A generalized-*RF* distribution was established by assigning equal weights to each of the *RF* distributions from the five formations listed above. This was done for three values of stage spacing—50 ft, 500 ft and 1,000 ft—yielding a generalized-*RF* distribution for each case.

7. The generalized-*RF* distributions were multiplied by the $OOIP_{sh\_oil}$ distribution (using Latin Hypercube sampling) to generate the TRR_{sh_oil} distribution for each formation.

8. The aggregate country-wise, region-wise (from all formations in a region) and total (from all formations studied) original-in-place and technically-recoverable shale oil were computed by summing resources from individual formations, both arithmetically

(assuming perfect correlation between production from individual formations) and statistically (assuming zero correlation between production from individual formations).

2. ASSESSMENT OF REGION-WISE AND TOTAL ORIGINAL-IN-PLACE SHALE OIL

The first phase of this study consisted of estimating the distribution of $OOIP_{sh\_oil}$ in 93 formations in the 36 countries listed in Table 1.1 and subsequently establishing the region-wise $OOIP_{sh\_oil}$ aggregate distributions and the total $OOIP_{sh\_oil}$ for all formations considered together.

Volumes of shale oil that have been generated ($O_{gen,tot}$) to date in the oil window were computed from kerogen kinetics and $TOC_{avg,pd}$. Next, the maximum available pore space (PV_{max}) for hydrocarbon retention within the formation was calculated volumetrically. The maximum volume of original-in-place shale oil in the formation ($OOIP_{max}$), prior to inclusion of previously omitted assessment criteria, was set equal to the minimum of $O_{gen,tot}$ and PV_{max} (Kuchinskiy, Gentry, and Hill 2012). Modifier distributions that account for previously omitted assessment criteria were used to modify $OOIP_{max}$ into the $OOIP_{sh\_oil}$ for each formation.

The $OOIP_{sh\_oil}$ distributions for all formations within a region were aggregated both arithmetically and statistically to generate the probabilistic estimates of $OOIP_{sh\_oil}$ for each region. Furthermore, the $OOIP_{sh\_oil}$ for all 93 formations were aggregated arithmetically and statistically to obtain the probabilistic estimate of total $OOIP_{sh\_oil}$ in all 36 countries combined.

The rest of this section is organized as follows: Section 2.1 details the workflow for arriving at the $OOIP_{sh\_oil}$ PDF for any formation. Section 2.2 concerns aggregation of

$OOIP_{sh\_oil}$ PDFs for individual formations into region-wise and total distributions. I present the results of this section in Section 2.3 and compare these with previous original-in-place resource assessments.

2.1 Workflow for Establishing Formation-wise $OOIP_{sh\_oil}$ Distributions

2.1.1 *Selection of Formations*

First, the countries within each geographical region that are potentially shale-oil resource-rich were identified. This was followed by volumetric assessments of a number of prospective formations within each country thus identified. My work covers 93 formations from 67 global basins in 36 countries. Out of the 93 formations, 88 have been assessed by EIA and ARI (2013). The remaining five are well-studied formations from four US basins. According to Li (2011), there are around 161 onshore oil and gas basins in the world. This implies that this study accounts for around 41% of all global oil and gas basins.

2.1.2 *Assignment of PDFs to Uncertain Parameters*

A list of key uncertain parameters included in my estimation of shale-oil resources is given in Table 1.2. These parameters form the input distributions to my model. The process of assigning PDFs to each parameter is described below:

2.1.2.1 Prospective Area (A)

For the assessment of unconventional resources, USGS has developed a probabilistic methodology that incorporates the uncertainty in areal extent of an 'assessment unit' in the form of triangular distributions (Schmoker 1999). The extreme values of the distribution represent the assessor's uncertainty about a single unknown

value of prospective area. **Table 2.1** shows the minimum, mode and maximum for the triangular distributions assigned to 15 international assessment units studied by the USGS.

Table 2.1—Probability distributions assigned to areal extent of assessment units by USGS (Numbers may not match exactly due to round-off)

Assessment unit	Country	Prospective area of assessment unit (1,000 acres)			Extrema normalized by the mode (no units)	
		Min	Mode	Max	(Max-Mode)/Mode	(Mode-Min)/Mode
Taoudeni (Brownfield et al. 2016)	Mali	22	10,500	21,500	1.0	1.0
Central Sumatra-Brown Shale (Schenk et al. 2015a)	Indonesia	4	603	3,967	5.6	1.0
Sargelu (Schenk et al. 2015c)	Iraq	13	3,911	13,037	2.3	1.0
Agua Nueva (USGS 2014)	Mexico	100	704	1,100	0.6	0.9
Tampico Pimienta (USGS 2014)	Mexico	100	695	2,100	2.0	0.9
Tampico Agua Nueva (USGS 2014)	Mexico	1,052	2,104	2,735	0.3	0.5
Toarcian, Paris Basin (Schenk et al. 2015b)	France	3	269	1,485	4.5	1.0
Lotharingian, Paris basin (Schenk et al. 2015b)	France	3	337	691	1.1	1.0
Cambrian-Ordovian (Brownfield et al. 2015)	Baltic	0	4,944	19,775	3.0	1.0
Silurian (Brownfield et al. 2015)	Baltic	79	1,963	7,851	3.0	1.0
Sirhan (Schenk et al. 2014b)	Jordan	0	29	290	9.0	1.0
East Safawi (Schenk et al. 2014b)	Jordan	0	86	860	9.0	1.0
Phitsanulok (Schenk et al. 2014a)	Thailand	100	205	250	0.2	0.5
Norte (USGS 2011)	Uruguay	213	2,132	3,198	0.5	0.9
Polish Foredeep (USGS 2012)	Poland	0	760	1,900	1.5	1.0
			Average of normalized extrema		2.9	0.9

However, Salazar, McVay, and Lee (2010) argued that triangular distributions are prone to judgmental bias unless the assessor is objectively certain about the extreme values of the distribution. In their improved methodology, the area of the assessment unit was modeled as a lognormal distribution. This was adopted in this study.

The median (P50) of the lognormal distribution was set to the value of prospective area of the formation in the oil window, as specified by EIA and ARI (2013). In order to specify the degree of uncertainty in prospective area, I normalized the values of the extrema (in Table 2.1) with respect to the value of the central tendency (mode) to compute the average normalized extrema assigned by the USGS. The average value of the normalized maxima was computed to be 2.9. This value was used to specify the spread of the lognormal distribution for prospective area in my study, by setting the 95th percentile (P95) of the distribution such that

$$\frac{P95 - P50}{P50} = 2.9 \quad (1)$$

2.1.2.2 Average Net Pay (h_{avg})

Net pay refers to the subintervals within the gross formation thickness characterized by the availability of sufficient volumes of hydrocarbons as well as adequate reservoir quality so as to be of potential commercial interest (Worthington 2010). In case of conventional reservoirs, net pay is quantified by applying a series of cut-offs to various reservoir parameters (discriminators) **(Fig. 2.1)**.

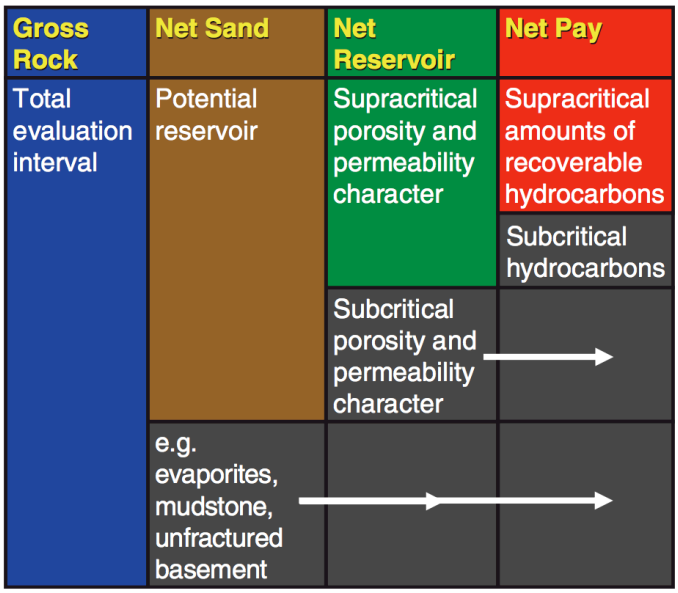

Fig. 2.1—Quantification of net pay in conventional reservoirs (Source: Worthington (2010)) (Reprinted with permission of Society of Petroleum Engineers)

Worthington and Majid (2013) modified this scheme for use in shale-gas reservoirs by redefining the discriminators for each of the intervals **(Fig. 2.2)**.

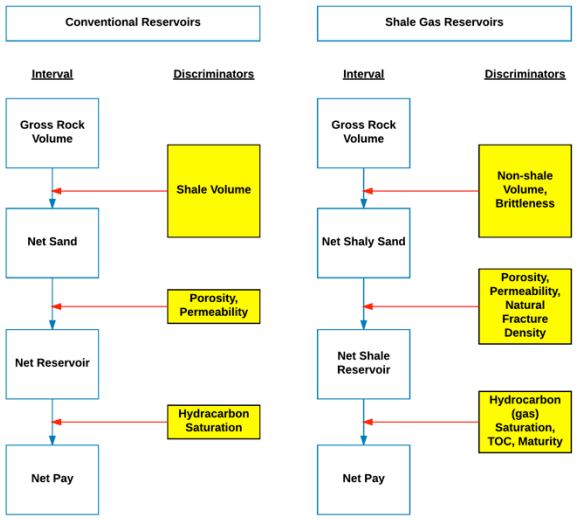

Fig. 2.2—Comparison of net pay in conventional reservoirs and in shale-gas reservoirs (Adapted from Worthington and Majid (2013))

EIA and ARI (2013) has published the "net organic shale thickness" and "gross organic shale thickness" of all international formations covered in my work. Comparing these terms with definitions of various thicknesses given by Worthington and Majid (2013), I assumed that the "gross organic thickness" takes into account the parameter cut-offs, namely $V_{nonshale}$, brittleness, porosity, permeability and natural fracture density. EIA and ARI (2013) computed the "net organic shale thickness" using a net-to-gross ratio applied to "gross organic shale thickness" in order to account for organically-barren rocks within the gross interval. Hence, it was further assumed that "net organic shale thickness" refers to Worthington's 'net pay' that takes into account the cut-off on TOC **(Fig. 2.3)**.

Even though net pay may be distributed according to any PDF form, the parameter to be used for volumetric assessment is the average net pay (h_{avg}) which, when multiplied by the prospective area, gives the total rock volume. Since h_{avg} is calculated by averaging the values of net pay at several locations, h_{avg} is expected to follow a normal distribution as a result of the central limit theorem (Murtha 2001). The median (P50) of this distribution was set to the value specified by EIA and ARI (2013) for each formation.

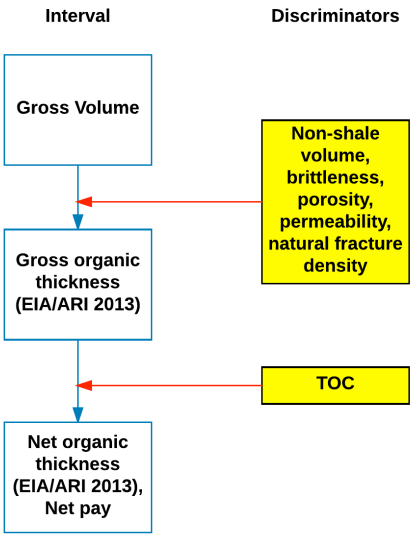

Fig. 2.3—Definition of net pay used in this study

Furthermore, since the net-to-gross ratio cannot be greater than unity, the average "gross organic shale thickness" may be assumed as an upper limit on h_{avg}. Hence, the 95th percentile of the distribution (P95) was set to this value.

2.1.2.3 Average Total Organic Carbon ($TOC_{avg,pd}$)

TOC refers to the percent by weight of organic carbon in the rock. A higher TOC in the formation, in general, signifies a greater hydrocarbon generative capacity, conditional on the percentage and type of kerogen (Types 1, 2 or 3) that accounts for the weight of organic carbon. Hydrocarbon generation proceeds with a decrease in average TOC from its original value at the time of sediment deposition ($TOC_{avg,i}$) to the present day value ($TOC_{avg,pd}$).

Similar to h_{avg}, $TOC_{avg,pd}$ for each formation was modeled as a normal distribution centered on the average value specified by EIA and ARI (2013). The degree

of uncertainty in $TOC_{avg,pd}$ was specified by setting the 95th percentile of the distribution (P95) at the maximum value of present day TOC cited by EIA and ARI (2013) for each formation, or 10 wt%, whichever is lower. This was done keeping in mind that, barring a few exceptions such as the North Nordegg formation ($TOC_{avg,pd}$ = 11 wt% (EIA and ARI 2013)), the upper limit on $TOC_{avg,pd}$ of mature shale exploration targets is just around 10 wt% (Alexander et al. 2011).

2.1.2.4 Vitrinite Reflectance (R_o%)

Vitrinite reflectance (R_o%), a measure of the thermal maturity of the formation, was assigned a triangular distribution with mode at the value specified by EIA and ARI (2013). The lower and upper limits of the distribution were set at 0.7 R_o% and 1.0 R_o% corresponding to the thermal maturity limits of the oil window as assumed by EIA and ARI (2013) in defining the prospective area.

2.1.2.5 Average Water Saturation ($S_{w,avg}$)

Since average water saturation values for studied formations has not been reported by EIA and ARI (2013), I assumed a normal distribution centered (P50) at 27.7%, based on published values (see Sections 3.4.2, 3.5.2, and 3.6.2) for three well-studied US formations (Bakken, Eagle Ford and Niobrara). The 95th percentile (P95) of the $S_{w,avg}$ distribution was set equal to 37.2%, which was computed as the average of published upper limits on water saturation for each of the above-mentioned formations **(Table 2.2)**.

Table 2.2—Computation of limits on water saturation using data from three US formations

Formation	Water saturation (%)	
	P50	**P95**
Bakken	25.1	37.5
Eagle Ford	19.0	25.0
Niobrara	39.0	49.0
Average value	27.7	37.2

2.1.3 *Computation of Porosity*

The total porosity (ϕ) was modeled as the sum of shale matrix porosity (ϕ_{mat}) and kerogen porosity (ϕ_{ker}) generated through the decomposition of organic matter in kerogen:

$$\phi = \phi_{mat} + \phi_{ker} \quad (2)$$

ϕ_{mat} was assigned a constant value of 5%, representative of the shale matrix (Li et al. 2015). The decomposition of kerogen into hydrocarbons and the subsequent development of organic porosity was modeled using an approach outlined by Modica and Lapierre (2012) **(Fig. 2.4)**.

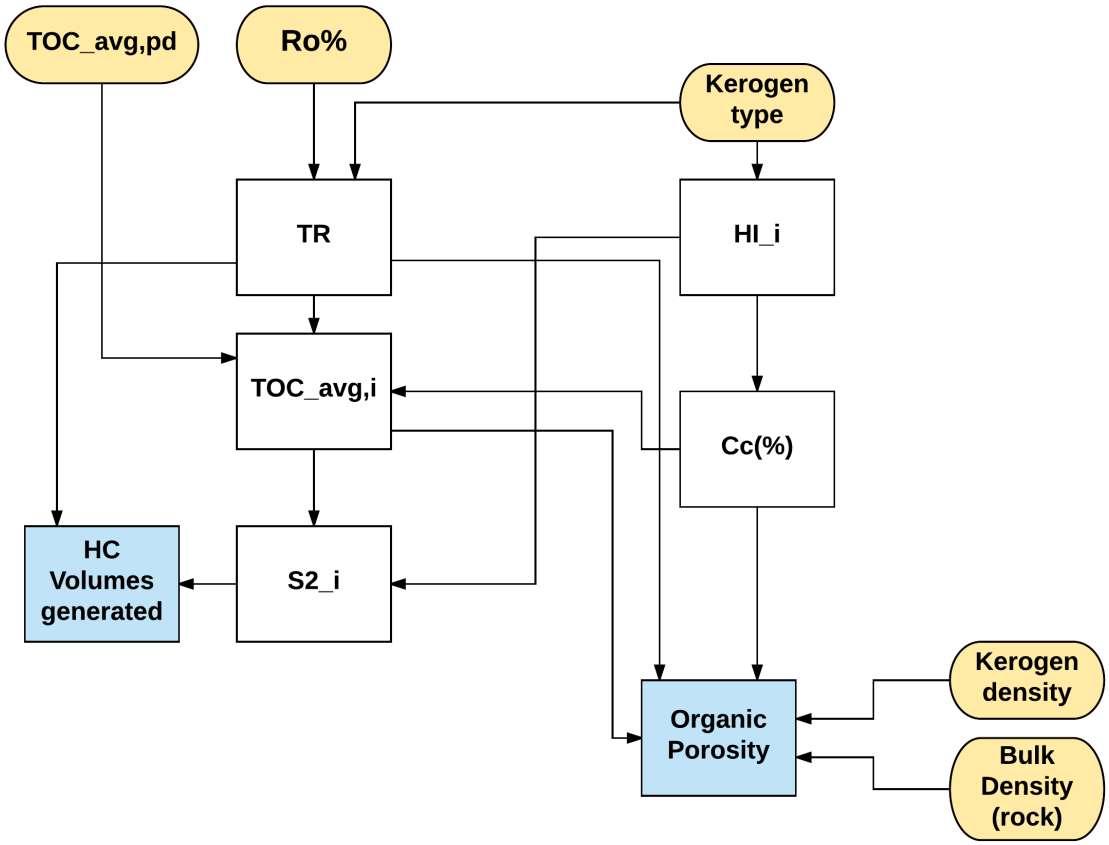

Fig. 2.4—Workflow for ϕ and O_{gen} computation, based on Modica and Lapierre (2012). Input parameters are shown in yellow ellipses and the outputs in blue boxes.

The extent of decomposition of organic matter is characterized by the carbon transformation ratio (TR) which was modeled as a function of $R_o\%$ and the predominant type of kerogen in the rock (reported by EIA and ARI (2013)). $TOC_{avg,i}$ was then computed from $TOC_{avg,pd}$ (reported by EIA and ARI (2013)) and TR. The volume of hydrocarbons generated to date (O_{gen}) due to TOC decomposition was then computed from $TOC_{avg,i}$ and initial hydrogen index (HI_i). The hydrogen index (HI) is a measure of the generative capacity of the rock and is defined as

$$HI = \frac{S2}{TOC} \tag{3}$$

where *S2* is the mass of hydrocarbons generated from 1 g of rock when subjected to thermal pyrolysis during a Rock-Eval study. A Rock-Eval study is a procedure used to assess the organic richness and maturity of a source-rock sample by heating it to progressively higher temperatures. In doing so, one can measure the mass of hydrocarbons initially present in the sample *(S1)* and that of hydrocarbons generated from source-rock kerogen *(S2)*, along with the mass of carbon dioxide released *(S3)* and that of residual carbon *(S4)* at the end of the study.

The procedure for the computation of ϕ_{ker} is detailed below.

1. HI_i was assigned a representative value based on the predominant kerogen type in the formation. If no information on the predominant kerogen type was available, Type 2 was assumed for marine depositional systems and Type 1 for lacustrine systems. The representative values of HI_i (Jarvie et al. 2007) assumed for each kerogen type are given in **Table 2.3**.

Table 2.3—Various kerogen types and associated HI_i assumed

Kerogen type	**HI_i (mg HC/g TOC)**
1	750
2	450
3	125

2. *TR* was computed from $R_o\%$. Modica and Lapierre (2012) used an empirical relationship between $R_o\%$ and *TR*, as reported by Bordenave et al. (1993) to compute *TR* for Type-2 kerogen:

$$TR = \frac{100\%}{1 + 20645.5\exp(-12.068 \times R_o\%)} \quad (4)$$

However, since this study includes formations rich in Type-1 and Type-3 kerogens as well, I modeled *TR* for each kerogen type using the same functional form as follows:

$$TR = \frac{100\%}{1 + A\exp(-B \times R_o\%)} \quad (5)$$

I used *TR* and $R_o\%$ reported by Waples and Marzi (1998) to compute the best-fit values for parameters *A* and *B* for each type of kerogen. However, as established by Waples and Marzi (1998), the relationship between $R_o\%$ and *TR* is dependent on the heating rate that the kerogen is subjected to. Therefore, I established a range of values for *A* and *B* for each kerogen type **(Table 2.4)** for heating rates that range from 0.5 ^{o}C/Ma to 10 ^{o}C/Ma. The established fits for each kerogen type are shown in **Fig. 2.5 to Fig. 2.7**.

Table 2.4—Parameter ranges for TR functional form for different kerogen types

	***A* upper limit**	***A* lower limit**	***B* upper limit**	***B* lower limit**
Type 1	3,411,947.8	2,239,740.8	16.8	16.3
Type 2	116,660,103.7	28,462,348.9	23.6	22.0
Type 3	143.1	40.1	4.4	3.2

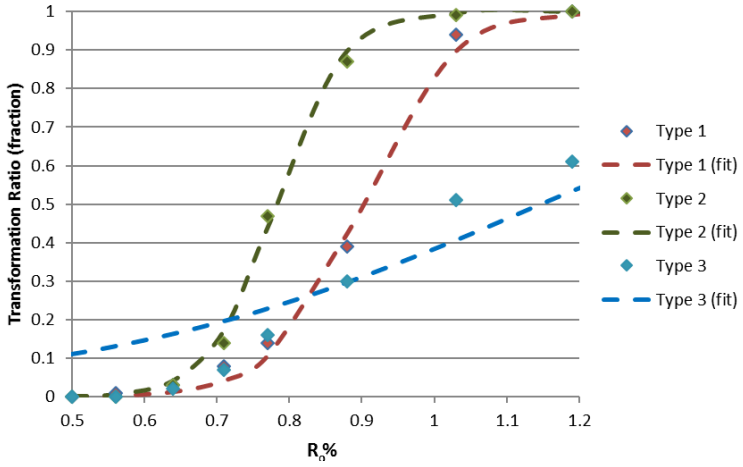

Fig. 2.5—Relationship between *TR* and vitrinite reflectance (R_o%) for different kerogen types heated at a rate of 0.5 ^{o}C/Ma in the oil window (data from Waples and Marzi (1998)). The fitted functional forms are also shown.

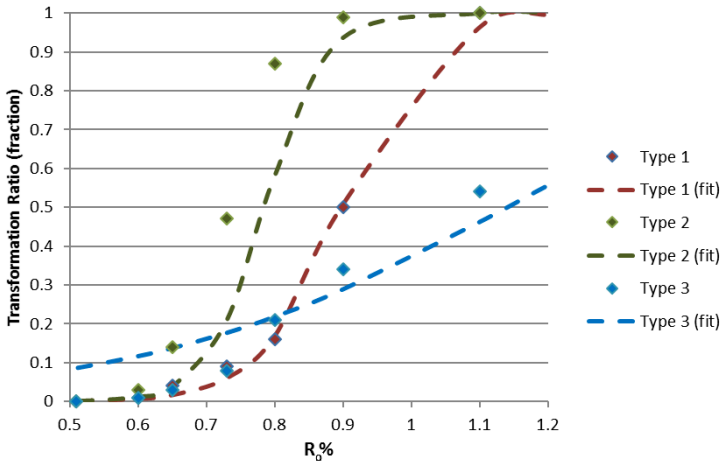

Fig. 2.6—Relationship between *TR* and vitrinite reflectance (R_o%) for different kerogen types heated at a rate of 2 ^{o}C/Ma in the oil window (data from Waples and Marzi (1998)). The fitted functional forms are also shown.

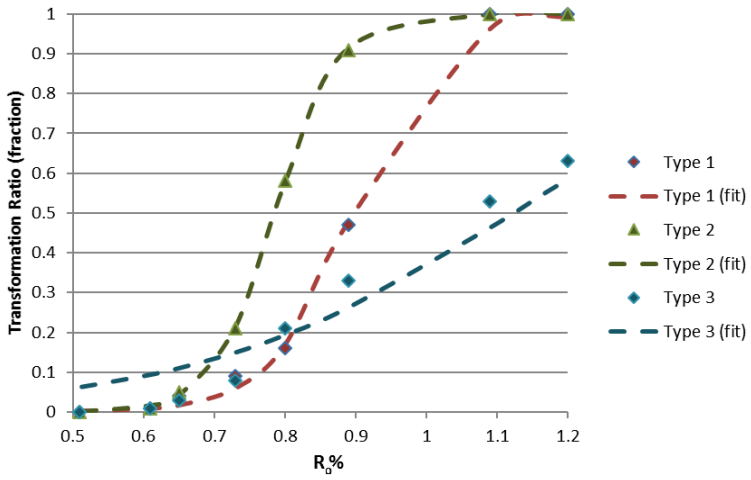

Fig. 2.7—Relationship between *TR* and vitrinite reflectance (R_o%) for different kerogen types heated at a rate of 10 °C/Ma in the oil window (data from Waples and Marzi (1998)). The fitted functional forms are also shown.

3. The percent convertible carbon *Cc (%)*, which represents the portion of $TOC_{avg,i}$ transformable into hydrocarbon, was calculated. *Cc (%)* is related to the kerogen type that makes up $TOC_{avg,i}$ and was estimated using a linear fit between HI_i and *Cc (%)*, derived by Modica and Lapierre (2012) using data from Daly and Edman (1987):

$$Cc(\%) = 0.0085 \times HI_i \tag{6}$$

4. $TOC_{avg,i}$ was computed as (Modica and Lapierre 2012)

$$TOC_{avg,i} = \frac{TOC_{avg,\,pd}}{1 - TR \times \dfrac{Cc(\%)}{100}} \tag{7}$$

5. ϕ_{ker} was computed as (Modica and Lapierre 2012)

$$\phi_{ker} = TOC_i \times Cc(\%) \times k \times TR \times \frac{\rho_b}{\rho_{ker}} \tag{8}$$

where factor of 1.118 accounts for the weight of kerogen per unit weight of convertible carbon, assuming that 95% of $TOC_{avg,i}$ is due to kerogen and that convertible carbon

accounts for 85% of convertible kerogen by weight (Modica and Lapierre 2012). ρ_b stands for the bulk density of rock, which was assumed to be 2.5 g/cc and ρ_{ker} for kerogen density, which was fixed at 1.2 g/cc (Okiongbo, Aplin, and Larter 2005).

2.1.4 *Computation of Initial Oil Formation Volume Factor (B_{oi})*

In this study, Standing's correlations (Velarde 1996) were used to estimate the oil formation volume factor (B_{oi}) from reservoir temperature (T_{res}), reservoir pressure (P_{res}), oil gravity in °API ($\gamma_{0,API}$), specific gas gravity (γ_g), and gas-oil ratio (GOR) (EIA and ARI 2013) for each of the formations. The procedure followed is detailed below.

1. T_{res} at the average depth of the formation (D) was estimated assuming a constant geothermal gradient (g_{therm}) and surface temperature (T_{surf}):

$$T_{res} = T_{surf} + (g_{therm} \times D) \tag{9}$$

g_{therm} ranges between 1.3 to 2.2 °F/100 ft (Peters, Curry, and Kacewicz 2012). An average value of 1.75 °F/100 ft was assumed in this report, unless EIA and ARI (2013) included the values for geothermal gradient for a particular formation. In addition, T_{surf} for all basins was assumed to equal 60 °F.

2. P_{res} at depth D was estimated assuming a constant atmospheric pressure (P_{atm}) and a subsurface pressure gradient (g_{press}), depending on the categorization of each formation as underpressured, normally pressured, slightly overpressured, moderately overpressured or highly overpressured by EIA and ARI (2013):

$$P_{res} = P_{atm} + (g_{press} \times D) \tag{10}$$

P_{atm} for all basins was assumed to equal 14.7 psi. Since EIA and ARI (2013) does not specify the pressure-gradient values for its categories, I converted each category into

a pressure-gradient range based on Miller's gas-shale-ranking scorecard (Bammidi 2011) **(Table 2.5)**.

Table 2.5—Pressure gradient categories and corresponding values

Category	**Pressure-gradient (psi/ft) range (Bammidi 2011)**	g_{press} **(psi/ft) assigned**
Underpressured	<0.4	0.35
Normally pressured	0.4-0.5	0.45
Slightly overpressured	0.5-0.6	0.55
Moderately overpressured	0.6-0.7	0.65
Highly overpressured	>0.7	0.75

3. *GOR* was calculated as the ratio between original-in-place associated gas and original-in-place shale oil in the formation, as assessed by EIA and ARI (2013). The bubble-point pressure (P_b) for the formation was computed from the *GOR* as (Velarde 1996)

$$P_b = 18.2 \times \left(\left(\frac{GOR}{\gamma_g} \right)^{0.83} \times 10^{y_g} - 1.4 \right) \tag{11}$$

where

$$y_g = 0.0125 \times \gamma_{o,API} - 0.00091 \times T_{res} \tag{12}$$

P_b thus computed, was compared to P_{res}. If $P_b > P_{res,}$ the reservoir was considered saturated.

4. The oil formation volume factor at bubble point (B_{ob}), was calculated as (Velarde 1996)

$$B_{ob} = 0.92 + 1.47 \times 10^{-4} \times \left(GOR \times \left(\frac{\gamma_g}{\gamma_o} \right)^{0.5} + 1.25 \times T_{res} \right) \quad (13)$$

where

$$\gamma_o = \frac{141.5}{\gamma_{o,API} + 131.5} \quad (14)$$

For a saturated reservoir, $B_{oi} = B_{ob}$.

5. If $P_b < P_{res}$, the formation was expected to be undersaturated and B_{oi} was calculated as

$$B_{oi} = B_{ob} \times \exp\left(c_o \left(P_b - P_{res}\right)\right) \quad (15)$$

where c_o represents the oil compressibility. A correlation provided by Vasquez and Beggs (1980) was used to calculate c_o and is given below:

$$c_o = \frac{-1.433 + 5R_s + 17.2T_{res} - 1180\gamma_g + 12.61\gamma_{o,API}}{P_{res} \times 10^5} \quad (16)$$

Here, the solution gas-oil ratio R_s=GOR for an undersaturated reservoir.

2.1.5 *Computation of Maximum Original-in-Place Shale Oil ($OOIP_{max}$)*

The initial hydrocarbon generation potential of the source rock ($S2_i$) in mg HC/gm rock was computed from HI_i and $TOC_{avg,i}$ (Chen, Jiang, and Lavoie 2016) (Fig. 2.4):

$$S2_i = HI_i \times TOC_{avg,i} \quad (17)$$

The volumes of generated oil to date (O_{gen}) were calculated in bbl/ac·ft by multiplying $S2_i$ with the carbon transformation ratio (TR) and a mass-to-volume conversion factor of 21.89 (Modica and Lapierre 2012):

$$O_{gen}\left(\frac{bbl}{ac\cdot ft}\right) = S2_i \times TR \times 21.89 \tag{18}$$

O_{gen} was then multiplied by the total rock volume in the formation to compute the total volume of oil generated ($O_{tot,gen}$). The total rock volume is equal to the prospective area (A) times the average net pay (h_{avg}):

$$O_{tot,gen} = O_{gen} \times A \times h_{avg} \tag{19}$$

However, due to the limit on the available pore volume in the formation, a fraction of the generated hydrocarbons may be expelled. The available pore volume (PV_{max}) was calculated volumetrically as

$$PV_{max} = \frac{A \times h_{avg} \times \phi \times \left(1 - S_{w,avg}\right)}{B_{oi}} \tag{20}$$

where A, h_{avg} and $S_{w,avg}$ were sampled from the specified distributions and ϕ and B_{oi} were calculated as explained previously.

The maximum volume of original-in-place oil in the formation, $OOIP_{max}$, was calculated as the minimum of O_{gen} and PV_{max} (Kuchinskiy, Gentry, and Hill 2012):

$$OOIP_{max} = \min\left(O_{tot,gen}, PV_{max}\right) \tag{21}$$

2.1.6 *Assignment of Modifier Distributions*

EIA and ARI (2013) modified the volumetrically computed resources using two kinds of judgmentally-assigned 'success factors': the play success factor and the prospective area success factor. I incorporated these factors into my study in the following manner:

a. Play-success-modifier distribution: Several of the formations covered by EIA and ARI (2013) (and included in this study) are speculative and hence have not been

geologically assessed to an adequate degree. This implies that there is considerable risk that the play will never become successful. EIA and ARI (2013) accounted for this risk by specifying a probability that at least some portion of play becomes productive based on prior developmental activities in the play and expert judgment. A play that has already seen some degree of development was assigned a 'play success factor' of 100%.

I included the play success probability into the assessment of $OOIP_{sh\_oil}$ by multiplying $OOIP_{max}$ by a 'play-success-modifier distribution' denoted by $p_{playsuccess}(m)$. This distribution was modeled as a Bernoulli random variable m, which takes the value of 1 if at least some portion of the play becomes productive, and a value of 0 otherwise. The probability density function for m is given by

$$p_{playsuccess}(m) = \begin{cases} s, & if \quad m = 1 \\ (1-s), & if \quad m = 0 \\ 0 & otherwise \end{cases} \tag{22}$$

where s stands for the 'play success factor' assigned by EIA and ARI (2013). In order to account for a probability of (1-s) with which no commercial discovery may be made on the play (i.e. $OOIP_{sh\_oil} = TRR_{sh\_oil} = 0$), $OOIP_{max}$ computed at each Monte Carlo iteration was multiplied by the random variable m that takes the value of 1 with a probability of s, and 0 otherwise. In this way, it is ensured that $OOIP_{max}$ is set to zero with a probability of (1-s).

b. Prospective-area-modifier distribution: The prospective area of a formation was established by EIA and ARI (2013) based on several criteria, namely depth, depositional environment, TOC and R_o%. The 'prospective area success factor' accounts for the productive portion of the established prospective area after the application of any

additional criteria (such as geological complexity that were not considered earlier) that may render some portion of the area unproductive. EIA and ARI (2013) assigns a single value to this factor.

I redefined the 'prospective area success factor' as the 'prospective-area modifier'—the portion of the prospective area that may be unproductive due to criteria that have not been included in assigning the prospective area.

The prospective-area modifier was modeled as a triangular distribution with the extreme values at 0 and 1 and the modal value at the factor cited by EIA and ARI (2013). This distribution was also multiplied to $OOIP_{max}$ to compute the deliverable $OOIP_{sh\_oil}$ distribution for each formation.

2.2 Resource Aggregation

The manner in which formation-level resource distributions are aggregated to the regional level plays an important role in the uncertainty that is captured by the resulting distributions. In other words, the variance of the resulting aggregate distribution is dependent on the approach used for aggregation.

Aggregation may be performed under the assumption that resource distributions in the various formations studied are dependent or independent of each other. Statistical aggregation involves summing up the various formation-level distributions, assuming a value for the correlation coefficient between the summand distributions. Statistical aggregation generally utilizes Monte Carlo simulation, wherein calculations (here summation) are performed on large randomly-generated samples from formation-level resource distributions in order to construct the PDF of the aggregate distribution. If the

PDF forms of the summand distributions are relatively simple (e.g. normal, lognormal or triangular), statistical aggregation can be done using analytical methods as well. In this study, I ran Monte Carlo simulations in order to establish the statistical aggregate distribution, assuming a correlation coefficient of zero between the summand distributions. However, there exists a possibility that at least some of the formations have common sedimentary histories that may result in some degree of correlation between them.

Arithmetic aggregation assumes 100% dependence (perfectly correlated) between the resources in each formation. Hence, the P10, P50 and P90 values for the aggregated resource distribution will be equal to the sum of the respective values for each of the formations considered for aggregation. Nevertheless, it is quite unlikely that the input parameter distributions for all formations considered are perfectly correlated. Perfect correlation would imply that if the 'actual' resource volume (established in some manner) in one formation (say, formation A) turns out to be the 60^{th} percentile value in the resource distribution for A, the actual value for another formation (say, formation B) should necessarily be the 60^{th} percentile value in the resource distribution for B.

The SPE-PRMS guidelines advocate the use of arithmetic summation for aggregation of resources beyond field, property or project levels in order to avoid underestimating the variance (and hence uncertainty) in higher levels of assessment (SPE et al. 2007). However, in this study, I used both arithmetic summation (assuming perfect correlation) and statistical summation (assuming perfect independence) in generating the region-wise and total resource estimates. This was done because the

correlation coefficient between the formation-wise distributions is unknown. Therefore, the true aggregate distribution is expected to be in between the arithmetically-aggregated and statistically-aggregated distributions.

2.3 $OOIP_{sh\_oil}$ Resource Distributions

In this section, I present the results of the region-wise and total $OOIP_{sh\_oil}$ assessments carried out using the procedure detailed in Sections 2.1 to 2.2. First, I present the region-wise distributions and P10-P50-P90 estimates obtained by means of statistical and arithmetic aggregation. Subsequently, the total $OOIP_{sh\_oil}$ distribution and the corresponding P10-P50-P90 estimates obtained via statistical and arithmetic aggregation are also presented.

2.3.1 *Region-wise Results*

The $OOIP_{sh\_oil}$ distributions for the seven regions, obtained using statistical and arithmetic aggregation of $OOIP_{sh\_oil}$ distributions of the studied formations in each region, highlight the large uncertainty in region-wise estimates **(Fig. 2.8 and Fig. 2.9).** The ratios of P90 to P10 **(Table 2.6 and Table 2.7)** are indicative of the degree of uncertainty in the aggregated estimates**.** The estimates reported by EIA and ARI (2013) are very close to the P10 values obtained through statistical aggregation, yet more optimistic than the P50 values computed using arithmetic aggregation (Table 2.6 and Table 2.7). The EIA and ARI estimates shown represent the volumes of original-in-place oil only and exclude condensates.

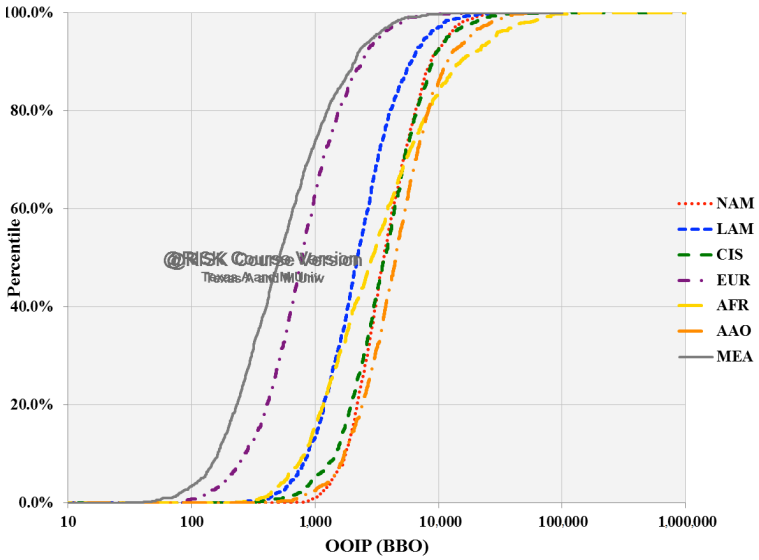

Fig. 2.8—Region-wise $OOIP_{sh\_oil}$ distributions generated using statistical aggregation

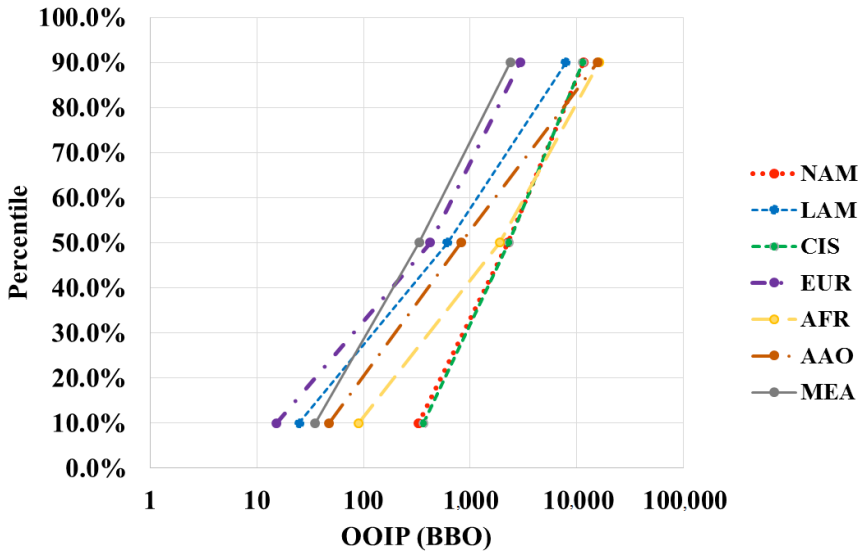

Fig. 2.9—Region-wise $OOIP_{sh\_oil}$ P10-P50-P90 estimates generated using arithmetic aggregation

Table 2.6—Region-wise $OOIP_{sh\_oil}$ P10-P50-P90 estimates generated using statistical aggregation

Region	$OOIP_{sh\_oil}$ (1,000 BBO)			P90/P10	Reported $OOIP_{sh\_oil}$ (1,000 BBO) (EIA and ARI 2013)
	P10	P50	P90		
NAM	1.77	3.62	8.67	5	1.28
LAM	0.87	2.22	5.97	7	0.92
CIS	1.46	3.64	8.85	6	1.46
EUR	0.27	0.78	2.39	9	0.24
AFR	0.82	2.89	15.11	18	1.07
AAO	1.72	4.51	11.66	7	1.48
MEA	0.16	0.52	2.10	13	0.51

Table 2.7—Region-wise $OOIP_{sh\_oil}$ P10-P50-P90 estimates generated using arithmetic aggregation

Region	$OOIP_{sh\_oil}$ (1,000 BBO)			P90/P10	Reported $OOIP_{sh\_oil}$ (1,000 BBO) (EIA and ARI 2013)
	P10	P50	P90		
NAM	0.33	2.26	11.47	35	1.28
LAM	0.03	0.61	7.84	314	0.92
CIS	0.37	2.31	11.39	31	1.46
EUR	0.02	0.42	2.95	193	0.24
AFR	0.09	1.91	16.19	179	1.07
AAO	0.05	0.82	15.50	324	1.48
MEA	0.04	0.33	2.39	67	0.51

Both statistically- and arithmetically-aggregated estimates are characterized by high uncertainty, with the lowest value of P90/P10 around 5—for statistically-aggregated $OOIP_{sh\_oil}$ in NAM (Table 2.6 and Table 2.7). As expected, due to perfect correlation between formation-wise distributions, the ratio is much higher in the case of arithmetic aggregation than in that of statistical aggregation.

Comparing the ratios for each region using both methods, the resource distributions of NAM and CIS seem to entail the lowest degrees of uncertainty (Table 2.6 and Table

2.7). These regions also hold high P10 volumes, using both aggregation methods (Fig. 2.8 and Fig. 2.9). This indicates the presence of substantial volumes of in-place resources at comparatively high levels of certainty in NAM and CIS.

AAO holds a P10 volume comparable to NAM and CIS using statistical aggregation (Table 2.6 and Fig. 2.8). However, arithmetic aggregation of AAO resources reveals a relatively low value for the P10 volume (Table 2.7 and Fig. 2.9). This may be explained by the fact that the total number of formations assessed, and thereby the number of formation-wise distributions aggregated, in the case of AAO is much higher than in other regions. Due to the greater number of summands, statistical aggregation would result in the P10 getting pushed further toward the mean. However, the arithmetically-aggregated P10 estimate is the sum of P10 values of all AAO formation-wise distributions, several of which are close to zero due to the high degree of speculation in these formations. This results in a low P10 estimate and thereby a high P90/P10 ratio in the case of arithmetic aggregation in AAO (Table 2.7).

The results for LAM may also be reasoned along the same lines (Table 2.6 and Table 2.7). AAO and LAM are expected to hold potentially large, albeit highly uncertain, volumes of in-place resources. These results should be revised once the prospective formations in these regions are sufficiently de-risked so that the uncertainties in the estimates may be reduced.

There also exists a high degree of uncertainty in the estimates for AFR, using both arithmetic and statistical aggregation (Table 2.6 and Table 2.7). This is due to the presence of formations with large uncertainty in net pay along with high values of

prospective area. Since the 95th percentiles of the prospective area for these formations are calculated using Eq. 1, it is expected that P90 estimates of $OOIP_{sh\_oil}$ of these formations will be very high (Table 2.6 and Table 2.7). Hence, both statistical and arithmetic aggregation of the resources in these formations lead to a high value of P90/P10 in AFR.

It has to be stressed that the assessment results for MEA are highly likely to be inconclusive since this study did not cover several potentially shale-oil-rich countries in the region.

2.3.2 *Total Results*

The total $OOIP_{sh\_oil}$ distributions obtained using both statistical and arithmetic aggregation highlight the large degree of uncertainty, particularly in the case of arithmetic aggregation (**Fig. 2.10**). The P90/P10 ratio of total $OOIP_{sh\_oil}$ obtained using statistical aggregation is merely 2.9, with the P50 value being less than twice the P10 value and the P90 values, less than twice the P50 value **(Table 2.8).** This is an effect of statistically aggregating several formation-wise distributions resulting in an increasingly-narrower aggregate distribution. This effect exposes the risk of underestimating uncertainty while aggregating resource distributions without accounting for possible correlations between them.

However, the arithmetically aggregated resource estimates entail a high degree of uncertainty with P90/P10 = 74.9 **(Table 2.9).** The P50 value is much closer to the P10 value than it is to the P90 value. This is the result of arithmetically aggregating several distributions that are heavily right-skewed.

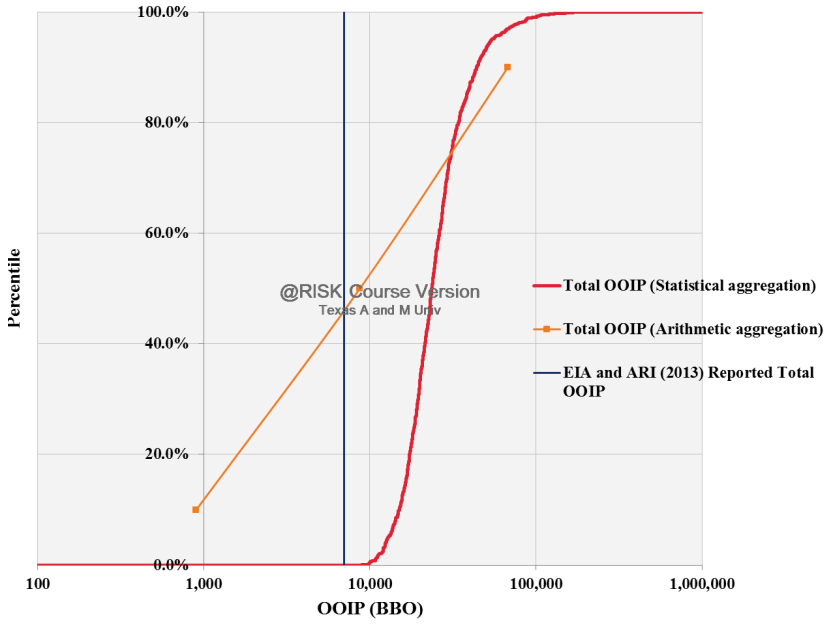

Fig. 2.10—Total $OOIP_{sh\_oil}$ distribution generated using statistical and arithmetic aggregation

Table 2.8—Total $OOIP_{sh\_oil}$ P10-P50-P90 estimates generated using statistical aggregation

Region	$OOIP_{sh\_oil}$ (1,000 BBO)			P90/P10	Reported $OOIP_{sh\_oil}$ (1,000 BBO) (EIA and ARI 2013)
	P10	P50	P90		
TOTAL	15.0	23.6	43.9	2.9	7.0

Table 2.9—Total $OOIP_{sh\_oil}$ P10-P50-P90 estimates generated using arithmetic aggregation

Region	$OOIP_{sh\_oil}$ (1,000 BBO)			P90/P10	Reported $OOIP_{sh\_oil}$ (1,000 BBO) (EIA and ARI 2013)
	P10	P50	P90		
TOTAL	0.9	8.7	67.7	74.9	7.0

2.4 Comparison with Previous Estimates

In this section, I compare the results of my study with those by EIA and ARI (2013) by plotting the P10, P50 and P90 values of $OOIP_{sh\_oil}$ for each formation against the deterministic estimates established in their report. Best-fit trendlines are plotted for P10, P50 and P90 in order to illustrate the relative magnitudes of my estimates to the previous ones **(Fig. 2.11).**

In general, EIA and ARI (2013) estimates lie within the computed P10 and P90 limits (Fig. 2.11). It is also worth noting that, even though my P50 estimates of $OOIP_{sh\_oil}$ are lesser than the best estimates published by EIA and ARI (2013) for most formations, the P50 trendline has a slope greater than unity due to the estimates for a few formations being much higher than the EIA and ARI (2013) estimates (Fig 2.11). These effects may be attributed to my methodology wherein I estimate the total porosity available using kerogen kinetics in contrast to the EIA and ARI's volumetric assessment using analogous porosities where data is absent.

The high porosities associated with formations with high $TOC_{avg,pd}$ account for the significantly higher P50 estimates, compared to EIA and ARI (2013) estimates (Fig 2.11). Likewise, P90 estimates that are lower than the EIA and ARI (2013) estimates are those of formations with low $TOC_{avg,pd}$ (which result in a low porosity estimate, based on my methodology), and thereby low $OOIP_{sh\_oil}$ estimates (Fig 2.11).

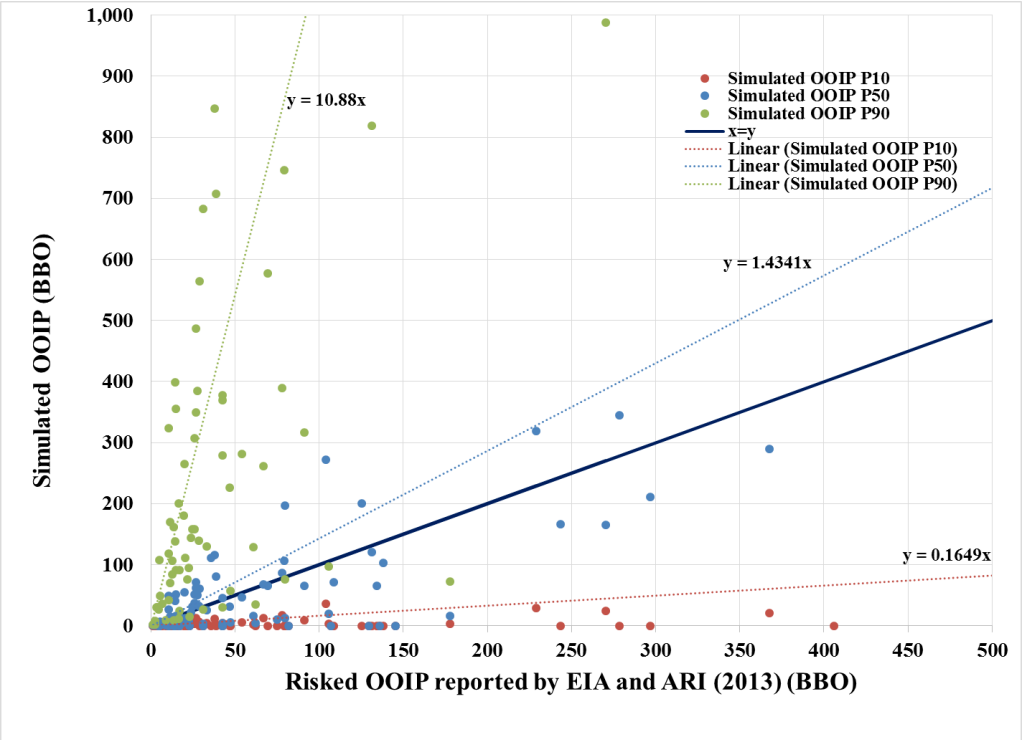

Fig. 2.11—Comparison between formation-wise probabilistic $OOIP_{sh\_oil}$ estimates from my study with the respective deterministic values cited by EIA and ARI (2013)

Fig. 2.12 and Fig. 2.13 compare my region-wise $OOIP_{sh\_oil}$ for each aggregation method, with the previous assessment of shale-oil resources by EIA and ARI (2013) (excluding condensate volumes). The large P90 values computed using my methodology recognize the high degree of uncertainty in region-wise resource estimates.

In general, EIA and ARI (2013) estimates are conservative compared to my region-wise P50 values computed via both arithmetical aggregation as well as statistical aggregation (Fig. 2.12 and Fig. 2.13). The notable exceptions are LAM and AAO, in the case of arithmetic aggregation (Fig. 2.13). However, the P50 obtained via statistical

aggregation exceeds the EIA and ARI (2013) estimates for these regions (Fig. 2.12). This effect may be attributed to the heavily right-skewed formation-wise resource distributions in these regions, which result from the low play-success and prospective-area modifiers assigned.

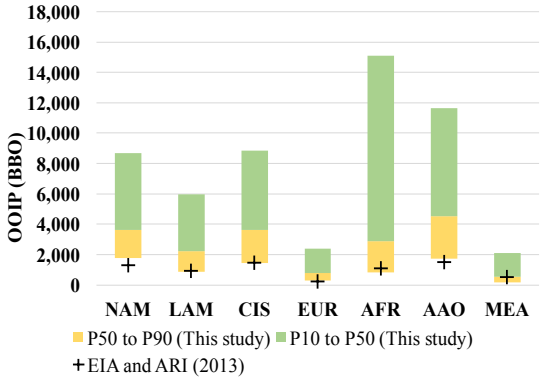

Fig. 2.12—*OOIP*$_{sh\_oil}$ ranges computed using statistical aggregation of formation-wise *OOIP*$_{sh\_oil}$ compared with *OOIP* values cited by EIA and ARI (2013)

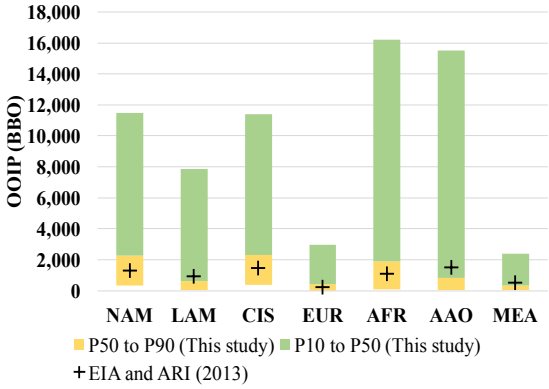

Fig. 2.13—*OOIP*$_{sh\_oil}$ ranges computed using arithmetic aggregation of formation-wise *OOIP*$_{sh\_oil}$ compared with *OOIP* values cited by EIA and ARI (2013)

3. RECOVERY FACTOR EVALUATION FOR FIVE US SHALE-OIL FORMATIONS

3.1 Introduction

In this section, oil recovery factors (*RF*) from five US shale-oil formations—Bakken, Eagle Ford, Wolfcamp, Niobrara and Avalon—are assessed using reservoir simulation. The recovery-factor (*RF*) distributions for each of these formations were established for three values of stage spacing—50 ft, 500 ft and 1,000 ft. Subsequently, generalized-recovery-factors for each value of stage spacing were generated, which were later used to compute TRR_{sh_oil} distributions in each of the 93 formations.

The rest of the section is organized as follows: In this section, I summarize a few previous assessments of US shale-oil resources. Section 3.2 briefly reviews the technology employed for hydrocarbon production from shale-oil reservoirs—horizontal drilling and hydraulic fracturing. Section 3.3 details the methodology and the reservoir model that I used to simulate production from the five US formations. Sections 3.4 to 3.8 present the input distributions to the model and simulation results for the five formations.

EIA and INTEK (2011) estimated the remaining technically-recoverable volumes of undeveloped shale-oil resources in discovered plays in the Lower 48 states to be 24 billion barrels (as of January 2009). EIA and INTEK (2011) conducted their assessment deterministically, based on the area, well spacing and the average expected ultimate recovery for each play. They also applied "effective recovery factors" that account for:

a. Prior knowledge about the play

b. Prior experience about production trends and response to recovery technologies

c. Produced volumes and proved reserves (in developed areas) that have not been included in the estimates

The EIA and INTEK (2011) report covered four shale-oil plays—Bakken, Eagle Ford, Monterey Santos and Avalon/Bone Spring. The results of this assessment are summarized in **Table 3.1**.

Table 3.1—Results of EIA and INTEK (2011) assessment of US shale-oil remaining technically-recoverable volumes (as of July 2011)

Shale oil play	Area (sq mile)	TRR (BBO)	Average EUR (MBO/well)
Eagle Ford	3,323	3.35	300
Bakken	6,522	3.59	550
Monterey Santos	1,752	15.42	550
Avalon/Bone Spring	1,313	1.58	300

Apart from the EIA and INTEK (2011) report, assessments of US continuous-oil accumulations (which comprise shale-oil and tight-oil formations) are regularly conducted by the USGS. The USGS (USGS 2015) published a list of assessed US continuous-oil accumulations comprising 11 continuous-oil provinces **(Table 3.2)**. These assessments of undiscovered technically-recoverable resources were conducted using the 'FORSPAN' methodology explained in Section 1.2.

Table 3.2—USGS resource assessments of various continuous-oil accumulations in the US (USGS 2015)

Province	Formation(s)	Mean TRR undiscovered (BBO)
Williston Basin	Bakken and Three Forks	7.38

Table 3.2 Continued

Province	Formation(s)	Mean TRR undiscovered (BBO)
Gulf Coast Region	Cretaceous strata	1.73
Northern Alaska	Brookian, Kingak, Shublik	0.00-2.00
Appalachian Basin	Ordovician Utica, Point Pleasant	0.94
Permian Basin	Spraberry	0.51
Paradox Basin	Cane Creek, Gothic, Chimney rock Hovenweep	0.47
Powder River Basin	Mowry, Niobrara	0.42
Anadarko Basin	Woodford	0.39
Southwestern Wyoming	Niobrara	0.1
Hanna, Laramie, Shirley Basins	Niobrara	0.04
Denver Basin	Niobrara, Carlile	0.04
Uinta-Piceance Basin	Green River	0.04
Montana Thrust Belt	Marias River	0.03
Big Horn Basin	Mowry	0.005

3.2 Drilling and Completion Techniques

In general, shale-oil formations are characterized by extremely low permeability that precludes the use of conventional vertical wells for resource extraction. Therefore, in order to produce commercial quantities of oil per well, the contact area between the wellbore and the formation has to be increased by drilling horizontal laterals.

Wellbores are at first drilled vertically to a specified depth, after which they are turned at an increasing angle until they run parallel to the target formation (Canadian Society for Unconventional Resources 2012). Based on a study conducted by EIA and

IHS (2016) using data from four unconventional plays, the cost of drilling an average horizontal well ranges from $1.8 MM to $2.6 MM and accounts for 27% to 38% of the total capital cost associated with a horizontal well.

To improve the effective permeability of the reservoir, hydraulic fracturing is performed wherein fracture networks are created by pumping in large volumes of fluid into the formation at pressures that exceed the fracture pressure of the rock. The pumped fluid is generally water-based, with a number of additives that make up around 0.5% to 3.0% of the total influent fluid volume. Once fracture networks are created, proppants are pumped into the fractures to keep them from closing once the fracture fluid is lost (Canadian Society for Unconventional Resources 2012). The cost of completing a horizontal well accounts for around 60% to 71% of the total well capital cost (EIA and IHS 2016).

Through the years, operators have been achieving higher well performance through technological innovations, some of which are listed below (EIA and IHS 2016):

- Use of longer laterals
- Better geosteering that ensures well placement in highly productive intervals
- Multi-pad drilling
- Increased fracture stages, proppant amounts and better fracture-fluid systems (cross-linked and slick water)
- Optimized spacing and stacking of laterals

3.3 Reservoir Model

In this study, I modeled a multistage horizontal lateral of length 5,000 ft in each of the five formations **(Fig. 3.1)**, wherein each stage is considered to consist of a single fully-penetrating hydraulic fracture 0.001 ft wide.

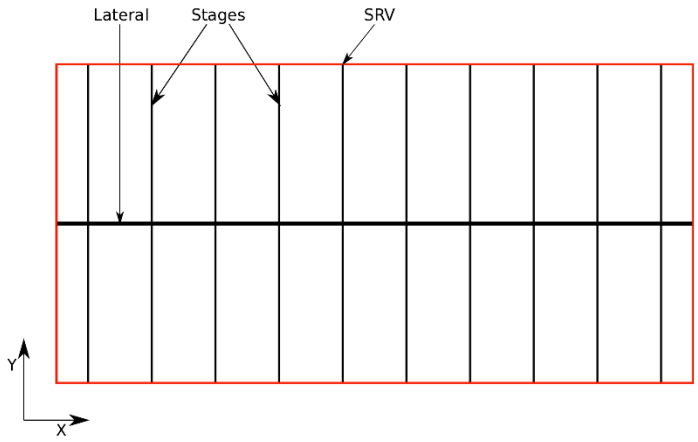

Fig. 3.1—Horizontal well overview

The stimulated reservoir volume (SRV) was assumed to be delimited by the hydraulic-fracture length $2x_f$ in the Y-direction, hydraulic-fracture height h_f (assumed to be equal to net pay) in the Z-direction, and the well length L in the X-direction **(Fig. 3.2)**. The stages were spaced along the well at a separation of d_s. Since each stage consists of only one hydraulic fracture, the hydraulic-fracture spacing d_f is equal to the stage spacing d_s.

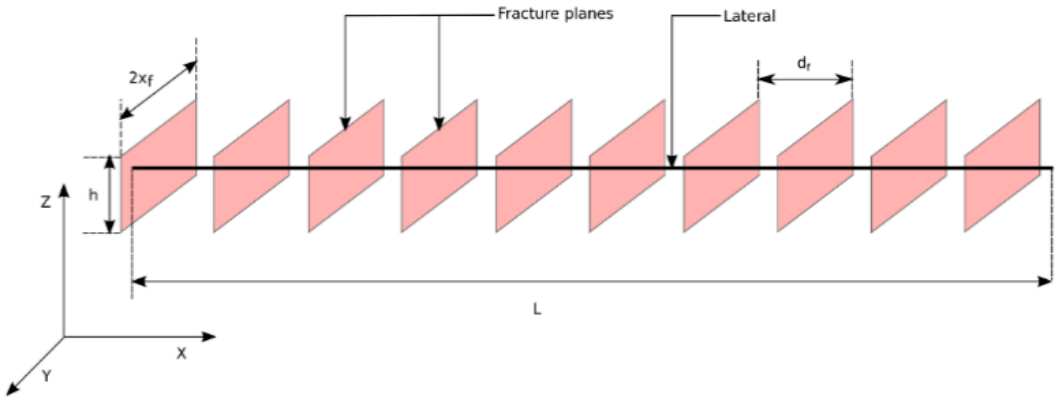

Fig. 3.2—Well definition and spatial limits of SRV

Due to the low matrix permeability of shale-oil reservoirs, the contribution from the unstimulated matrix to hydrocarbon production was assumed insignificant. Hence, the wells were laid out in such a way that the SRV's touch each other in order to maximize recovery (Yesiltepe 2015). Therefore, I assumed that the well spacing d_{well} is equal to $2x_f$ **(Fig. 3.3)**. Due to identical production trends from Well 1 and Well 2, there exists a no-flow boundary midway between the wells in the X-Z plane (Fig. 3.3). Since each hydraulic fracture was assumed identical in properties and dimensions, hydrocarbon flow into adjacent hydraulic fractures results in a no-flow boundary midway between the hydraulic fractures, as with adjacent wells. It was sufficient to simulate flow into a single hydraulic fracture in order to calculate the production from the entire SRV (which would equal the production from one fracture times the number of stages in the SRV).

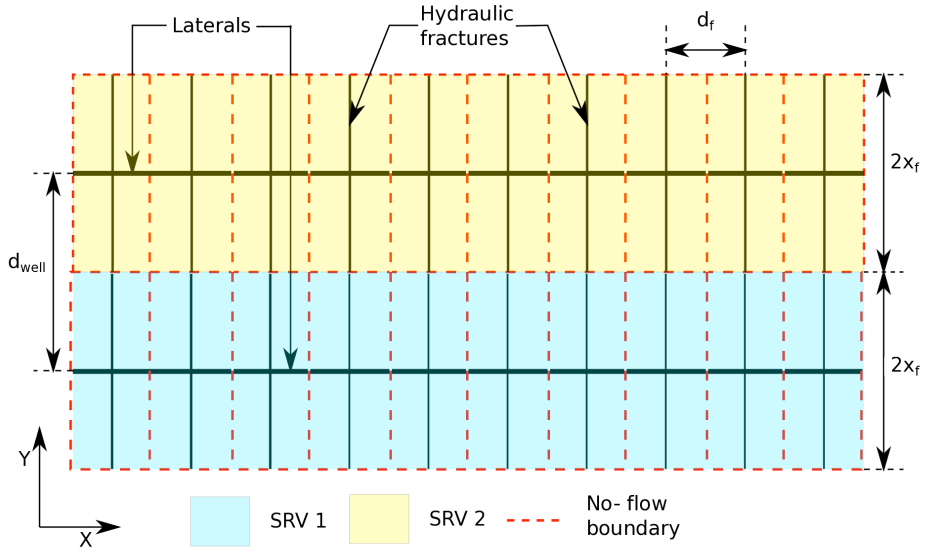

Fig. 3.3—Well spacing and no-flow boundaries

Hydrocarbon flow directly from the SRV into the wellbore was neglected. The hydraulic fracture was modeled as proposed by Chaudhary (2011). This method was originally developed in order to study the sensitivity of Eagle Ford liquids production to various reservoir parameters such as hydraulic-fracture spacing, half-length and conductivity, rock compressibility, flowing bottom-hole pressure and matrix permeability.

A single hydraulic fracture of half-length x_f and width 0.001 ft was modeled using a logarithmically-refined gridding scheme in order to simulate the pressure drop near the fracture **(Fig. 3.4).** The hydraulic fracture was assumed to have a dimensionless fracture conductivity F_{cD}=100.

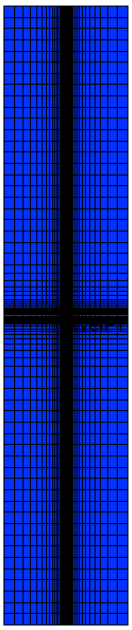

Fig. 3.4—Hydraulic-fracture model used

For the ease of simulation, the hydraulic fracture of width 0.001 ft was modeled as a conduit of width $w_{conduit} = 2$ ft, maintaining the same dimensionless fracture conductivity. The permeability of the conduit $k_{conduit}$ is thus given by,

$$k_{conduit} = \frac{F_{cD} \times k_{matrix} \times x_f}{w_{conduit}} \quad (23)$$

The flux into the hydraulic fracture remains constant along the length of the fracture, away from the wellbore.

The model was initialized to the estimated average P_{res} for each formation and production was simulated for 25 years, with a constant minimum-pressure constraint of 1,000 psi. The number of stages (n_s) is computed as

$$n_s = \frac{L}{d_s} \quad (24)$$

The technically-recoverable shale oil from a well of n_s stages is calculated as its cumulative production during a well-life of 25 years. Therefore,

$$TRR_{sh\_oil\_well} = n_s \times N_{p,stage} \tag{25}$$

where $N_{p,stage}$ is the cumulative production from a single stage in 25 years. The drainage area of the well is expressed as

$$A_{well} = L \times (2x_f) \tag{26}$$

Furthermore, the recovery factor was computed as

$$RF = \frac{TRR_{sh\_oil\_well}}{OOIP_{sh\_oil\_well}} \tag{27}$$

where $OOIP_{sh\_oil\_well}$ stands for the oil originally in place in the drainage area of the well, computed volumetrically.

The parameters d_s and well spacing d_{well} are controllable parameters that do not entail considerable uncertainty (Dong 2012). In addition to this, since I modeled the hydraulic fracture in such a way that $2x_f = d_{well}$, the uncertainty in x_f has also been ignored. Due to the model assumption that flux into the hydraulic fracture is constant along the length of the fracture, my choice of x_f barely affects the final cumulative production and *RF* from the prospective area. However, I computed the $TRR_{sh\_oil\_well}$ and *RF* for three different values of d_s—50 ft, 500 ft, and 1,000 ft. Commonly used stage spacing in the Bakken, Eagle Ford and Permian as of 2016 ranged from 250 to 350 ft (EIA and IHS 2016). However, in practice, each stage consists of several clusters of hydraulic fractures, which I did not account for in my study. Furthermore, the stage spacing is expected to reduce in the future, as operators seek to maximize recoveries from a single lateral. Therefore, *RF* distributions assuming 50-ft spacing is expected to

be closer to the actual *RF* distributions compared to those assuming 500-ft or 1,000-ft spacings.

Table 3.3 lists the model-input parameters that were held constant and assumed to be common to all five formations. Other parameters, specific to each formation, are covered in later sections dedicated to the respective formations.

Table 3.3—Constant model-input parameters common to all five formations

Model parameter	**Value assigned**
Compressibility of shale (psi)	5×10^{-6}
Hydraulic-fracture spacing (ft)	50, 500, 1,000
Hydraulic-fracture conductivity (dimensionless)	100
Hydraulic-fracture half-length (ft)	500
Hydraulic-fracture cell-width (ft)	2
Oil gravity (^{o}API)	40
Gas specific gravity (Air = 1.0)	0.8
Water formation volume factor (RB/STB)	1.06
Water compressibility (psi)	3.7×10^{-6}
Water density (lb/ft^3)	59.2
Initial gas saturation S_{gi} (fraction)	0
Relative permeability to gas (k_{rg}) at irreducible oil saturation (S_{oirr})	1

The relative-permeability tables for the shale matrix are calculated using the model **(Table 3.4)** provided by Cullick et al. (2014).

Table 3.4—Relative-permeability parameters for shale matrix (Cullick et al. 2014)

Model parameter	**Value assigned**
Initial gas saturation (S_{gi})	0
Irreducible oil saturation (S_{oirr})	$0.863\times(1-S_{wi})$
Corey oil exponent (N_o)	3
Corey gas exponent (N_g)	3
Relative permeability to gas at S_{oirr} (k_{rg} at S_{oirr})	1

The relative-permeability tables for the hydraulic fractures were computed using values provided by Chaudhary (2011) **(Table 3.5)**.

Table 3.5—Relative-permeability parameters for hydraulic fractures (Chaudhary 2011)

Model parameter	Value assigned
Initial gas saturation (S_{gi})	0
Irreducible oil saturation (S_{oirr})	0.1
Corey oil exponent (N_o)	1.5
Corey gas exponent (N_g)	1
Relative permeability to gas at S_{oirr} (k_{rg} at S_{oirr})	1

CMOST (Computer Modelling Group Ltd. 2013a) was used to assign probability distributions to uncertain parameters such as porosity, permeability, connate water saturation and net pay based on parameter ranges from published literature. The parameter values for porosity, water saturation, and net pay were sampled from normal distributions and permeability from lognormal distributions with the 5th and 95th percentiles at the average lower and average upper limits of cited ranges. The details of the parameter distributions for each formation are given in later sections, dedicated to the respective formations. 990 simulations were run using the IMEX black oil simulator (Computer Modelling Group Ltd. 2013b) for each of the studied formations and the *RF* distributions were fitted using @RISK software (Palisade Corporation 2015).

3.4 Bakken

3.4.1 *Introduction*

The Upper Devonian-Lower Mississippian Bakken formation is a shale-oil resource located in the Williston basin of Montana and North Dakota **(Fig. 3.5)**. The

Williston basin, which was formed as an intracratonic depression on the North American craton, has an areal extent of around 300,000 sq mile covering portions of North and South Dakota, and Montana along with parts of Manitoba and Saskatchewan in Canada (Pollastro, Roberts, and Cook 2010). Despite sediment deposition having begun as early as the Cambrian, major basin subsidence and filling took place, starting from the Ordovician.

The Bakken formation, present within the central deeper portions of the Williston basin, is organic-rich and consists of siliciclastic rocks. EIA and INTEK (2011) estimated the US acreage of the Bakken play to be approximately 6,522 sq mile. It is sandwiched between the Devonian Three Fork and the Mississippian Lodgepole formations. The Bakken formation may be roughly delineated into three members:

- Lower shale member that consists of organic-rich black marine mudstone (primary source rock)
- Middle member with varying lithology—sandstone, siltstone, dolomite and mudstone
- Upper shale member that consists of organic-rich black marine mudstone (primary source rock)

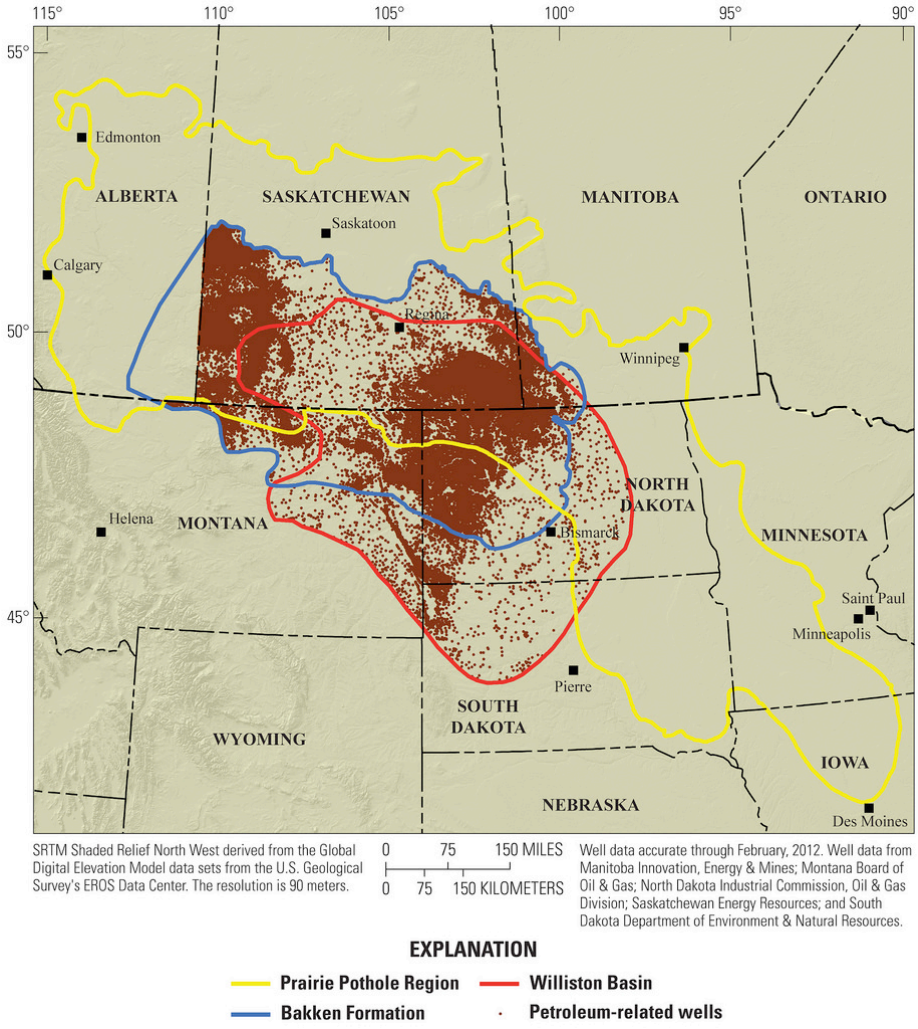

Fig. 3.5—Location of the Williston basin and the areal extent of the Bakken formation (Reprinted from Flickr (Plains and Prairies LLC 2013))

Production from upper Bakken started during the 1980s from several fields in North Dakota. However, horizontal drilling in the Bakken took off in 2000 at the Elm Coulee field and the rig count and daily production steadily increased until the drop in oil prices during late 2014 **(Fig. 3.6 and Fig. 3.7)**.

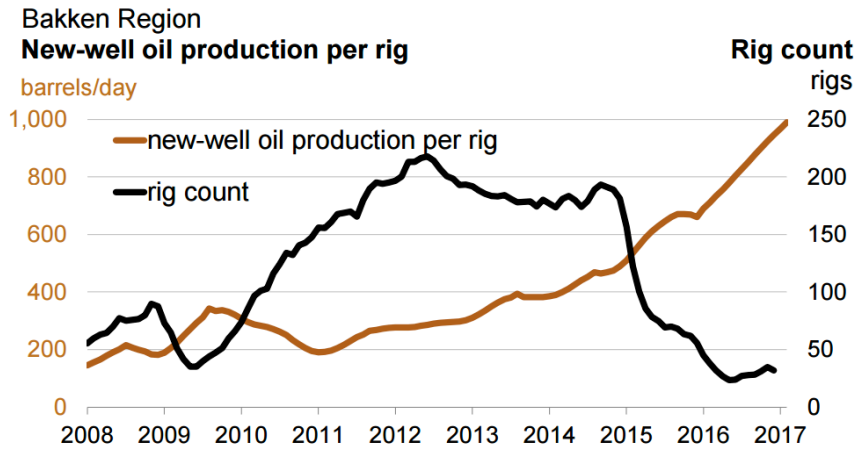

Fig. 3.6—Bakken rig-count trend (Reprinted from EIA (2017))

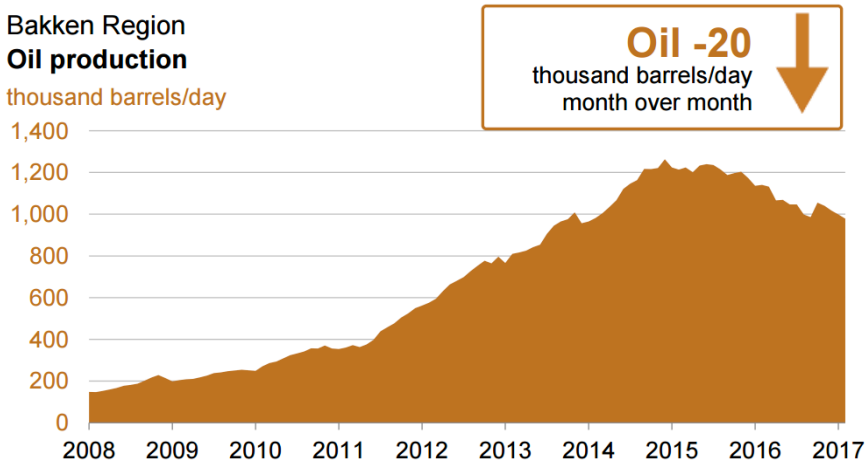

Fig. 3.7—Bakken average daily production trend (Reprinted from EIA (2017))

3.4.2 *Reservoir Properties*

The Bakken formation occurs at depths between 8,000 and 10,000 ft (Theloy and Sonnenberg 2012). It is moderately overpressured with pressure gradients ranging from 0.6 to 0.7 psi/ft (Sarg 2012). I assumed a constant depth of 9,500 ft along with a pressure gradient of 0.65 psi/ft, which were computed as the averages of the respective ranges. I

used a constant reservoir pressure of 6,190 psia in my model, which was computed from the assumed depth and pressure gradient. The reservoir temperature was calculated to be 226 ^{o}F based on the assumed depth and a calculated geothermal gradient of 0.0175 ^{o}F/ft (see Section 2.1.4). The *GOR* in formation is variable with values ranging from 400 scf/bbl reported in the Parshall field (Jarvie 2012) through 872 scf/bbl in the Sanish field (Jarvie 2012) to 1,230 scf/bbl in the Antelope field (LeFever and Nordeng 2015). I assumed a constant *GOR* of 834 scf/bbl, which is the average of the above three values. A summary of constant reservoir parameters values used is given in **Table 3.6**.

I compiled a list of published ranges **(Table 3.7)** for the uncertain parameters (net pay, porosity, water saturation and matrix permeability) for which values are sampled from probability distributions using CMOST.

Since the values for net pay, porosity and water saturation are sampled from normal distributions, the average of lower limits of the published ranges for each parameter was set as the 5th percentile ($P5_{normal}$) for the respective normal distributions.

$$P5_{normal} = \left(\frac{\sum_{i=1}^{n} low_i}{n_r} \right) \tag{28}$$

where low_i stands for the lower limits of each of the published ranges and n_r for the number of published ranges that are considered.

Similarly, the average of upper limits of the published ranges for each parameter was set as the 95th percentile ($P95_{normal}$) for the respective normal distributions.

$$P95_{normal} = \left(\frac{\sum_{i=1}^{n} high_i}{n_r} \right) \tag{29}$$

where $high_i$ stands for the upper limits of each of the published ranges and n_r for the number of published ranges that are considered.

Since the matrix permeability values are sampled from a lognormal distribution, the 5th percentile ($P5_{lognormal}$) value was computed as

$$P5_{lognormal} = \exp\left(\frac{\sum_{i=1}^{n} \ln low_i}{n_r} \right) \tag{30}$$

where low_i stands for the lower limits of each of the published ranges and n_r for the number of published ranges that are considered.

Similarly the 95th percentile ($P95_{lognormal}$) for the lognormal distribution was computed as

$$P95_{lognormal} = \exp\left(\frac{\sum_{i=1}^{n} \ln high_i}{n_r} \right) \tag{31}$$

where $high_i$ stands for the upper limits of each of the published ranges and n_r for the number of published ranges that are considered.

Table 3.6—List of constant reservoir parameters for the Bakken formation used in this study and their ranges cited in literature

Parameter	From published literature	Used in this study
Depth (ft)	8,000 to 11,000 (Theloy and Sonnenberg 2012)	9,500

Table 3.6 Continued

Pressure Gradient (psi/ft)	0.6 to 0.7 (Sarg 2012)	0.65
GOR (scf/bbl)	1,230 (LeFever and Nordeng 2015) 400 (Jarvie 2012) 872 (Jarvie 2012)	834
T_{res} (^{o}F)		226 (Calculated)

Table 3.7—List of uncertain parameters for the Bakken formation, their cited ranges and the ranges assumed in this study

Parameter	**Source**	**Range**		**Assumed range**	
		Upper limit	**Lower limit**	**P5**	**P95**
Net Pay (ft)	(Simenson, Sonnenberg, and Cluff 2011); Simenson (2010)	80	130	67.5	140
	Tran, Sinurat, and Wattenbarger (2011)	-	140		
	Beckwith (2013)	55	150		
Porosity (%)	Sarg (2012)	4	8	3.7	10.7
	Simenson, Sonnenberg, and Cluff (2011)	1	11		
	Cohen (2008)	8	12		
	Kieschnick and Suarez-Rivera (Dolomitic mudstone – dolomite members)	2.3	9.28		
	Kieschnick and Suarez-Rivera (Silty/Sandy mudstone – sandstone members)	3.32	13.26		
Permeability (md)	Sarg (2012)	0.001	0.15	0.00015	0.092
	Kieschnick and Suarez-Rivera (Dolomitic mudstone – dolomite members)	0.000021	0.001		
	Kieschnick and Suarez-Rivera (Silty/Sandy mudstone – sandstone members)	0.000135	1.2917		
	Tran, Sinurat, and Wattenbarger (2011)	0.0003	3.36		
	Kumar, Hoffman, and Prasad (2013)	0.0001	0.01		

Table 3.7 Continued

Parameter	Source	Range		Assumed range	
		Upper limit	Lower limit	P5	P95
Water Saturation (%)	Cohen (2008)	15	25	12.8	37.5
	Kieschnick and Suarez-Rivera (Dolomitic mudstone – dolomite members)	8.56	44.95		
	Kieschnick and Suarez-Rivera (Silty/Sandy mudstone – sandstone members)	2.47	30.16		
	Simenson (2010)	25	50		

3.4.3 *Results*

The resource distributions and recovery-factor distributions for a single stage during a 25-year well life (as explained in Section 3.3) were generated by simulating 990 instances using the input parameters given in Table 3.7. The resulting distributions for $OOIP_{sh\_oil\_well}$ and $TRR_{sh\_oil\_well}$ for d_s =50 ft are given in **Fig. 3.8** and **Fig. 3.9**, respectively. The *RF* distributions for d_s =50 ft, 500 ft and 1,000 ft are given in **Fig. 3.10**.

It is worth noting that the steep slopes of the *RF* distributions for 500-ft and 1,000-ft stage spacings indicate that the 50th and 95th *RF* percentiles are very close in value. This effect is attributable to the minimum-pressure constraint imposed on the well, due to which further recovery is limited. Furthermore, at 50-ft stage spacing, the *RF* distribution is very narrow, implying that the probability of obtaining a high *RF* (~8 to 9%) is very high, regardless of other input parameters.

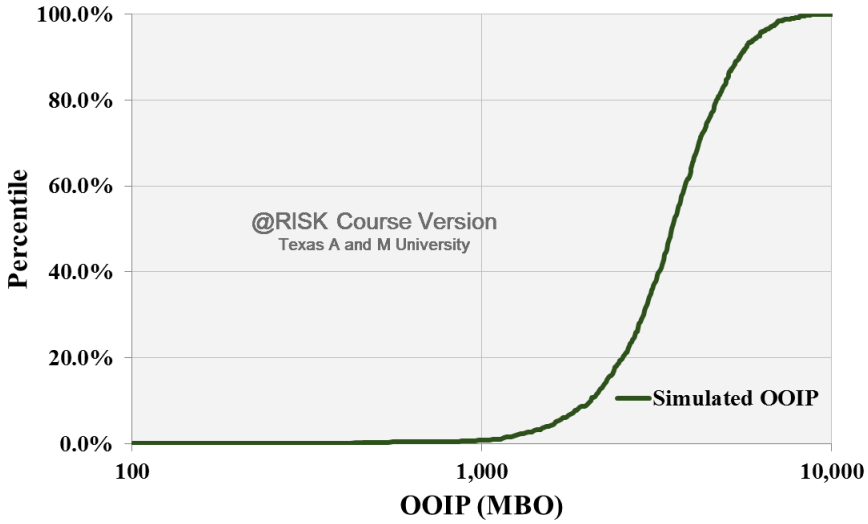

Fig. 3.8—*OOIP*$_{sh\_oil\_well}$ distribution for Bakken formation.

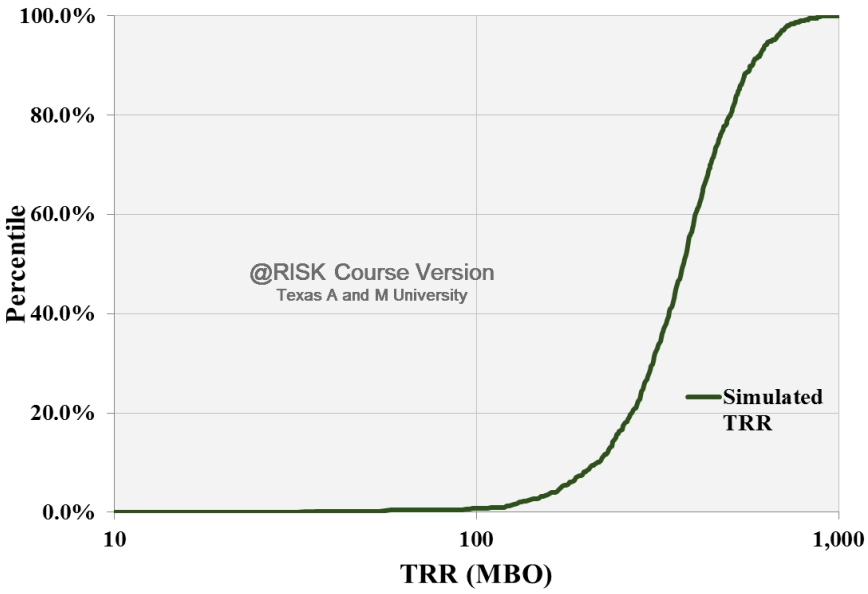

Fig. 3.9—*TRR*$_{sh\_oil\_well}$ distribution for Bakken formation for d_s = 50 ft.

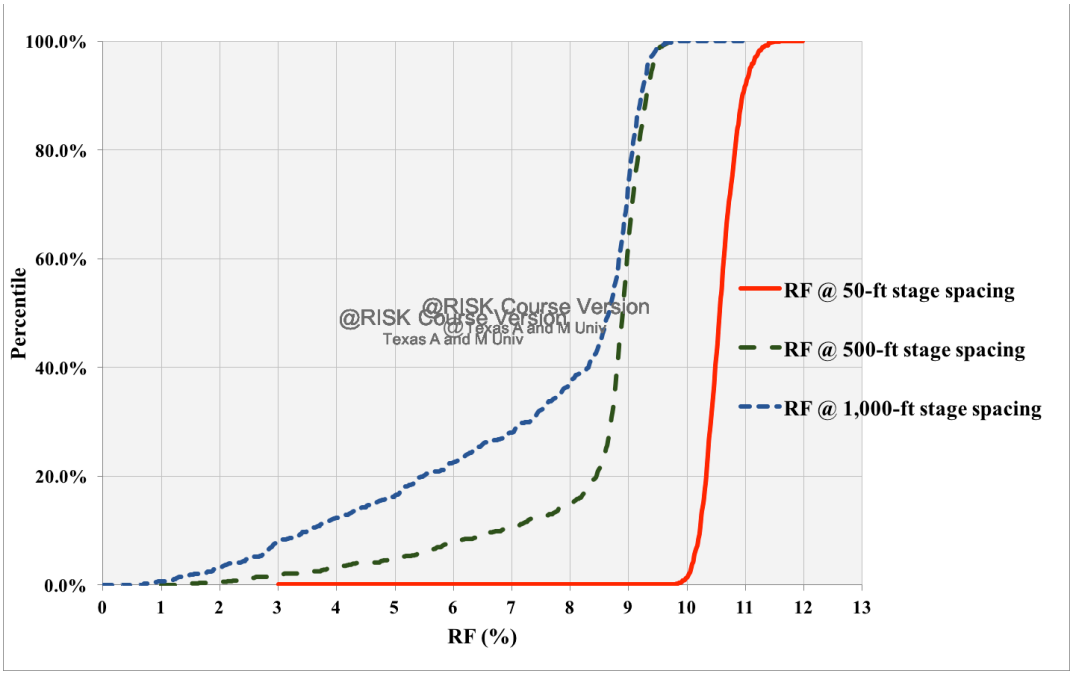

Fig. 3.10—*RF* distributions for the Bakken formation for d_s = 50 ft, 500 ft and 1,000 ft.

3.5 Eagle Ford

3.5.1 *Introduction*

The Cretaceous Eagle Ford formation is located in the Maverick basin in Texas and extends southward into the northeastern part of Mexico, occupying parts of the Sabinas and Burgos basins (Velasco 2013). From northwest to southeast, the Eagle Ford transitions from a black-oil to gas-condensate and ultimately to a dry-gas play (Tian, Ayers, and McCain Jr. 2013). EIA and INTEK (2011) estimated the areal extent of the oil window to be 2,233 sq mile.

The Eagle Ford formation overlies the Buda Limestone and is overlain by and acts as a source rock for the Austin Chalk. The formation may be broadly delineated into two units:

- The brittle and carbonate-rich Upper Eagle Ford
- The more ductile and shale- and TOC-rich Lower Eagle Ford

Eagle Ford lithology is dominated by calcite, accounting for 50 to 60% of the formation, followed by clay (20 to 30%) and quartz (5 to 10%). Therefore, the formation is most appropriately classified as muddy limestone rather than as shale (Weijermars et al. 2017).

Even though the Eagle Ford was initially developed as a gas play in 2008, the decline in gas prices and the then-prevalent high oil prices fueled its development as an oil play (Weijermars et al. 2017). Until early 2015, the Eagle Ford rig count and daily production had been increasing at a rapid rate, before taking a steep dip post the oil glut of the late 2014 **(Fig. 3.11 and Fig. 3.12)**.

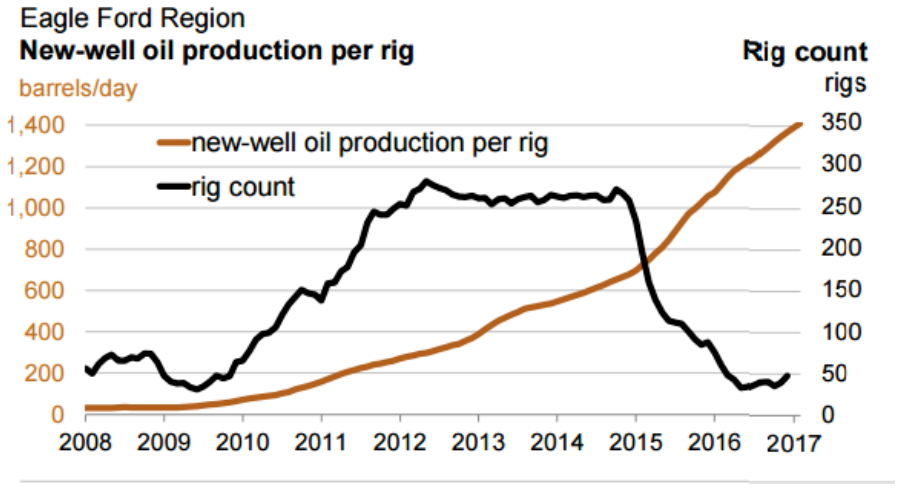

Fig. 3.11—Eagle Ford rig-count trend (Reprinted from EIA (2017))

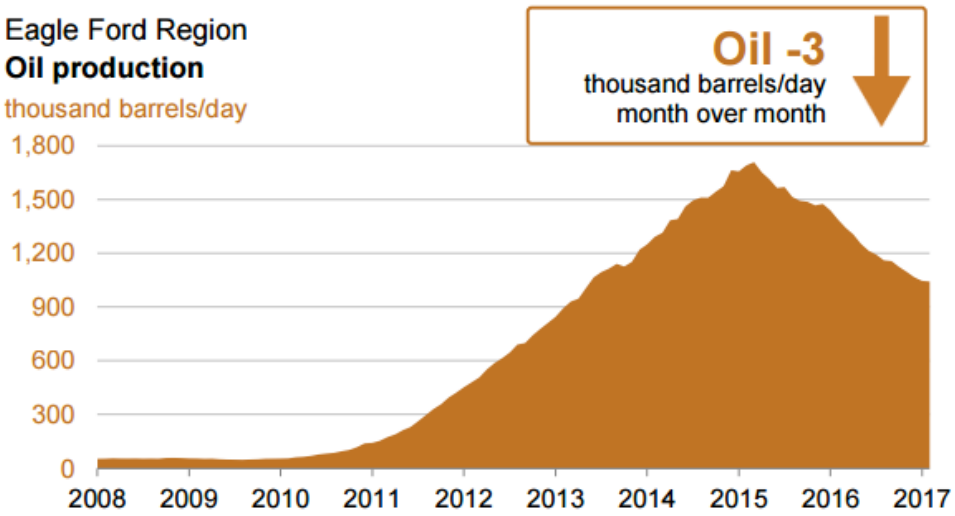

Fig. 3.12—Eagle Ford daily production trend (Reprinted from EIA (2017))

3.5.2 *Reservoir Properties*

The Eagle Ford formation occurs at depths between 5,000 and 11,500 ft (Amoss et al. 2011). It is a highly-overpressured formation with pressure gradients ranging from 0.66 to 0.82 psi/ft (Tian, Ayers, and McCain Jr. 2013). A constant depth of 8,250 ft was assumed along with a pressure gradient of 0.74 psi/ft, which were computed as the averages of the given ranges. I used a constant reservoir pressure of 6,120 psia that was computed from the assumed depth and pressure gradient. The reservoir temperature was calculated to be 204 ^{o}F, based on the assumed depth and a geothermal gradient of 0.0175 ^{o}F/ft (calculated in Section 2.1.4). The *GOR* in the formation ranges from 700 to 1,000 scf/bbl. I set the *GOR* constant at the average value of 850 scf/bbl. A summary of constant reservoir parameters values used is given in **Table 3.8**.

I compiled a list of published ranges **(Table 3.9)** for the uncertain parameters (net pay, porosity, water saturation and matrix permeability) and computed the P5 and P95 values for each distribution as explained in Section 3.4.

Table 3.8—List of constant reservoir parameters for the Eagle Ford formation used in this study and their ranges cited in literature

Parameter	From published literature	Used in this study
Depth (ft)	5,000 to 11,500 (Amoss et al. 2011)	8,250
Pressure Gradient (psi/ft)	0.66 to 0.82 (Tian, Ayers, and McCain Jr. 2013)	0.74
GOR (scf/bbl)	700 to 1,000 (Tian, Ayers, and McCain Jr. 2013)	850
T_{res} (^{o}F)		204 (Calculated)

Table 3.9—List of uncertain parameter for the Eagle Ford formation, their cited ranges and the ranges assumed in this study

Parameter	Source	Range		Assumed range	
		Lower limit	Upper limit	P5	P95
Net Pay (ft)	Smith et al. (2013)	79	131	137	301
	Cerón, Walls, and Diaz (2013)	256	328		
	Cho et al. (2016)	50	300		
	Beckwith (2013)	200	300		
	Wust, Cui, and Nassichuk (2014)	98	295		
	Amoss et al. (2011)	140	450		
Porosity (%)	Walls et al. (2011)	2	16	5.9	12.9
	Smith et al. (2013)	7	15		
	Mullen (2010)	5	14		
	Schlumberger (2012)	6	10		
	Mendoza, Aular, and Sousa (2011)	9	12		
	Amoss et al. (2011)	6	9		
Permeability (md)	Walls et al. (2011)	0.0000001	0.001	0.000023	0.00065
	Cerón, Walls, and Diaz (2013)	-	0.001		
	Schlumberger (2012)	0.0002	0.0006		

Table 3.9 Continued

Parameter	Source	Range		Assumed range	
		Lower limit	Upper limit	P5	P95
	Amoss et al. (2011)	0.0007	0.002		
	Lalehrokh and Bouma (2014)	0.00002	0.0001		
Water Saturation (%)	Amoss et al. (2011)	13.0	25.0	13.0	25.0

3.5.3 *Results*

The resource distributions and recovery-factor distributions for a single stage during a 25-year well life (as explained in Section 3.3) were generated by simulating 990 instances using the input parameters given in Table 3.9. The resulting distributions for $OOIP_{sh\_oil\_well}$ and $TRR_{sh\_oil\_well}$ for d_s =50 ft are given in **Fig. 3.13 and Fig. 3.14**. The *RF* distributions for d_s =50 ft, 500 ft and 1,000 ft are given in **Fig. 3.15**.

In the case of 500-ft and 1,000-ft stage spacing, the *RF* distribution is not as steep as it is in the case of the Bakken. This may be due to the lower permeability in the Eagle Ford, compared to the Bakken. However, at 50-ft stage spacing, the Eagle Ford offers maximum *RF* subject to the minimum-pressure constraint, regardless of variations in other input parameters.

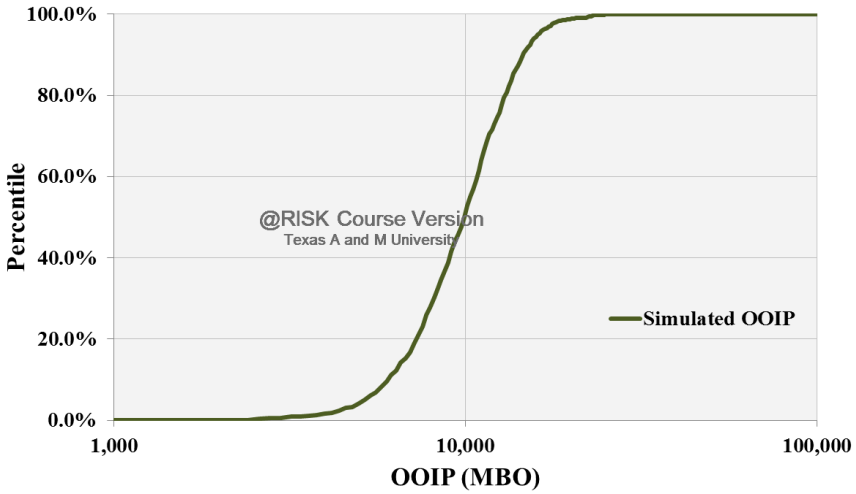

Fig. 3.13—*OOIP*$_{sh\_oil\_well}$ distribution for Eagle Ford formation.

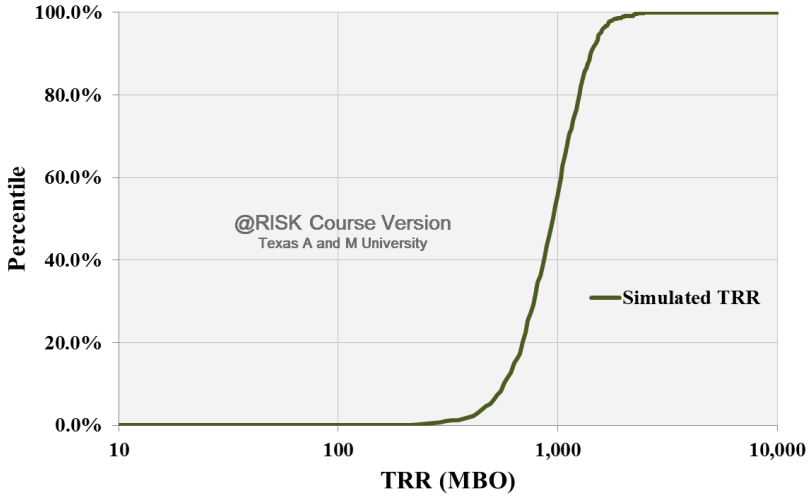

Fig. 3.14—*TRR*$_{sh\_oil\_well}$ distribution for Eagle Ford formation for d_s = 50 ft

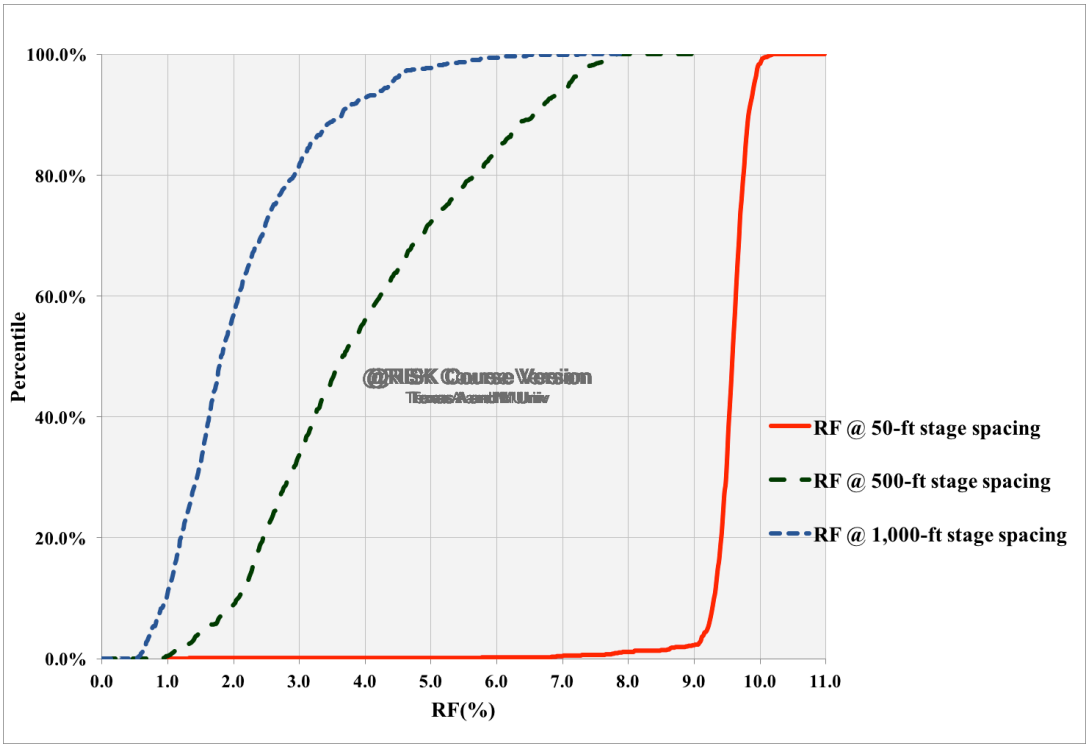

Fig. 3.15—*RF* distributions for the Eagle Ford formation for d_s = 50 ft, 500 ft and 1,000 ft.

3.6 Niobrara

3.6.1 *Introduction*

The Upper Cretaceous Niobrara formation is present throughout the Central Rocky Mountain region **(Fig. 3.16)** and is predominantly composed of chalk, marl and calcareous shale. In this study, I focused on the Niobrara formation in the Denver-Julesberg basin—a large asymmetric basin formed during the Laramide Orogeny. The areal extent of the Niobrara formation has been placed at 14,000 sq mile (Kennedy, Luo, and Kusskra 2016).The chalk units are considered the reservoir rocks, which are sourced from high-TOC marls (Sonnenberg 2016). The Niobrara shale overlies unconformably

on the Carlile shale and is overlain by the Pierre shale. The Niobrara formation is currently productive in the Wattenberg field of Colorado (Cho et al. 2016). The rig count and daily production trends in the Niobrara region are shown in **Fig. 3.17 and Fig. 3.18**.

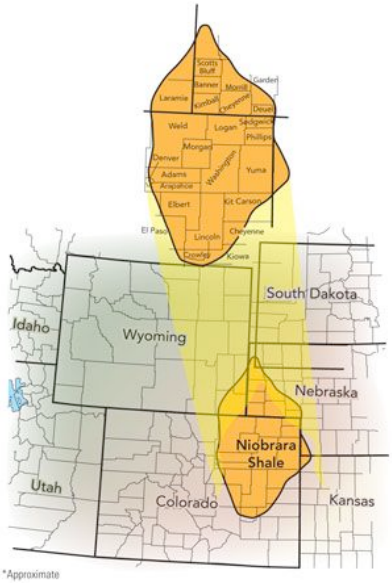

Fig. 3.16—Niobrara shale map (Source: Oil and Gas Financial Journal (2016)) (Reprinted with the permission of Oil and Gas Financial Journal)

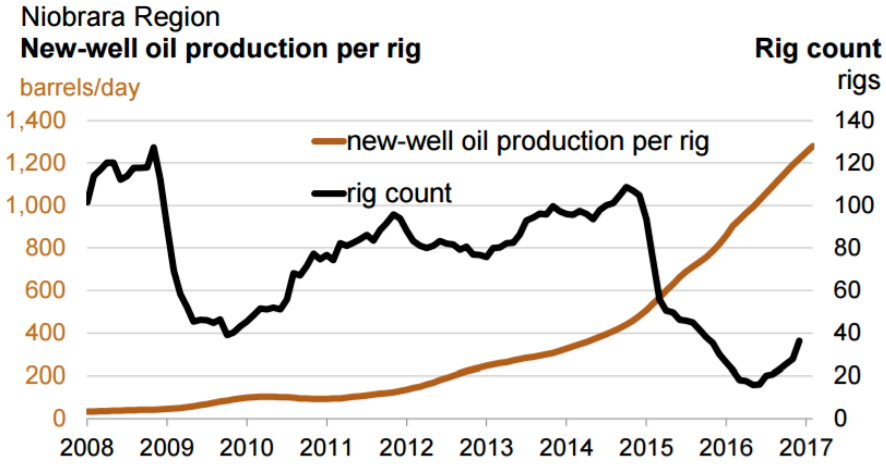

Fig. 3.17—Niobrara rig-count trend (Reprinted from EIA (2017))

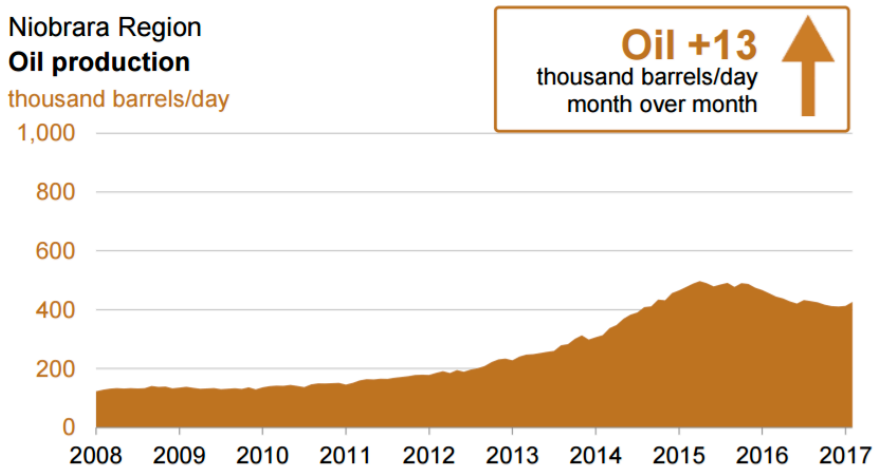

Fig. 3.18—Niobrara daily production trend (Reprinted from EIA (2017))

3.6.2 *Reservoir Properties*

The Niobrara formation occurs at an average depth of 8,000 ft (Sonnenberg 2012). Since it is normally pressured (EIA and ARI 2013), I assumed an average pressure gradient of 0.45 psi/ft, based on the pressure categorization given in Table 2.5. I used a constant reservoir pressure of 3,614 psia, computed from the average depth and pressure gradient. The reservoir temperature was calculated to be 200 ^{o}F based on the assumed depth and a geothermal gradient of 0.0175 ^{o}F/ft (calculated in Section 2.1.4). Various sources cite different ranges for *GOR*s such as 656 to 1,730 scf/bbl (Jarvie 2012) and 300 to 900 scf/bbl (Dyman and Condon 2005; Finn and Johnson 2005). In this study, I set the *GOR* for the formation constant at a value of 897 scf/bbl, which was computed as the average of the above ranges. A summary of constant reservoir parameters values used is given in **Table 3.10**.

I compiled a list of published ranges **(Table 3.11)** for the uncertain parameters (net pay, porosity, water saturation and matrix permeability) and computed the P5 and

P95 values for each distribution as explained in Section 3.4. It is to be noted that I used published ranges from Niobrara formations in other basins (Greater Green River and Powder Basins) for want of publicly-available data on uncertain parameters in the Denver-Julesberg basin.

Table 3.10—List of constant reservoir parameters for the Niobrara formation used in this study and their ranges cited in literature

Parameter	From published literature	Used in this study
Depth (ft)	8,000 (Sonnenberg 2012)	8,000
Pressure Gradient (psi/ft)	0.45 (EIA and ARI 2013)	0.45
GOR (scf/bbl)	656 to 1,730 (Jarvie 2012) 300 to 900 (Dyman and Condon 2005; Finn and Johnson 2005)	897
T_{res} (^{o}F)		200 (Calculated)

Table 3.11—List of uncertain parameter for the Niobrara formation, their cited ranges and the ranges assumed in this study

Parameter	Source	Range		Assumed range	
		Lower limit	Upper limit	P5	P95
Net Pay (ft)	Hovey (2011)	300	600	270	800
	Hovey (2011) (Greater Green River Basin)	900	1,800		
	Drillinginfo (2012)	50	600		
	Anna (2010)	50	600		
	Finn and Johnson (2005)	50	400		
Porosity (%)	Matthies (2014)	-	10	6.6	10.8
	Hovey (2011)	8	10		
	Hovey (2011) (Greater Green River Basin)	4	14		
	Hovey (2011) (Powder River Basin)	5.5	7.5		

Table 3.11 Continued

Parameter	Source	Range		Assumed range	
		Lower limit	Upper limit	P5	P95
	Sonnenberg (2012)	8	10		
	Drillinginfo (2012)	8	10		
	Sonnenberg and Taylor	8	10		
	Welker, Stright, and Anderson (2013)	5	15		
Permeability (md)	Ford et al. (2012)	0.0065	0.3	0.0065	0.144
	Matthies (2014)	-	0.1		
	Hovey (2011)	-	3		
	Hovey (2011) (Greater Green River Basin)	-	0.1		
	Sonnenberg and Taylor	-	0.01		
	Sonnenberg (2012)	-	0.1		
Water Saturation (%)	Anna (2010)	29	49	29	49

3.6.3 *Results*

The resource distributions and recovery-factor distributions for a single stage during a 25-year well life (as explained in Section 3.3) were generated by simulating 990 instances using the input parameters given in Table 3.11. The resulting distributions for $OOIP_{sh\_oil\_well}$ and $TRR_{sh\_oil\_well}$ for d_s =50 ft are given in **Fig. 3.19 and Fig. 3.20**. The *RF* distributions for d_s =50 ft, 500 ft and 1,000 ft are given in **Fig. 3.21**. The *RF*s obtained are much lower compared to the Bakken and Eagle Ford, due to low initial reservoir pressure and comparatively higher water saturation.

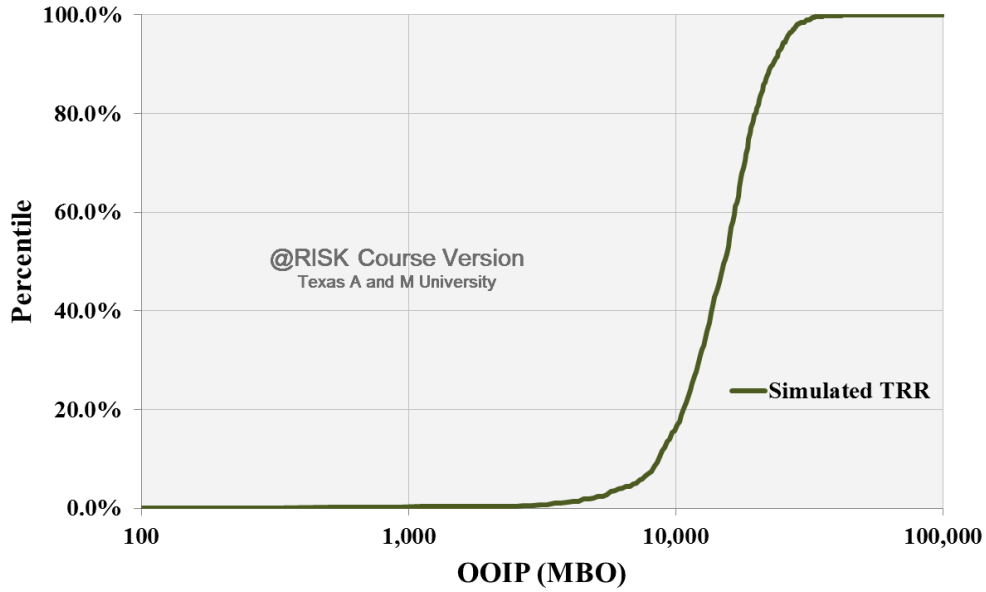

Fig. 3.19—*OOIP*$_{sh\_oil\_well}$ distribution for Niobrara formation.

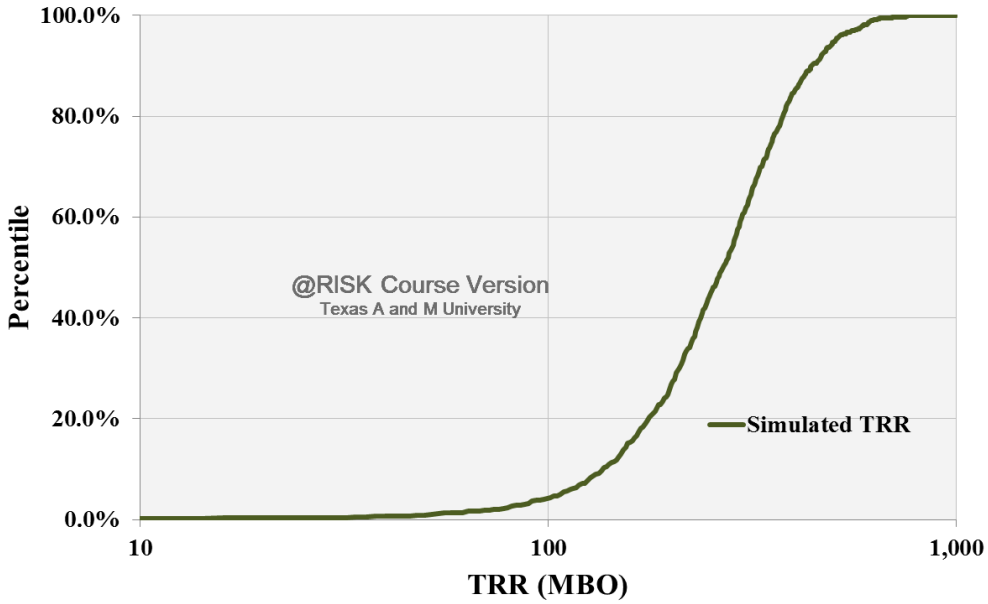

Fig. 3.20—*TRR*$_{sh\_oil\_well}$ distribution for Niobrara formation for d_s = 50 ft.

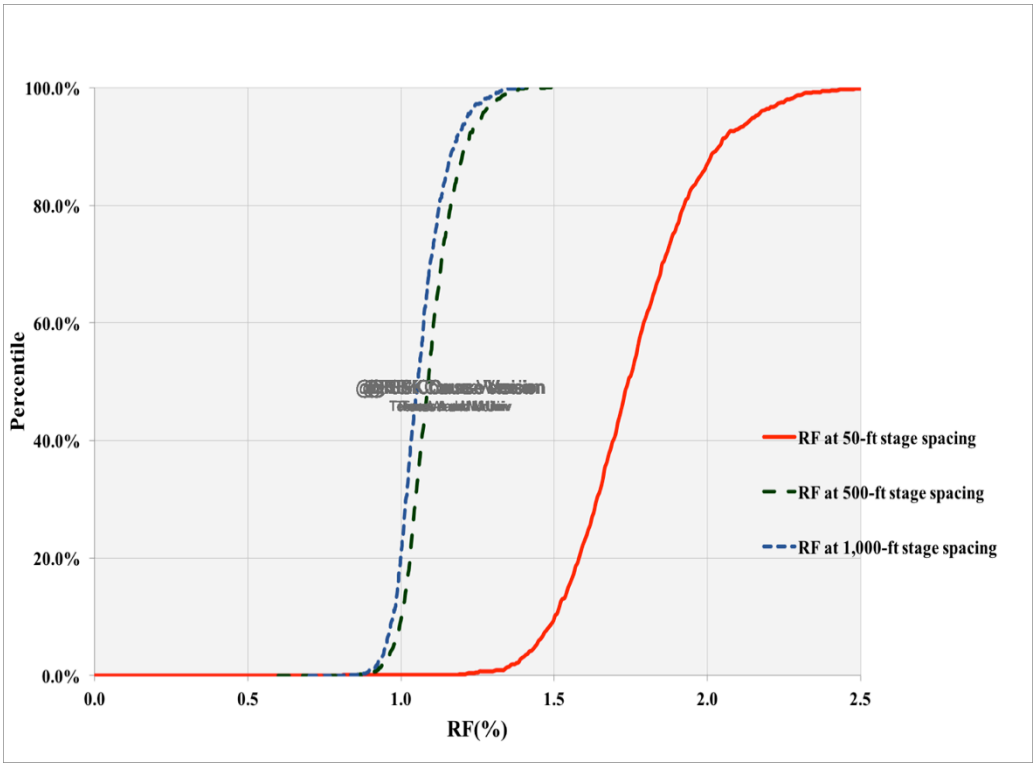

Fig. 3.21—*RF* distributions for the Niobrara formation for d_s = 50 ft, 500 ft and 1,000 ft.

3.7 Avalon

3.7.1 *Introduction*

The Lower Permian Avalon shale of the Delaware sub-basin (within the Permian Basin) covers parts of southeast New Mexico and west Texas **(Fig. 3.22)**. It consists of organic-rich siliciclastic mudstones interbedded with fine-grained carbonate strata. It is worth mentioning that the Avalon shale refers to a target interval for hydrocarbon exploration within the first Bone Spring carbonate formation rather than a formal stratigraphic unit. It has also been referred to as the Leonard shale depending on locations (Stolz 2014).

The Avalon shale has been delineated into three intervals:

- Mud-rich Lower Avalon
- Carbonate-rich Middle Avalon
- Mud-rich Upper Avalon

EIA and INTEK (2011) estimated the areal extent of the Avalon shale to be approximately 1,313 sq mile. The rig count and daily production in the Permian region are shown in **Fig. 3.23 and Fig. 3.24**.

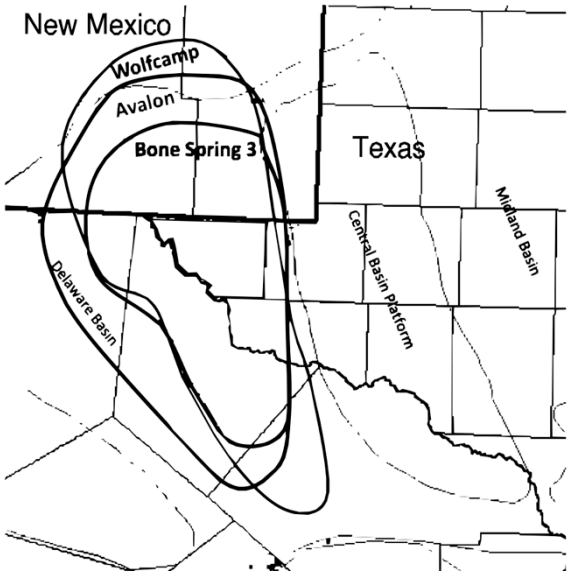

Fig. 3.22—Avalon shale map (Adapted from Royal Dutch Shell (2012))

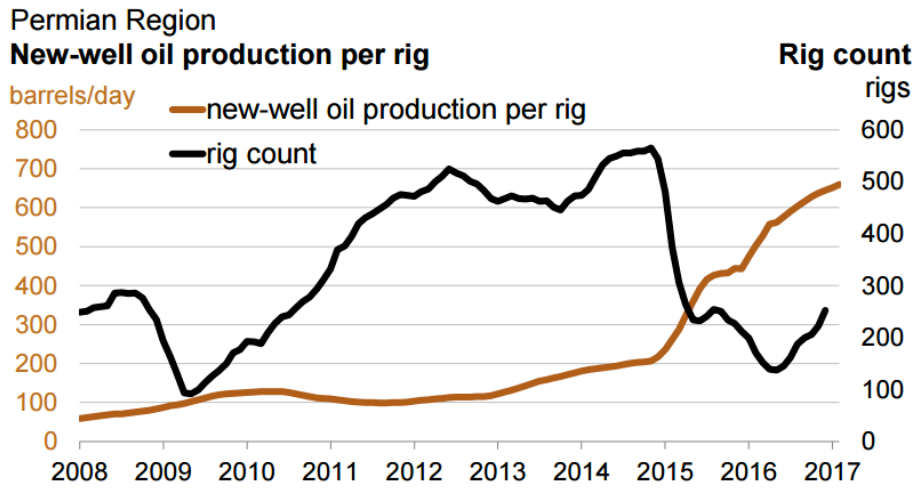

Fig. 3.23—Permian region rig-count trend (Reprinted from EIA (2017)). The shown trend is not limited to a particular formation. It is indicative of drilling activity within the entire Permian region.

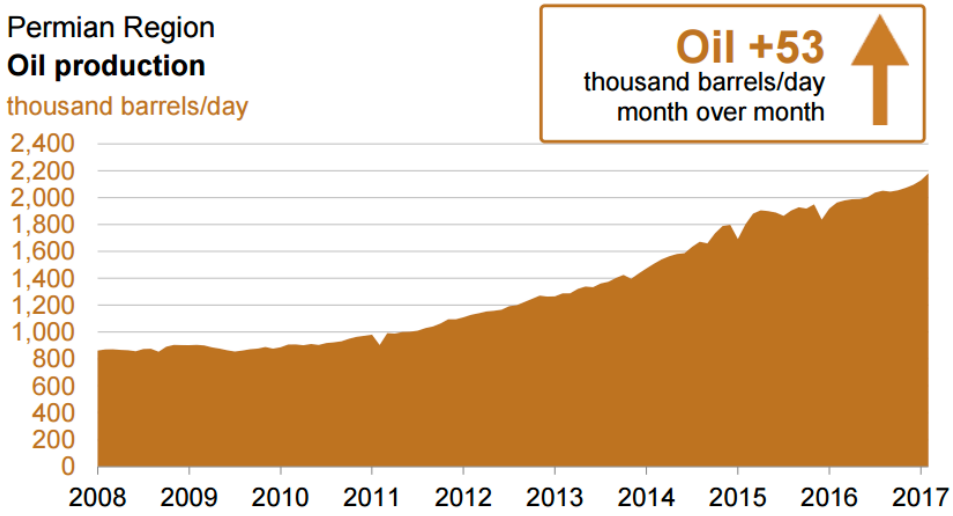

Fig. 3.24—Permian region daily production trend (Reprinted from EIA (2017)). The shown trend is not limited to a particular formation. It is indicative of drilling activity within the entire Permian region.

3.7.2 *Reservoir Properties*

The Avalon formation occurs at depths between 6,500 and 9,500 ft (Kelly et al. 2012). Since it is slightly overpressured (EIA and ARI 2013), I assumed a pressure gradient of 0.55 psi/ft, based on the pressure categorization given in Table 2.5. I used a constant reservoir pressure of 4,277 psia, computed from an assumed depth of 7,750 ft (computed as the average of the given range) and the assumed pressure gradient. The reservoir temperature was calculated to be 196 ^{o}F based on the assumed depth and a geothermal gradient of 0.0175 ^{o}F/ft (calculated in Section 2.1.4). The *GOR* ranges from 1,000 to 2,500 scf/bbl (Apache Corporation 2013) and a constant value of 1,750 scf/bbl was used in the study. A summary of constant reservoir parameters values used is given in **Table 3.12**.

I compiled a list of published ranges (**Table 3.13**) for the uncertain parameters (net pay, porosity and matrix permeability) and computed the P5 and P95 values for each distribution as explained in Section 3.4. However, I was not able to find published ranges on water saturation in the Avalon formation. Therefore, the upper and lower limits on porosity and water saturation in the Bakken, Eagle Ford and Niobrara formations (computed in Table 3.7, Table 3.9 and Table 3.11) were used to regress a linear relationship between upper and lower porosity limits and the corresponding water saturation limits **(Fig. 3.25)**. This relationship, given by S_w=2.6752×ϕ+0.0515, was used to calculate the upper and lower limits on water saturation in the Avalon shale from the corresponding limits on porosity.

Table 3.12—List of constant reservoir parameters for the Avalon formation used in this study and their ranges cited in literature

Parameter	From published literature	Used in this study
Depth (ft)	6,500 to 9,000 (Kelly et al. 2012)	7,750
Pressure Gradient (psi/ft)	0.55 (EIA and ARI 2013)	0.55
GOR (scf/bbl)	1,000 to 2,500 (Apache Corporation 2013)	1,750
T_{res} (^{o}F)		196 (Calculated)

Table 3.13—List of uncertain parameter for the Avalon formation, their cited ranges and the ranges assumed in this study

Parameter	Source	Range		Assumed range	
		Lower limit	Upper limit	P5	P95
Net Pay (ft)	Stolz, Franseen, and Goldstein (2015)	900	1,700	900	1,150
	Menchaca (2013)	-	600		
Porosity (%)	Stolz, Franseen, and Goldstein (2015)	1	16	8.5	17.0
	Menchaca (2013)	16	18		
Permeability (md)	Stolz, Franseen, and Goldstein (2015)	0.00001	0.001	0.00001	0.01
	Menchaca (2013)	-	0.1		
Water Saturation (%)	-	-	-	27.0 (Extrapolated)	49.8 (Extrapolated)

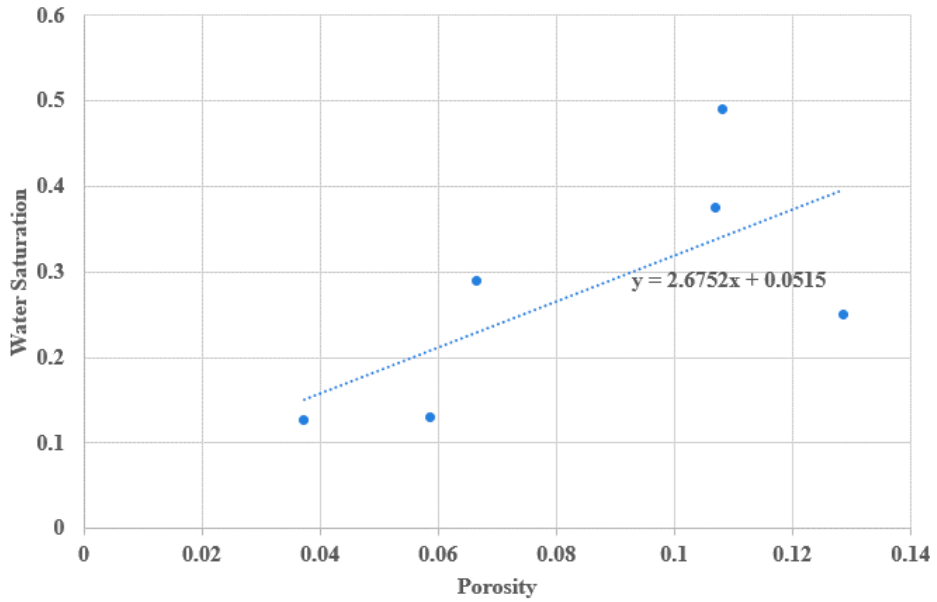

Fig. 3.25—Upper and lower limits on porosity and water saturation for three formations used to regress a linear relationship between porosity and water saturation.

3.7.3 *Results*

The resource distributions and recovery-factor distributions for a single stage during a 25-year well life (as explained in Section 3.3) were generated by simulating 990 instances using the input parameters given in Table 3.13. The resulting distributions for $OOIP_{sh\_oil\_well}$ and $TRR_{sh\_oil\_well}$ for d_s =50 ft are given in **Fig. 3.26 and Fig. 3.27**. The *RF* distributions for d_s =50 ft, 500 ft and 1,000 ft are given in **Fig. 3.28**. Similar to the Niobrara, the *RF*s obtained in the Avalon are much lower compared to the Bakken and the Eagle Ford, due to comparatively high water saturation and *GOR*.

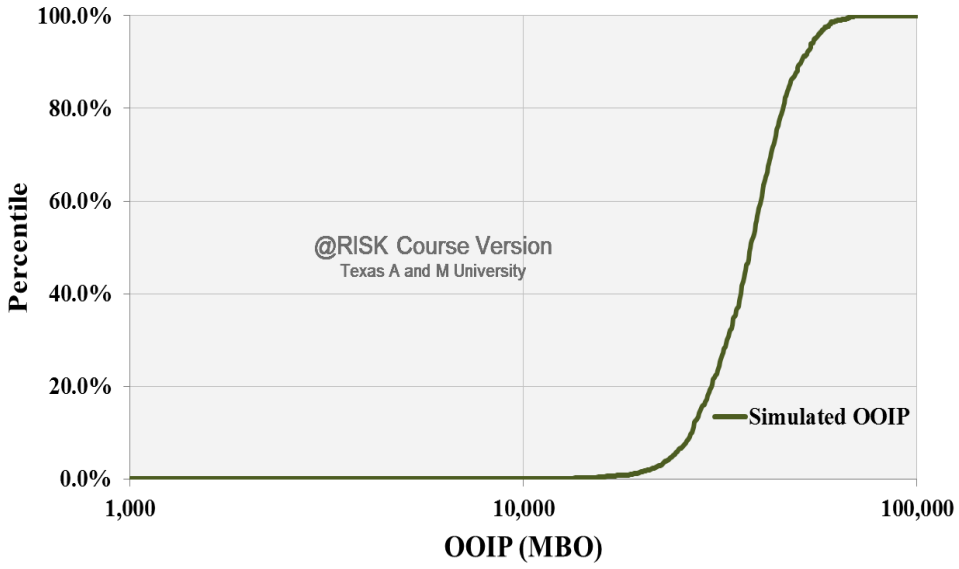

Fig. 3.26—*OOIP*$_{sh\_oil\_well}$ distribution for Avalon formation.

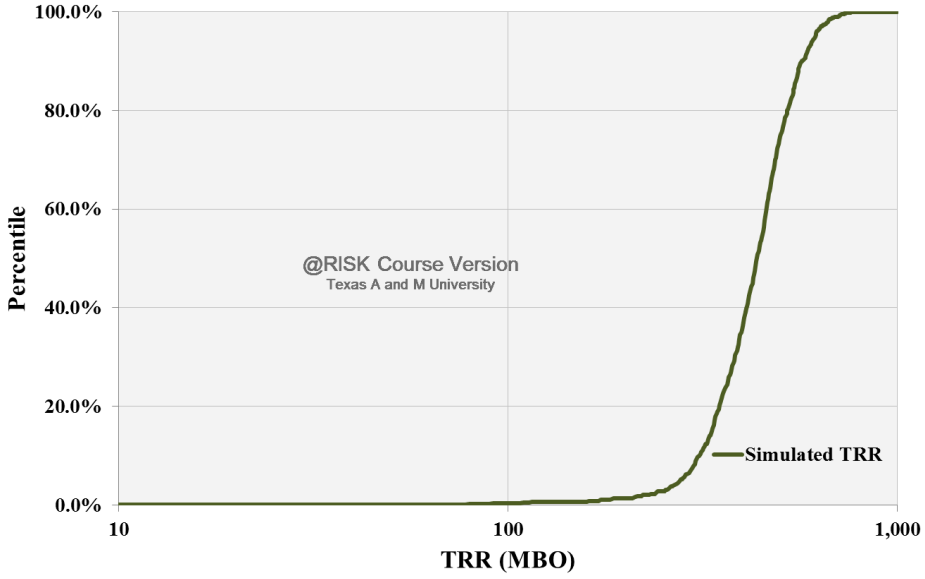

Fig. 3.27—*TRR*$_{sh\_oil\_well}$ distribution for Avalon formation for d_s = 50 ft.

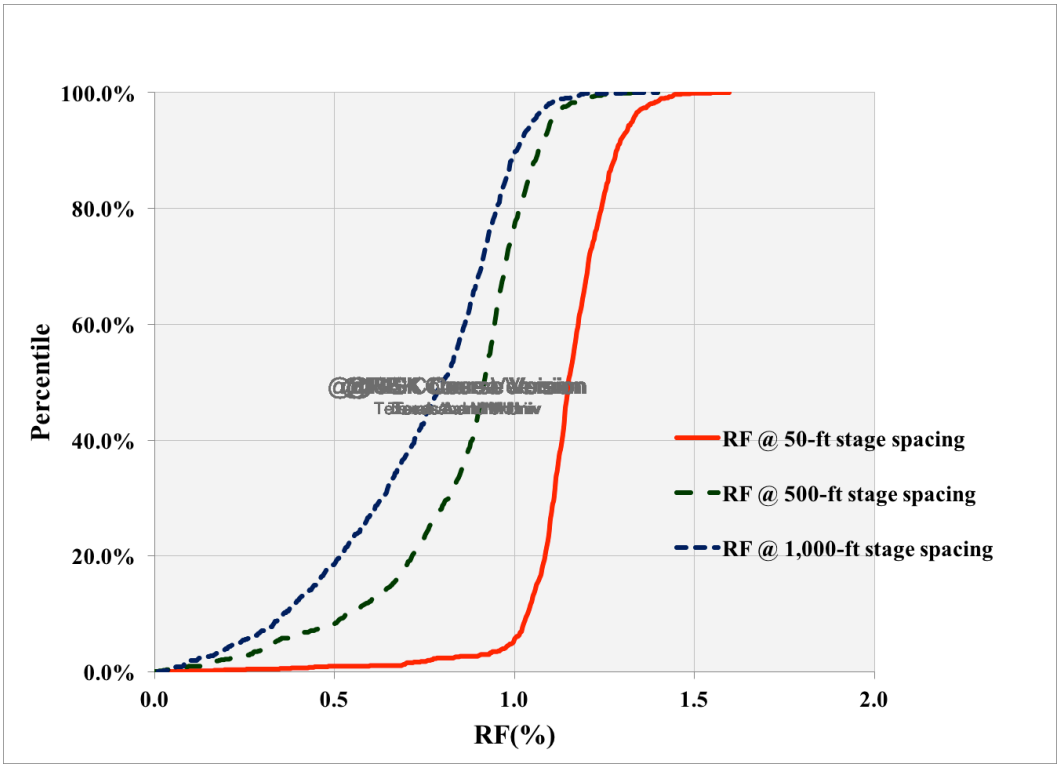

Fig. 3.28—*RF* distributions for the Avalon formation for d_s = 50 ft, 500 ft and 1,000 ft.

3.8 Wolfcamp

3.8.1 *Introduction*

The Pennsylvanian-Permian Wolfcamp shale in the Midland sub-basin (of the Permian Basin) is located in west Texas **(Fig. 3.29)** and has been an active target for hydrocarbon exploration in the Permian, with over 3,000 horizontal wells drilled to date. The formation consists of interbedded fine-grained organic-rich siliciclastic muds along with organic-poor clay-rich mud and fine-grained carbonates (USGS 2016).

The shale has been divided into four stratigraphic units—Wolfcamp A, B, C and D, based on log signatures as well as drilling practices.

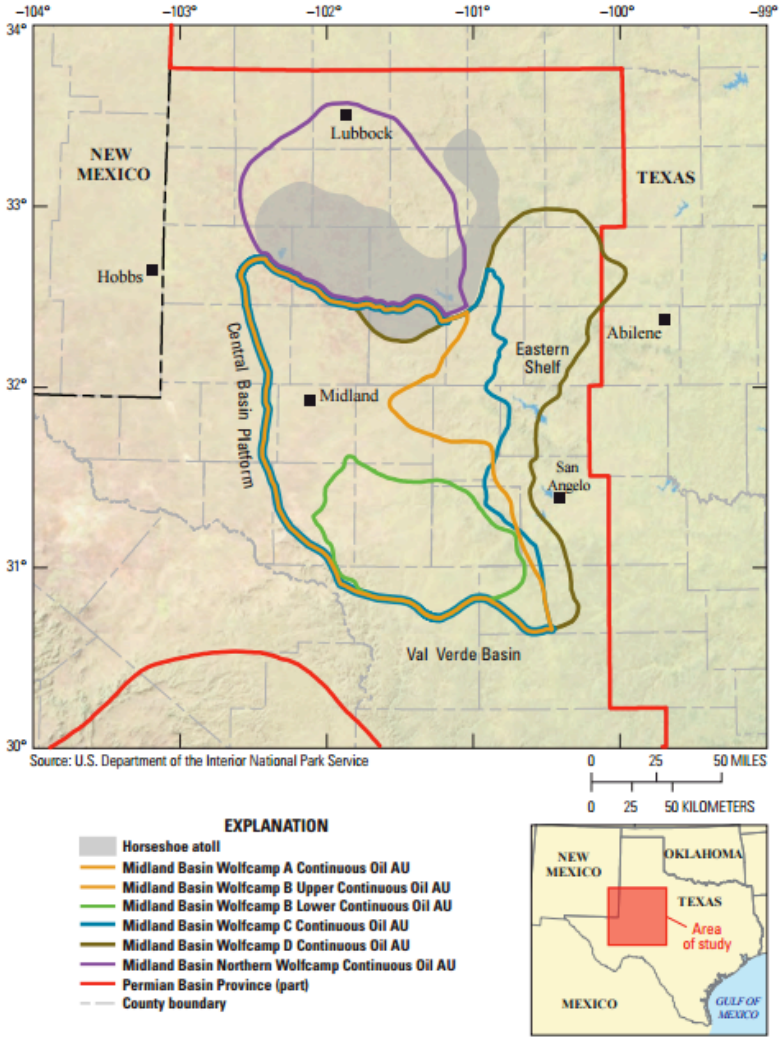

Fig. 3.29—Wolfcamp shale map (Reprinted from USGS (2016))

3.8.2 *Reservoir Properties*

The Wolfcamp formation occurs at depths between 5,800 and 7,000 ft (Kelly et al. 2012). The pressure gradient in the region is around 0.7 psi/ft (Menchaca 2013). I used a constant reservoir pressure of 4,495 psia, computed from an assumed depth of 6,400 ft and the given pressure gradient. The reservoir temperature was calculated to be 172 ^{o}F based on the assumed depth and a geothermal gradient of 0.0175 ^{o}F/ft (calculated

in Section 2.1.4). The *GOR* averages around 800 scf/bbl (Scott 2014). A summary of constant reservoir parameters values used is given in **Table 3.14**.

I compiled a list of published ranges **(Table 3.15)** for the uncertain parameters (net pay, porosity and matrix permeability) and computed the P5 and P95 values for each distribution as explained in Section 3.4. However, as with Avalon shale, I was not able to find published ranges on water saturation. Therefore, the regressed linear relationship obtained in Section 3.7 was used to compute the upper and lower limits on water saturation from the respective limits on porosity (Fig. 3.25).

Table 3.14—List of constant reservoir parameters for the Wolfcamp formation used in this study and their ranges cited in literature

Parameter	From published literature	Used in this study
Depth (ft)	5,800 to 7,000 (Kelly et al. 2012)	6,400
Pressure Gradient (psi/ft)	0.7 (Menchaca 2013)	0.7
GOR (scf/bbl)	800 (Scott 2014)	800
T_{res} (^{o}F)		172 (Calculated)

Table 3.15—List of uncertain parameter for the Wolfcamp formation, their cited ranges and the ranges assumed in this study

Parameter	Source	Range		Assumed range	
		Lower limit	Upper limit	P5	P95
Net Pay (ft)	Kelly et al. (2012)	544	680	722	926.7
	Pettegrew, Qiu, and Zhan (2016)	-	1,000		
	www.wolfcamp-shale.com (2014)	900	1,100		
Porosity (%)	Kelly et al. (2012)	9.4	12	5.5	11.3

Table 3.15 Continued

Parameter	Source	Range		Assumed range	
		Lower limit	Upper limit	P5	P95
	www.wolfcamp-shale.com (2014)	4	12		
	Walls and Morcote-Rios (2015)	3	14		
	Nutech Energy	7.5	11		
	OGJ (2013)	4	10		
	Menchaca (2013)	5	9		
Permeability (md)	www.wolfcamp-shale.com (2014)	-	1	0.0001	0.023
	Walls and Morcote-Rios (2015)	0.00002	0.008		
	Pettegrew, Qiu, and Zhan (2016)	0.00058	0.00155		
Water Saturation (%)	-	-	-	19.2	34.2

3.8.3 *Results*

The resource distributions and recovery-factor distributions for a single stage during a 25-year well life (as explained in Section 3.3) were generated by simulating 990 instances using the input parameters given in Table 3.15. The resulting distributions for $OOIP_{sh\_oil\_well}$ and $TRR_{sh\_oil\_well}$ for d_s =50 ft are given in **Fig. 3.30 and Fig. 3.31**. The *RF* distributions for d_s =50 ft, 500 ft and 1,000 ft are given in **Fig. 3.32**. The Wolfcamp formation offers favorable *RF*s between 6% and 7% in the case of 50-ft stage spacing. However the *RF*s are lower than those in the Bakken and the Eagle Ford, possibly due to a lower initial reservoir pressure.

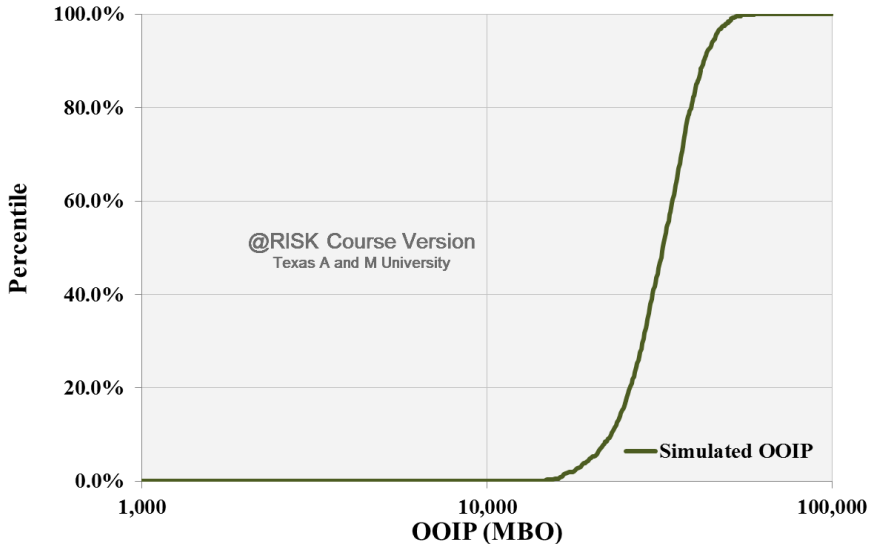

Fig. 3.30—*OOIP*$_{sh\_oil\_well}$ distribution for Wolfcamp formation.

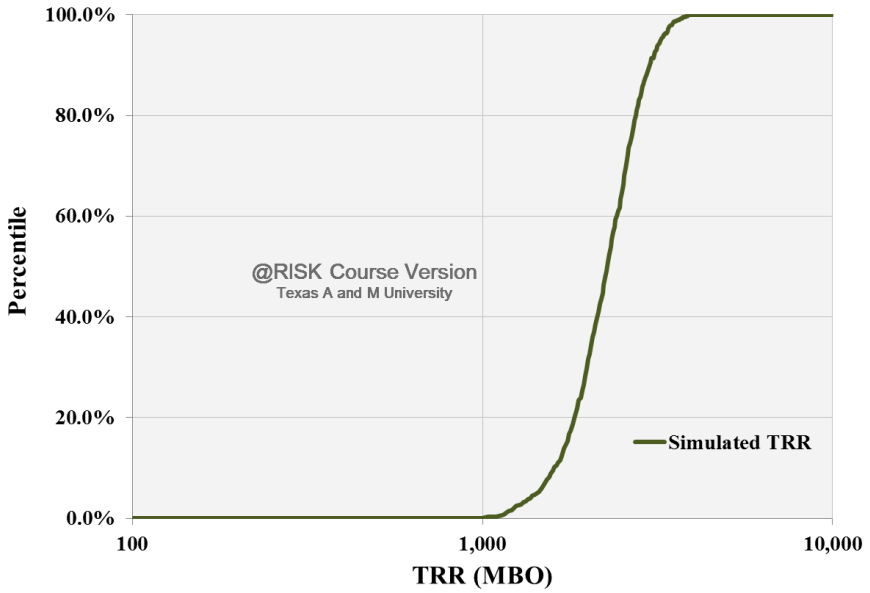

Fig. 3.31—*TRR*$_{sh\_oil\_well}$ distribution for Wolfcamp formation for d_s = 50 ft.

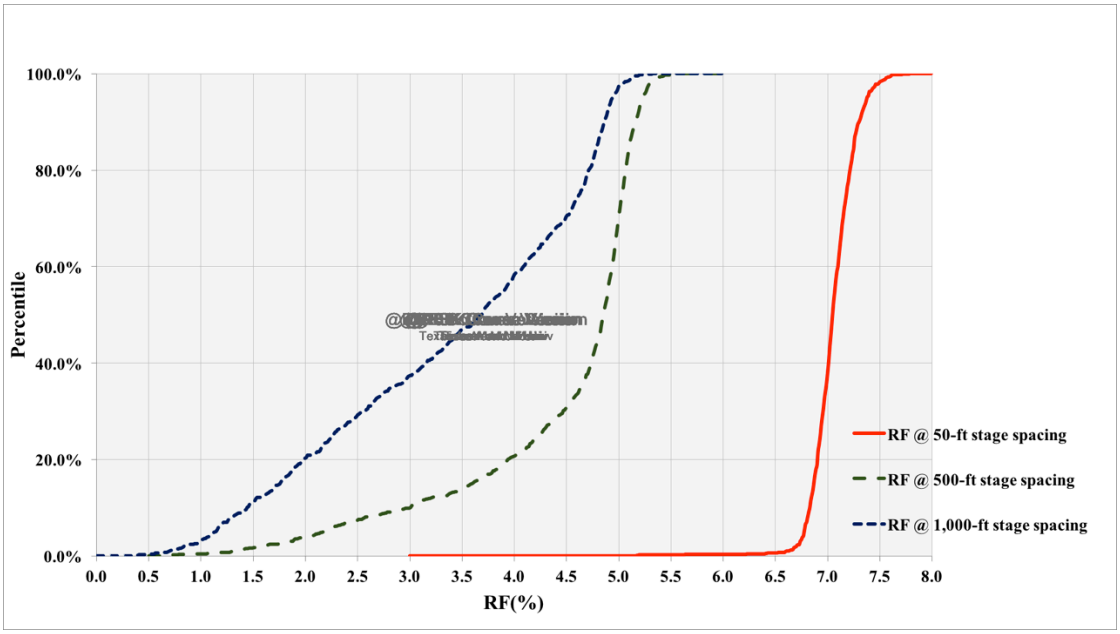

Fig. 3.32—*RF* distributions for the Wolfcamp formation for d_s = 50 ft, 500 ft and 1,000 ft.

3.9 Synthesis of Generalized-*RF* Distributions

The results of my simulation study of five US shale-oil formations are summarized in **Table 3.16**. The Bakken, Eagle Ford and Wolfcamp formations offer favorable recovery factors greater than 5% when a stage spacing of 50 ft is used. This may be attributed to high initial reservoir pressures, low *GOR*s and low water saturations in these formations. Based on the five formations considered here, I computed generalized-*RF* distributions for production from shale-oil formations to establish the formation-wise TRR_{sh_oil} for each of the 93 formations studied, and subsequently, the region-wise and total TRR_{sh_oil} (covered in Section 4). Generalized-*RF* distributions were computed for each value of stage spacing by assigning equal weights to all 4,950 instances of *RF* from the five formations and fitting an appropriate cumulative probability distribution using

@RISK software. The best-fit distribution for the three stage spacings are given in **Table 3.17** and the respective fits are plotted in **Fig 3.33 to Fig. 3.35**.

Table 3.16—Summary of model inputs and resulting $OOIP_{sh\_oil\_well}$, $TRR_{sh\_oil\_well}$ and *RF* distributions for five US formations

	Formations				
Parameter	**Bakken**	**Eagle Ford**	**Avalon**	**Wolfcamp**	**Niobrara**
Depth assumed (ft)	9,500	8,250	7,750	6,400	8,000
Initial P_{res} (psi)	6,190	6,120	4,277	4,495	3,614
GOR assumed (scf/bbl)	834	850	1,750	800	896
T_{res} (^{o}F)	226	204	196	172	200
Net Pay (P5) (ft)	67.5	137.2	900	722	270
Net Pay (P95) (ft)	140	300.7	1,150	926.7	800
Porosity (P5) (%)	3.7	5.8	8.5	5.5	6.6
Porosity (P95) (%)	10.7	12.8	17.0	11.3	10.8
Permeability (P5) (md)	0.00015	0.000023	0.00001	0.0001	0.0064
Permeability (P95) (md)	0.0092	0.00065	0.01	0.023	0.144
Water Saturation (P5) (%)	12.8	13.0	27.0	19.2	29.0
Water Saturation (P95) (%)	37.5	25.0	48.8	34.25	49.0
$OOIP_{sh\_oil\_well}$ (P5) (1,000 MBO)	1.6	5.3	24.2	20.2	7.3
$OOIP_{sh\_oil\_well}$ (P50) (1,000 MBO)	3.50	10.1	37.9	32.5	15.4
$OOIP_{sh\_oil\_well}$ (P95) (1,000 MBO)	6.23	16.3	55.1	46.0	26.1

Table 3.16 Continued

	Formations				
Parameter	**Bakken**	**Eagle Ford**	**Avalon**	**Wolfcamp**	**Niobrara**
$TRR_{sh\_oil\_well}$ (d_s = 50 ft) (P5) (MBO)	173.1	503.3	279.4	1,448.1	108.1
$TRR_{sh\_oil\_well}$ (d_s = 50 ft) (P50) (MBO)	374.3	968.1	437.0	2,290.1	269.7
$TRR_{sh\_oil\_well}$ (d_s = 50 ft) (P95) (MBO)	656.2	1,581.9	617.8	3,245.9	507.7
RF (d_s = 50 ft) (P5) (%)	10.1	9.2	1.0	6.8	1.4
RF (d_s = 50 ft) (P50) (%)	10.6	9.6	1.2	7.1	1.7
RF (d_s = 50 ft) (P95) (%)	11.1	9.9	1.3	7.4	2.2
RF (d_s = 500 ft) (P5) (%)	5.0	1.6	0.3	2.2	1.0
RF (d_s = 500 ft) (P50) (%)	8.9	3.7	0.9	4.9	1.1
RF (d_s = 500 ft) (P95) (%)	9.4	7.1	1.1	5.2	1.3
RF (d_s = 1,000 ft) (P5) (%)	2.6	0.8	0.2	1.1	1.0
RF (d_s = 1,000 ft) (P50) (%)	8.7	1.8	0.8	3.7	1.1
RF (d_s = 1,000 ft) (P95) (%)	9.3	4.4	1.1	5.0	1.2

Table 3.17—Generalized-*RF* distributions for each case of stage spacing considered

Stage spacing (ft)	**Best-fit CDF form**
50	Uniform
500	Triangular
1,000	Gamma

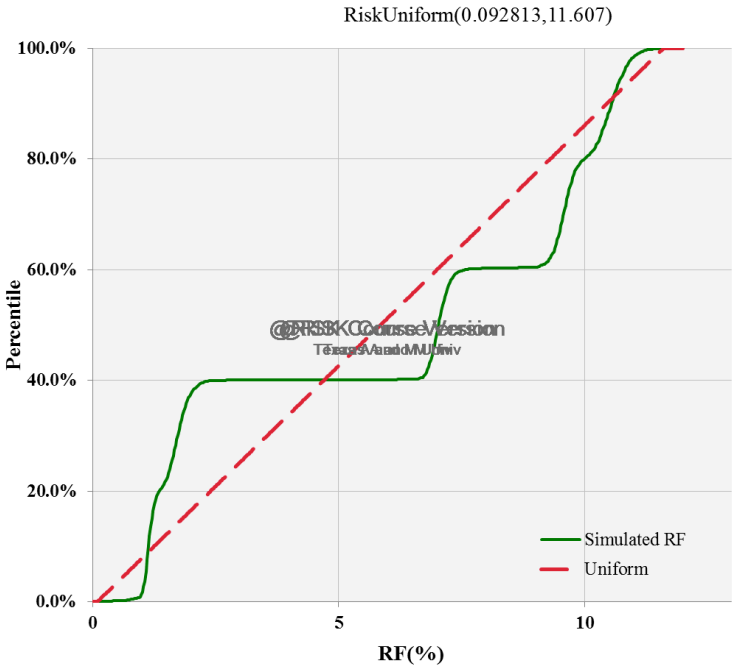

Fig. 3.33—Generalized-*RF* distribution fit for d_s = 50 ft

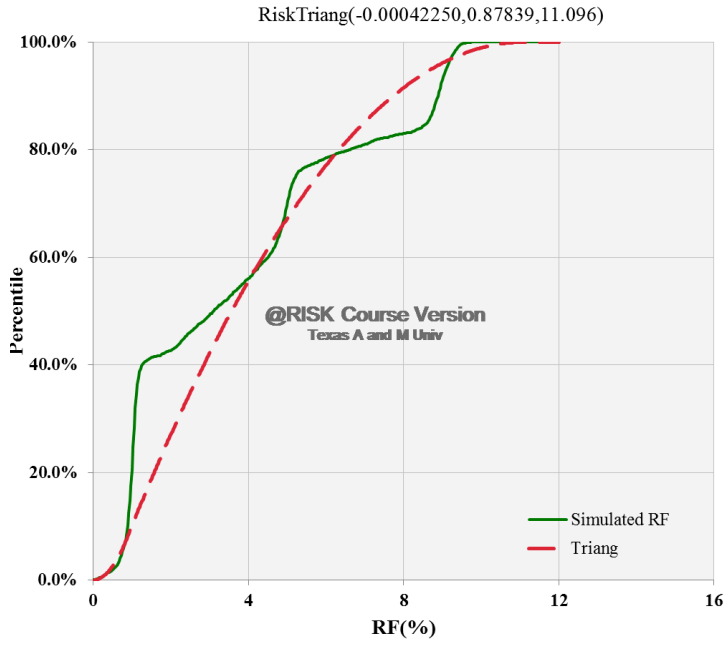

Fig. 3.34—Generalized-*RF* distribution fit for d_s = 500 ft

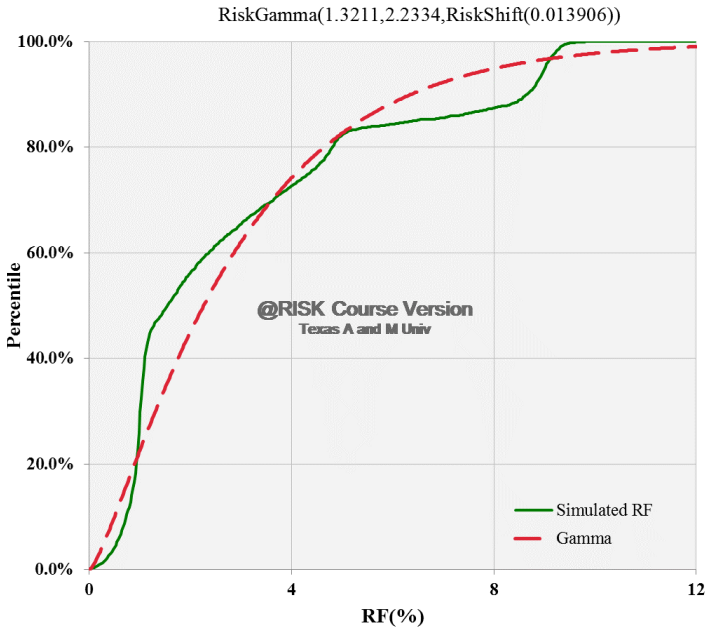

Fig. 3.35—Generalized-*RF* distribution fit for d_s = 1,000 ft

4. ASSESSMENT OF REGION-WISE AND TOTAL TECHNICALLY-RECOVERABLE SHALE-OIL RESOURCES

In this section, I apply the generalized-*RF* distributions computed in Section 3 to the $OOIP_{sh\_oil}$ distributions from Section 2 to establish the region-wise and total TRR_{sh_oil} distributions. This was done by using Monte Carlo simulation wherein randomly-sampled values from the *RF* distributions and the $OOIP_{sh\_oil}$ distributions for each formation are multiplied together to establish the TRR_{sh_oil} distribution for each of the 93 formations. @RISK software was used for generating the TRR_{sh_oil} distribution by means of Latin Hypercube sampling from input distributions. Subsequently, the resulting formation-wise resource distributions were aggregated statistically and arithmetically (as explained in Section 2.2) to establish the region-wise and total TRR_{sh_oil} estimates.

In Section 4.1, I cover the region-wise results following statistical and arithmetic aggregation of formation-wise TRR_{sh_oil} for all three cases of stage spacing considered. In Section 4.2, I compute the total TRR_{sh_oil} via statistical and arithmetical aggregation of TRR_{sh_oil} from individual formations, for each value of stage spacing. In Section 4.3, I compare my results to prior assessments of shale-oil resources.

4.1 Region-wise Results

A comparison of the region-wise TRR_{sh_oil} distributions obtained via statistical aggregation **(Fig. 4.1 to Fig. 4.3)** with those obtained via arithmetic aggregation **(Fig. 4.4 to Fig. 4.6)** highlights not only the high uncertainty in both estimates but also the wider spread of arithmetically-aggregated estimates for each stage spacing considered.

The degree of uncertainty, indicated by P90/P10, ranges from 13 to 44 in case of statistical aggregation **(Table 4.1 to Table 4.3)** and from 64 to 697 in case of arithmetic aggregation **(Table 4.4 to Table 4.6).**

As with $OOIP_{sh\_oil}$ estimates, the amount of uncertainty associated with TRR_{sh_oil} in NAM and CIS are considerably lower than other regions for all stage spacings considered (Table 4.1 to Table 4.6). AAO and LAM also seem to show comparatively lower degrees of uncertainty, using statistical aggregation (Table 4.1 to Table 4.3).

A high degree of uncertainty is observed in AFR using both arithmetic and statistical aggregation, since the P90 estimates are consistently very high (Table 4.1 to Table 4.6). This is due to the presence of a number of formations with large prospective area and highly uncertain net pay, which results in high P90/P10 for individual formations as well as the AFR aggregate.

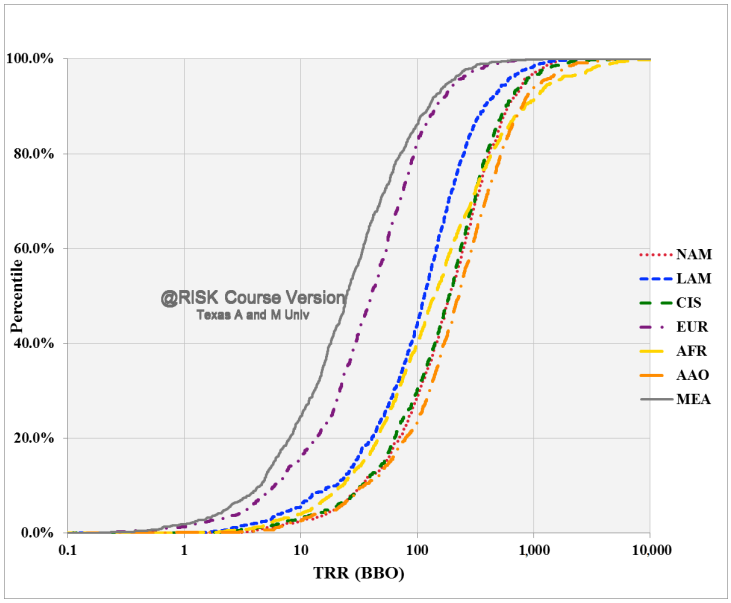

Fig. 4.1—Statistically-aggregated region-wise TRR_{sh_oil} distributions for d_s = 50 ft

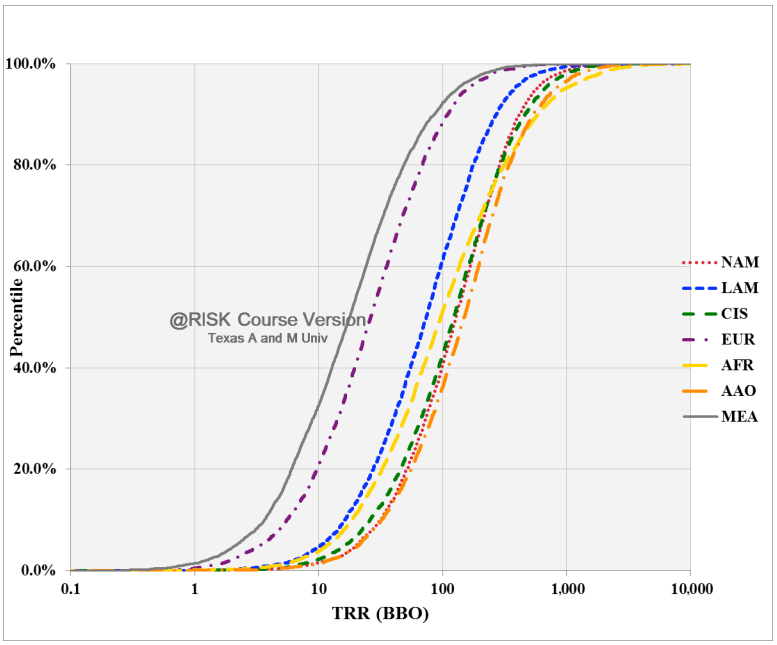

Fig. 4.2—Statistically-aggregated region-wise TRR_{sh_oil} distributions for d_s = 500 ft

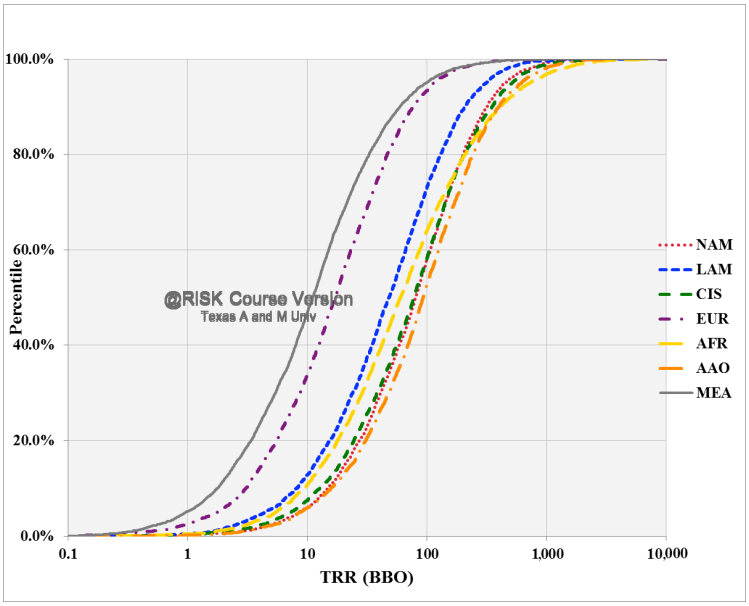

Fig. 4.3—Statistically-aggregated region-wise TRR_{sh_oil} for d_s = 1,000 ft

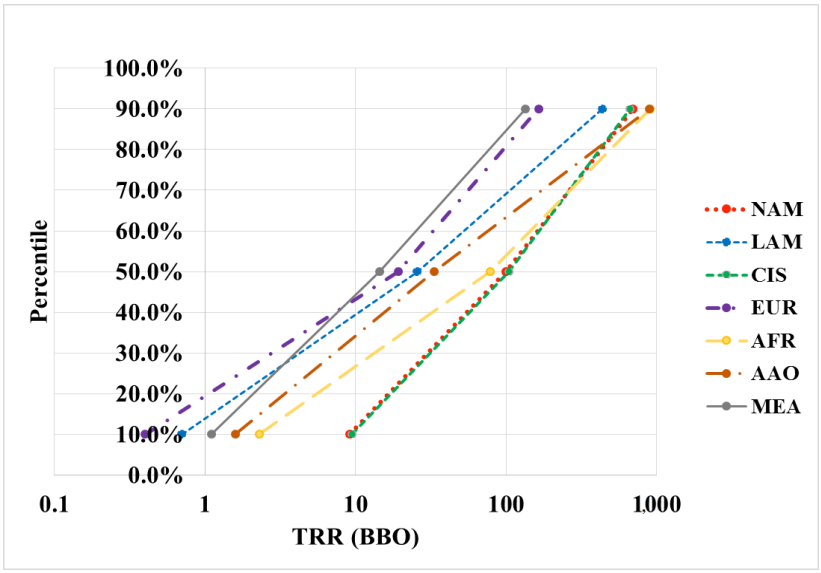

Fig. 4.4—Arithmetically-aggregated region-wise TRR_{sh_oil} P10-P50-P90 estimates for d_s = 50 ft

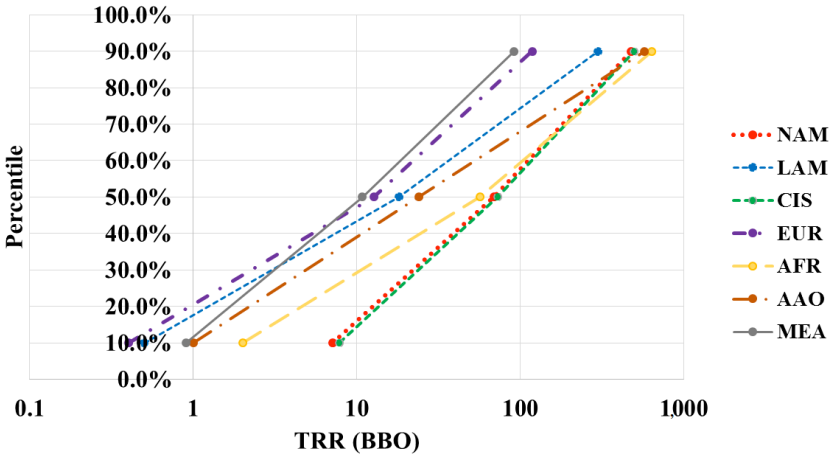

Fig. 4.5—Arithmetically-aggregated region-wise TRR_{sh_oil} P10-P50-P90 estimates for d_s = 500 ft

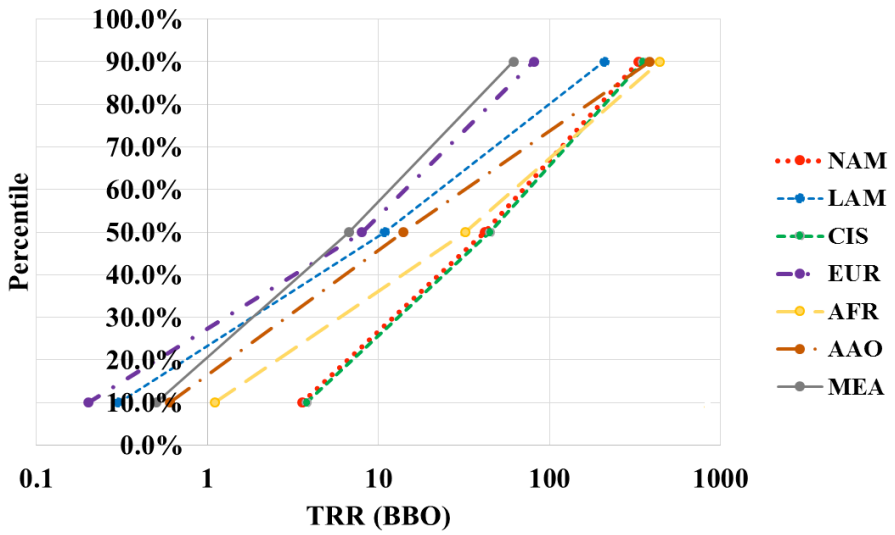

Fig. 4.6—Arithmetically-aggregated region-wise TRR_{sh_oil} P10-P50-P90 estimates for d_s = 1,000 ft

Table 4.1—TRR_{sh_oil} for d_s = 50 ft (BBO) (Statistically Aggregated)

	This study				EIA and ARI (2013)	McGlade (2012)		
Region	**P10**	**P50**	**P90**	**P90/P10**		**Low**	**Central**	**High**
NAM	33.3	189.1	605.7	18	93.7	36	57	136
LAM	20.1	115.1	377.9	19	47.9	42	45	54
CIS	33.6	187.0	576.9	17	84.7	3	42	95
EUR	5.9	39.7	143.9	24	10.7	19	21	25
AFR	22.3	140.8	833.7	37	44.6	35	38	46
AAO	34.4	227.6	799.4	23	65.3	14	53	109
MEA	4.5	24.6	126.4	28	28.8	3	21	45

Table 4.2—TRR_{sh_oil} for d_s = 500 ft (BBO) (Statistically Aggregated)

	This study				EIA and ARI (2013)	McGlade (2012)		
Region	**P10**	**P50**	**P90**	**P90/P10**		**Low**	**Central**	**High**
NAM	31.5	128.4	418.7	13	93.7	36	57	136
LAM	16.3	73.9	271.3	17	47.9	42	45	54
CIS	25.9	123.2	460.4	18	84.7	3	42	95

Table 4.2 Continued

	This study				EIA and ARI (2013)	McGlade (2012)		
Region	**P10**	**P50**	**P90**	**P90/P10**		**Low**	**Central**	**High**
EUR	5.5	26.3	109.0	20	10.7	19	21	25
AFR	18.5	96.7	584.9	32	44.6	35	38	46
AAO	32.1	149.6	544.3	17	65.3	14	53	109
MEA	3.7	17.8	85.6	23	28.8	3	21	45

Table 4.3—TRR_{sh_oil} for d_s = 1,000 ft (BBO) (Statistically Aggregated)

	This study				EIA and ARI (2013)	McGlade (2012)		
Region	**P10**	**P50**	**P90**	**P90/P10**		**Low**	**Central**	**High**
NAM	14.9	80.0	316.3	21	93.7	36	57	136
LAM	8.1	48.0	206.5	26	47.9	42	45	54
CIS	12.7	77.3	349.0	28	84.7	3	42	95
EUR	3.0	17.0	76.0	25	10.7	19	21	25
AFR	9.4	60.0	409.9	44	44.6	35	38	46
AAO	15.7	92.7	394.8	25	65.3	14	53	109
MEA	1.7	11.0	59.2	35	28.8	3	21	45

Table 4.4—TRR_{sh_oil} for d_s = 50 ft (BBO) (Arithmetically Aggregated)

	This study				EIA and ARI (2013)	McGlade (2012)		
Region	**P10**	**P50**	**P90**	**P90/P10**		**Low**	**Central**	**High**
NAM	9.1	99.2	698.4	77	93.7	36	57	136
LAM	0.7	25.7	437.4	625	47.9	42	45	54
CIS	9.5	103.8	667.6	70	84.7	3	42	95
EUR	0.4	19.2	164.8	412	10.7	19	21	25
AFR	2.3	78.5	909.1	395	44.6	35	38	46
AAO	1.6	33.4	894.2	559	65.3	14	53	109
MEA	1.1	14.4	134.8	123	28.8	3	21	45

Table 4.5—TRR_{sh_oil} for d_s = 500 ft (BBO) (Arithmetically Aggregated)

	This study				EIA and ARI (2013)	McGlade (2012)		
Region	**P10**	**P50**	**P90**	**P90/P10**		**Low**	**Central**	**High**
NAM	7.1	69.2	473.3	67	93.7	36	57	136
LAM	0.5	18.1	298.5	597	47.9	42	45	54
CIS	7.8	72.7	496.8	64	84.7	3	42	95
EUR	0.4	12.7	118.3	296	10.7	19	21	25
AFR	2.0	56.9	636.2	318	44.6	35	38	46
AAO	1.0	23.9	570.3	570	65.3	14	53	109
MEA	0.9	10.8	91.4	102	28.8	3	21	45

Table 4.6—TRR_{sh_oil} for d_s = 1,000 ft (BBO) (Arithmetically Aggregated)

	This study				EIA and ARI (2013)	McGlade (2012)		
Region	**P10**	**P50**	**P90**	**P90/P10**		**Low**	**Central**	**High**
NAM	3.6	42.0	330.0	92	93.7	36	57	136
LAM	0.3	10.8	209.2	697	47.9	42	45	54
CIS	3.8	44.6	350.0	92	84.7	3	42	95
EUR	0.2	8.0	80.8	404	10.7	19	21	25
AFR	1.1	32.3	438.9	399	44.6	35	38	46
AAO	0.6	13.9	386.1	644	65.3	14	53	109
MEA	0.5	6.7	61.4	123	28.8	3	21	45

4.2 Total Results

As in the case of region-wise aggregate TRR_{sh_oil} distributions, the total TRR_{sh_oil} distributions also show a large uncertainty using both statistical and arithmetic aggregation (but more so in the case of arithmetic aggregation) **(Fig. 4.7 to Fig. 4.8).** The ranges of TRR_{sh_oil} obtained using either aggregation method are wider than those reported by McGlade (2012) (Fig. 4.7 to Fig. 4.8).

The P90/P10 ratio for the total aggregate, obtained using statistical aggregation **(Table 4.7**), is less than those of individual regions and this may be explained by the shift of P10 and P90 limits toward the mean while statistically aggregating a large number of resource distributions (Table 4.1 to Table 4.3). However, no such observation can be made in case of arithmetic aggregation **(Table 4.8).**

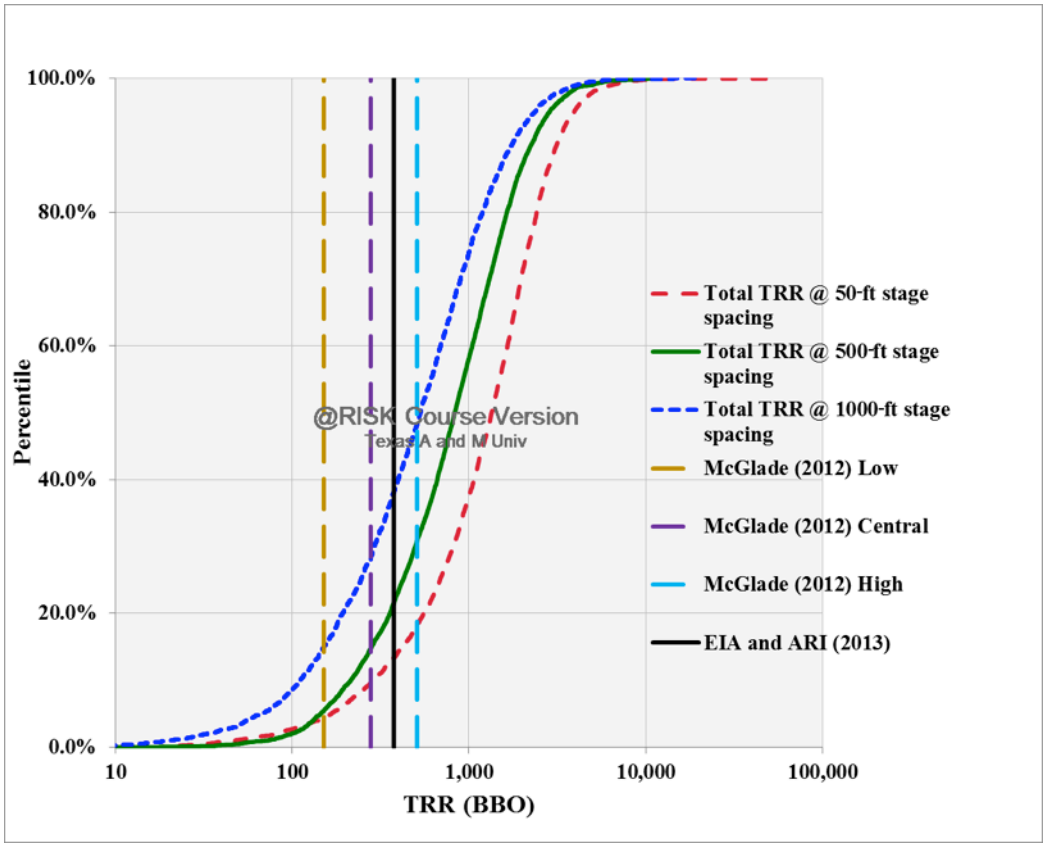

Fig. 4.7—Statistically-aggregated total TRR_{sh_oil} distributions for d_s = 50, 500 and 1,000 ft

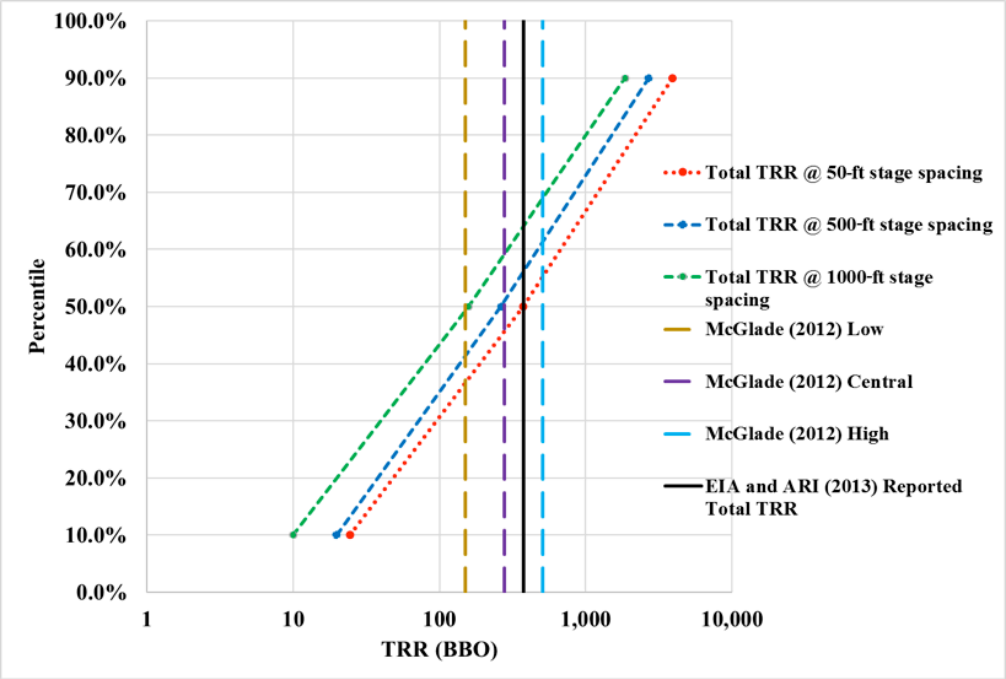

Fig. 4.8—Arithmetically-aggregated total TRR_{sh_oil} distributions for d_s = 50, 500 and 1,000 ft

Table 4.7—Total TRR_{sh_oil} (BBO) (Statistically Aggregated)

	This study				EIA and ARI (2013)	McGlade (2012)		
Stage spacing (ft)	P10	P50	P90	P90/P10		Low	Central	High
50	250.4	1,302.1	3,092.8	12	375.7	151	278	508
500	226.0	857.8	2,253.0	10				
1,000	111.1	530.8	1,740.5	16				

Table 4.8—Total TRR_{sh_oil} (BBO) (Arithmetically Aggregated)

	This study				EIA and ARI (2013)	McGlade (2012)		
Stage spacing (ft)	P10	P50	P90	P90/P10		Low	Central	High
50	24.6	374.2	3,906.2	159	375.7	151	278	508
500	19.8	264.4	2,684.7	136				
1,000	10.0	158.4	1,856.3	186				

4.3 Comparison with Previous Estimates

In this section, I compare the results of my study with those by EIA and ARI (2013) by plotting the P10, P50 and P90 values of TRR_{sh_oil} for each formation against the deterministic estimates established in their report **(Fig. 4.9 to Fig. 4.11)**. My P50 estimates of TRR_{sh_oil} for 500-ft and 1,000-ft stage spacings fall well below the deterministic EIA and ARI (2013) estimates (Fig. 4.10 to Fig. 4.11) and those for 50-ft spacing are closest to the EIA and ARI estimates (Fig. 4.9). The P50 trendlines indicate that the P50 estimates for 500-ft and 1,000-ft stage spacings are, on average, 0.8 and 0.5 times the estimate obtained by EIA and ARI (Fig. 4.10 to Fig. 4.11). This may be due to the generalized-*RF* distributions that I have established for 500-ft and 1,000-ft spacings, the means of which are 3.28% and 2.68%, respectively. However, EIA and ARI (2013) assigned *RF*s in the following manner based on their judgment of geological complexity and the clay content in the formation:

- A "favorable" *RF* of 6% was assigned to basins with low clay content, geologic complexity and favorable reservoir properties such as reservoir pressure and oil-filled porosities.
- An "average" *RF* of 4 to 5% was assigned to basins with medium clay content, moderate complexity and 'average' reservoir properties.
- A "less favorable" *RF* of 3% was assigned to basins with medium to high clay content and moderate to high geologic complexity and below-average reservoir properties.

These assignments (EIA and ARI 2013) were based on a database of *RF*s from 28 US tight-oil plays, the unweighted average of which is around 3.5%. It is worth mentioning that, out of the 28 plays considered, only 10 plays have *RF*s greater than 4% and nine out of the 10 belong to either the Bakken-Three Forks formations or the Eagle Ford formation. Therefore, it is possible that EIA and ARI (2013) have overestimated the *RF* offered by "average" plays.

However, the P50 trendline for 50-ft stage spacing shows that the P50 estimate for a formation is, on average, 1.2 times the EIA and ARI estimate (Fig. 4.9). Nevertheless, the number of formations for which my P50 estimate is higher than the respective EIA and ARI estimate decreases with increase in the magnitude of the EIA and ARI estimate. This is evident from the observation that only three of the computed P50 estimates are above the x=y line for formations whose EIA and ARI estimates are greater than 4 BBO. Hence it is likely that the EIA and ARI have overestimated the risked TRR for several large formations, perhaps due to the optimistic assignment of *RF* to "average" and "less favorable" formations.

The computed P90 estimates exceed the EIA and ARI estimates for most formations, considering all stage-spacing cases (Fig. 4.9 to Fig. 4.11). Similarly, the computed P10 estimates for most formations fall below the respective EIA and ARI estimates (Fig. 4.9 to Fig. 4.11). As a result, the simulated probabilistic range obtained using all three stage spacing cases bracket the EIA and ARI estimates comfortably.

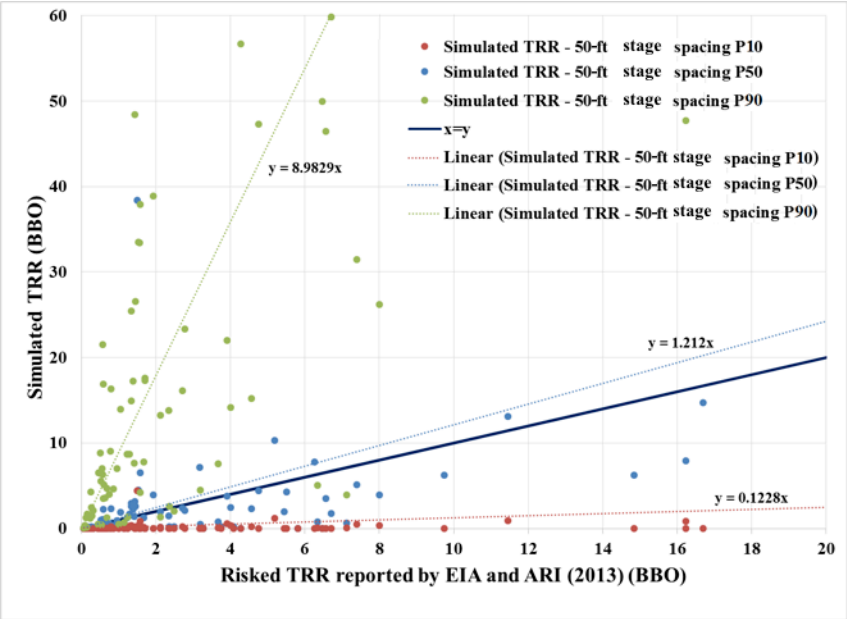

Fig. 4.9—Comparison between formation-wise probabilistic TRR_{sh_oil} estimates (d_s = 50 ft) from my study with the respective deterministic values cited by EIA and ARI (2013)

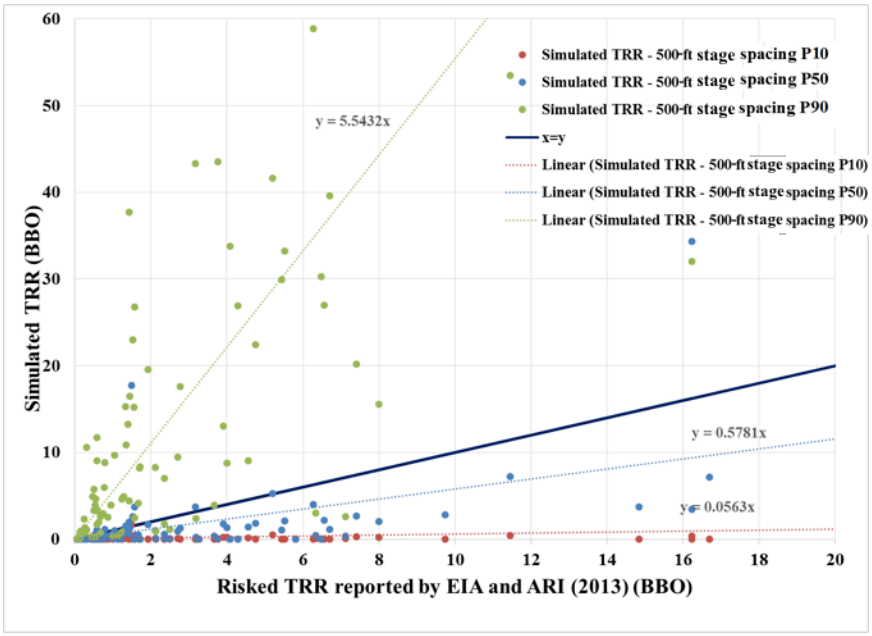

Fig. 4.10—Comparison between formation-wise probabilistic TRR_{sh_oil} estimates (d_s = 500 ft) from my study with the respective deterministic values cited by EIA and ARI (2013)

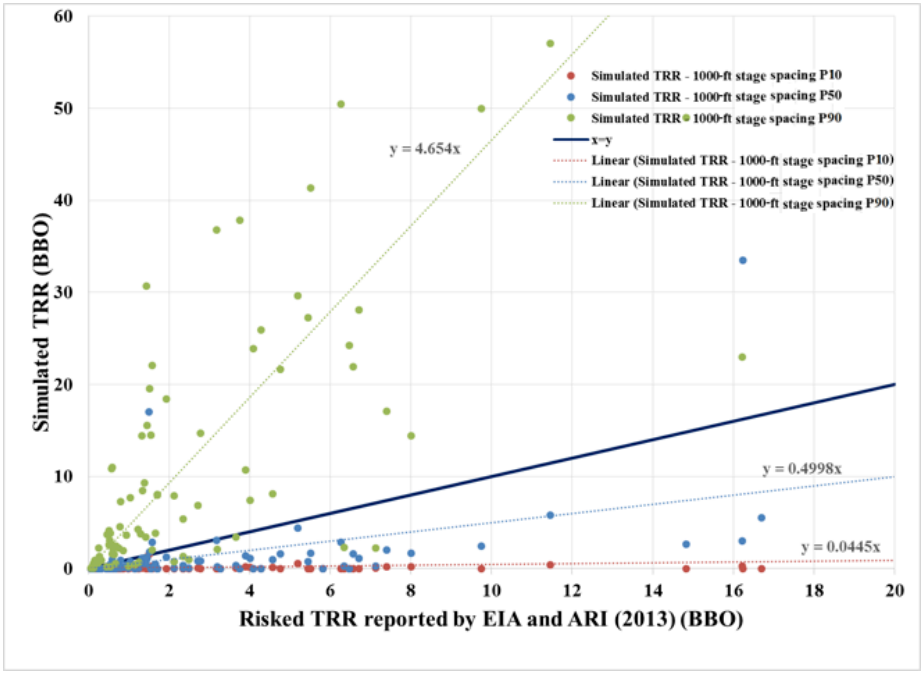

Fig. 4.11—Comparison between formation-wise probabilistic TRR_{sh_oil} estimates (d_s = 1,000 ft) from my study with the respective deterministic values cited by EIA and ARI (2013)

The region-wise P10-P90 range of TRR_{sh_oil} established by my study is substantially higher than the 'low'-'high' range computed by McGlade (2012) (**Fig. 4.12 to Fig. 4.17**). Moreover, McGlade's 'central' estimate is more conservative than the P50 estimates established in my study using both statistical and arithmetic aggregation, assuming 50-ft stage spacing (Fig. 4.12 to Fig. 4.13). However, McGlade's 'central estimates' seem to exceed the P50 estimates obtained using arithmetic aggregation, assuming stage spacings of 500 ft or 1,000 ft (Fig. 4.15 and Fig. 4.17). This is may be explained by the low *RF*s associated with higher values of stage spacing.

In general, EIA and ARI (2013) region-wise estimates are conservative when compared to the P50 estimates established via statistical aggregation, for any value of stage spacing (Fig. 4.12, Fig. 4.14 and Fig. 4.16). However, in the case of arithmetic aggregation, EIA and ARI (2013) region-wise estimates more conservative only when a stage spacing of 50 ft is assumed (Fig. 4.13).

Nevertheless, since stage spacing is expected to decrease (from a range of 250 to 350 ft in 2016) in future, one can safely assume that the estimates obtained considering 50-ft spacing is most likely to be closest to actual resource volumes.

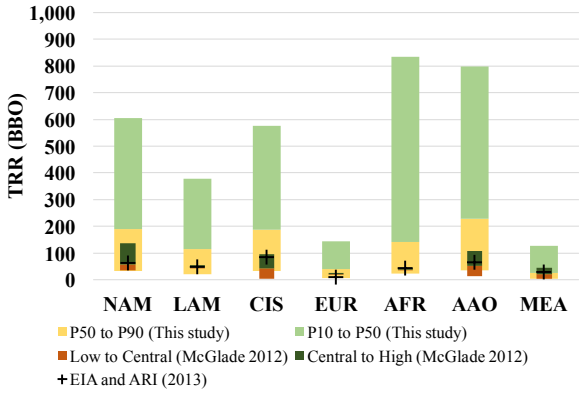

Fig. 4.12—TRR_{sh_oil} ranges computed using statistical aggregation of formation-wise TRR_{sh_oil} (d_s = 50 ft) compared with risked TRR values cited by EIA and ARI (2013) and TRR ranges cited by McGlade (2012)

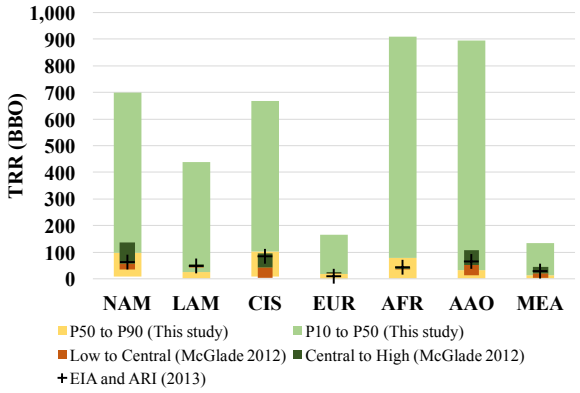

Fig. 4.13—TRR_{sh_oil} ranges computed using arithmetic aggregation of formation-wise TRR_{sh_oil} (d_s = 50 ft) compared with risked TRR values cited by EIA and ARI (2013) and TRR ranges cited by McGlade (2012)

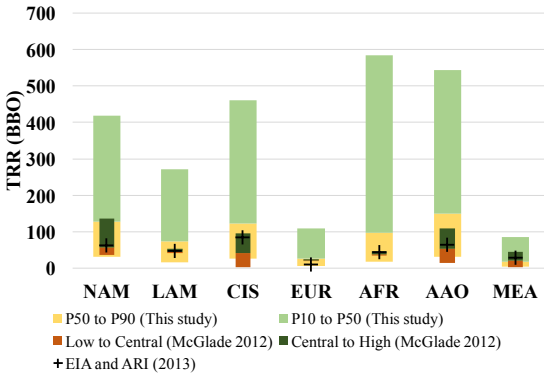

Fig. 4.14—TRR_{sh_oil} ranges computed using statistical aggregation of formation-wise TRR_{sh_oil} (d_s = 500 ft) compared with risked TRR values cited by EIA and ARI (2013) and TRR ranges cited by McGlade (2012)

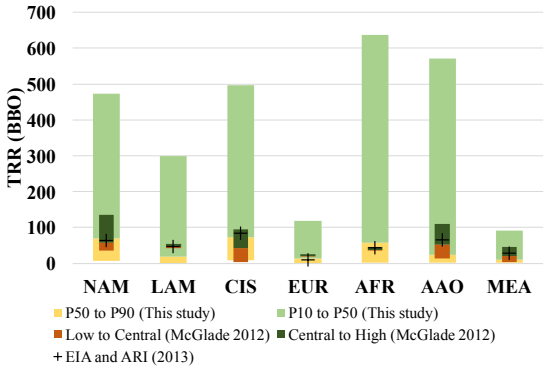

Fig. 4.15—TRR_{sh_oil} ranges computed using arithmetic aggregation of formation-wise TRR_{sh_oil} (d_s = 500 ft) compared with risked TRR values cited by EIA and ARI (2013) and TRR ranges cited by McGlade (2012)

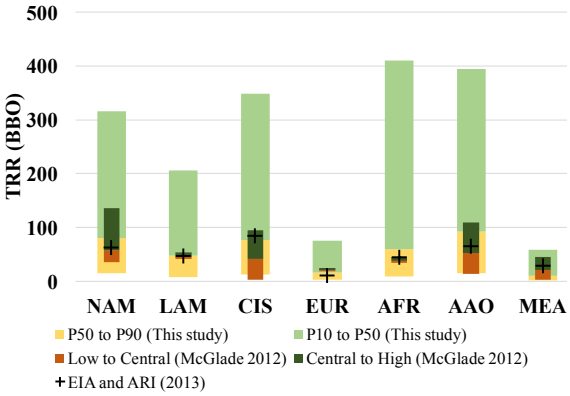

Fig. 4.16—TRR_{sh_oil} ranges computed using statistical aggregation of formation-wise TRR_{sh_oil} (d_s = 1,000 ft) compared with risked TRR values cited by EIA and ARI (2013) and *TRR* ranges cited by McGlade (2012)

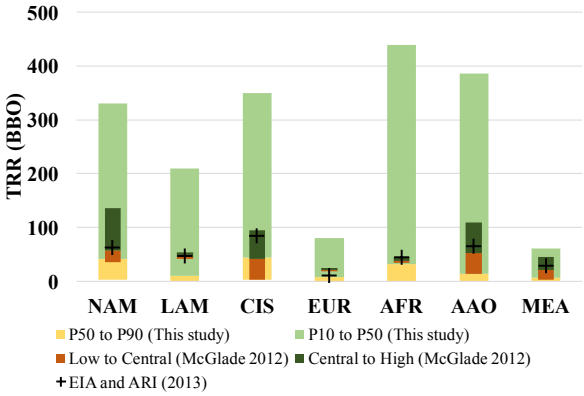

Fig. 4.17—TRR_{sh_oil} ranges computed using arithmetic aggregation of formation-wise TRR_{sh_oil} (d_s = 1,000 ft) compared with risked TRR values cited by EIA and ARI (2013) and TRR ranges cited by McGlade (2012)

5. CONCLUSIONS

I have probabilistically assessed 93 shale-oil formations in 67 basins from 36 countries in the seven global regions demarcated by Rogner (1997) and Dong (2012). This study accounts for 41% of all global petroleum basins. Based on my study, the following conclusions can be drawn:

- The probabilistic estimates of total $OOIP_{sh\_oil}$ and TRR_{sh_oil} for the 93 formations studied (assuming 50-ft stage spacing) are given in the following table. A key finding is the large degree of uncertainty in both $OOIP_{sh\_oil}$ and TRR_{sh_oil} estimates, denoted by the ratio P90/P10. The uncertainty is considerably larger in the case of arithmetic aggregation.

Table 5.1—Summary of calculated total $OOIP_{sh\_oil}$ and total TRR_{sh_oil} (for d_s= 50 ft) and the associated degrees of uncertainty for 93 global formations

	Statistical Aggregation				**Arithmetic Aggregation**			
	P10	**P50**	**P90**	**P90/P10**	**P10**	**P50**	**P90**	**P90/P10**
$OOIP_{sh\_oil}$ (1,000 BBO)	15.0	23.6	43.9	3	0.90	8.70	67.7	75
TRR_{sh_oil} (d_s = 50 ft) (1,000 BBO)	0.25	1.30	3.09	12	0.02	0.37	3.91	159

- The probabilistic estimates of $OOIP_{sh\_oil}$ and those of TRR_{sh_oil} (assuming 50-ft stage spacing) computed in this study using both statistical and arithmetic aggregation are greater than estimates from previous studies by EIA and ARI (2013) and McGlade (2012), as shown in the following table.

Table 5.2—Comparison of total $OOIP_{sh\_oil}$ and total TRR_{sh_oil} (for d_s= 50 ft) with estimates from previous assessments

	Statistical Aggregation			Arithmetic Aggregation			EIA and ARI (2013)	McGlade (2012)		
	P10	P50	P90	P10	P50	P90		Low	Cent-ral	High
$OOIP_{sh\_oil}$ (1,000 BBO)	15.0	23.6	43.9	0.9	8.70	67.7	7.0	-	-	-
TRR_{sh_oil} (d_s = 50 ft) (1,000 BBO)	0.25	1.30	3.09	0.02	0.4	3.91	0.38	0.15	0.28	0.51

- The distributions of shale-oil resources available are heavily dependent on the method of aggregation employed. Arithmetic aggregation of resources is likely more appropriate than statistical aggregation because it results in a wider spread of the aggregate total/region-wise distributions and hence circumvents the risk of underestimating uncertainty in such high-level estimates. However, the actual resource estimates are expected to fall between the statistically-aggregated and arithmetically-aggregated estimates.

6. LIMITATIONS AND FUTURE WORK

A major shortcoming of my study is that it does not cover highly prospective countries in the Middle East such as Saudi Arabia, Iraq and Iran due to unavailability of data on required input parameters. Hence the probabilistic estimates established in this study are highly likely to be conservative. The resource estimates should be revised when data from prospective formations in these countries are available.

The study did not cover the prospects for artificial lift and other technologies that may improve recovery efficiency. I also did not extend my investigation to other potentially uncertain parameters such as reservoir pressure, depth of formation, and relative-permeability exponents. This has been left for future research.

Another area in my study where there is room for improvement is the lack of delineation of the prospective area into sweet spots and non-sweet spots as carried out by USGS (Charpentier and Cook 2010). This delineation is recommended due to high heterogeneity in shale plays that accounts for widely different type curves for sweet spots and non-sweet spots.

Additionally, since the estimation of economically-recoverable resources is beyond the scope of this work, I did not take into consideration economic factors such as oil price and capital/operating costs, which may be very different in various parts of the world. The economic environment conducive to shale-oil development that prevails in North America may not apply globally. Hence, the commerciality of developing the established TRR is yet to be explored.

REFERENCES

Alexander, T., Baihly, J., Boyer, C. et al. 2011. Shale Gas Revolution. *Oilfield Review*.

Amoss, D., Angelico, B., Bachmann, J. et al. 2011. Eagle Ford Shale Not All Areas are Created Equal, Howard Weil Incorporated, New Orleans, LA (June 1).

Anna, L. O. 2010. Geological Assessment of Undiscovered Oil and Gas in the Powder River Basin Province, Wyoming and Montana. In *Total Petroleum Systems and Geologic Assessment of Undiscovered Oil and Gas in the Powder River Basin Province, Wyoming and Montana: U.S. Geological Survey Series DDS-69_U*, Chap. 1, 97.

Apache Corporation. 2013. Permian Bus Tour.

Bammidi, V. S. 2011. Unconventional Oil & Gas Resource Evaluation of the Woodford Shale in New Mexico. Master of Science, New Mexico Institute of Mining and Technology, Socorro, New Mexico (July 31, 2011).

Beckwith, R. 2013. California's Monterey Formation Zeroing in on a New Shale Oil Play? *Journal of Petroleum Technology* **65** (05). SPE-0513-0044-JPT. http://dx.doi.org/10.2118/0513-0044-JPT

Bordenave, M. L., Espitalie, J., Leplat, P. et al. 1993. The sedimentation of organic matter. In *Applied petroleum geochemistry*, 217-278. Paris, France, Technip.

Brownfield, M. E., Schenk, C. J., Charpentier, R. R. et al. 2015. Assessment of undiscovered conventional and continuous oil and gas resources of the Baltic Depression Province, 2014. http://dx.doi.org/10.3133/fs20153015

Brownfield, M. E., Schenk, C. J., Klett, T. R. et al. 2016. Assessment of undiscovered oil and gas resources of the Taoudeni Basin Province, Mali and Mauritania, 2015. http://dx.doi.org/10.3133/fs20163003

Budzik, P. and Ford, M. 2014. Oil and natural gas resource categories reflect varying degrees of certainty. *U.S Energy Information Administration*. http://www.eia.gov/todayinenergy/detail.php?id=17151 (accessed 10 February 2017).

Canadian Society for Unconventional Resources. 2012. Understanding Tight Oil. http://www.csur.com/sites/default/files/Understanding_TightOil_FINAL.pdf (accessed 11 May 2017.

Cander, H. 2012. What Are Unconventional Resources? A Simple Definition Using Viscosity and Permeability. AAPG Annual Convention and Exhibition, Long Beach, California, April 22-25, 2012.

Cerón, M. R., Walls, J. and Diaz, E. 2013. Comparison of Reservoir Quality from La Luna, Gacheta and Eagle Ford Shale Formations Using Digital Rock Physics. AAPG International Conference and Exhibition, Cartagena, Colombia, September 8-11, 2013.

Charpentier, R. R. and Cook, T. A. 2010. Improved USGS methodology for assessing continuous petroleum resources. 2.0 edition. *U.S. Geological Survey*.

Chaudhary, A. S. 2011. Shale Oil Production Performance from a Stimulated Reservoir Volume. Master of Science, Texas A&M University, College Station, TX (August 2011).

Chen, Z., Jiang, C. and Lavoie, D. 2016. Rock-Eval Pyrolysis Data Analysis and Kerogen Kinetics Comparison of Selected Producing and Potential Shale Gas Plays in Canadian Sedimentary Basins. AAPG 2016 Annual Convention and Exhibition, Calgary, Alberta, Canada, June 19-22, 2016.

Cho, Y., Eker, E., Uzun, I. et al. 2016. Rock Characterization in Unconventional Reservoirs: A Comparative Study of Bakken, Eagle Ford, and Niobrara Formations. SPE Low Perm Symposium, Denver, Colorado, USA. SPE-180239-MS. http://dx.doi.org/10.2118/180239-MS.

Cohen, D. 2008. An Unconventional Play In The Bakken. *Resilience*. http://www.resilience.org/stories/20080416/unconventionalplaybakken/ (accessed February 9 2017).

Colorado Oil & Gas Association. 2013. Oil shale vs Shale oil http://www.coga.org/wp-content/uploads/2015/08/1-Basics_OilShale.pdf.

CMOST, 2013a. Calgary, Alberta, Canada, Computer Modelling Group Ltd.,.

IMEX Three Phase Black Oil Reservoir Simulator, 2013b. Calgary, Alberta Canada, Computer Modelling Group Ltd,.

Cronquist, C. 2001. *Estimation and classification of reserves of crude oil, natural gas and condensate*, SPE book series: SPE.

Cullick, A. S., Carrillo, M., Clayton, C. et al. 2014. Well-spacing Study to Develop Stacked Tight Oil Pay in Midland Basin. SPE Unconventional Resources Conference, The Woodlands, Texas, USA. SPE-168992-MS. http://dx.doi.org/10.2118/168992-MS.

Daly, A. R. and Edman, J. D. 1987. Loss of Organic-Carbon from Source Rocks during Thermal Maturation. *AAPG Bulletin* **71** (5)

Dong, Z. 2012. A New Global Unconventional Natural Gas Assessment. Doctor of Philosophy, Texas A&M University, College Station, TX (August 2012).

Dong, Z., Holditch, S. A. and McVay, D. A. 2012. Global Unconventional Gas Resource Assessment. *SPE Economics & Management* **4** (04). SPE-148365-PA. http://dx.doi.org/10.2118/148365-PA

Dong, Z., Holditch, S. A. and McVay, D. A. 2013. Resource Evaluation for Shale Gas Reservoirs. *SPE Economics & Management* **5** (01). SPE-152066-PA

Dong, Z., Holditch, S. A., McVay, D. A. et al. 2014. Probabilistic Assessment of World Recoverable Shale Gas Resources. SPE/EAGE European Unconventional Conference and Exhibition Vienna, Austria, 25–27 February. SPE-167768-MS.

Drillinginfo. 2012. The Impacts of Faults and Fractures on Production in the Niobrara PRB. *Drillinginfo*. http://info.drillinginfo.com/what-impacts-to-faults-and-fractures-play-on-production-in-the-niobrara-prb/ (accessed February 13, 2017.

Dyman, T. S. and Condon, S. M. 2005. FORSPAN ASSESSMENT MODEL FOR CONTINUOUS ACCUMULATIONS--BASIC INPUT DATA FORM.

EIA. 2015a. Assumptions to the Annual Energy Outlook 2015, U.S Energy Information Administration, Washington D.C.

EIA. 2015b. World Shale Resource Assessments Summary tables. *EIA*. https://www.eia.gov/analysis/studies/worldshalegas/xls/Attachments_A_B_by_Country_ARI_EIA_World_Shale_Resources_122914.xlsx.

EIA. 2015c. World Shale Resources Assessments. *EIA*. https://www.eia.gov/analysis/studies/worldshalegas/ (accessed February 21 2017).

EIA. 2016. Annual Energy Outlook 2016 with Projections to 2040, EIA, Washington.

EIA. 2017. Drilling Productivity Report (January 2017).

EIA and ARI. 2013. Technically Recoverable Shale Oil and Shale Gas Resources: An Assessment of 137 Shale Formations in 41 Countries Outside the United States, Energy Information Agency, Washington.

EIA and IHS. 2016. Trends in U.S. Oil and Natural Gas Upstream Costs, IHS, Washington.

EIA and INTEK. 2011. Review of Emerging Resources: U.S. Shale Gas and Shale Oil Plays, INTEK, Washington (July 2011).

Finn, T. M. and Johnson, R. C. 2005. Niobrara Total Petroleum System in the Southwestern Wyoming Province: Petroleum Systems and Geologic Assessment of Oil and Gas in the Southwestern Wyoming Province, Wyoming, Colorado, and Utah.

Ford, J. R., Ashley, S. E., Justus, H. et al. 2012. Location of Tributary/Non-Tributary Line Niobrara Formation, Lower Pierre Shale, Carlile Formation, and Greenhorn Formation. Report No. 1402UPC01, Leonard Rice Engineers Inc. (February 20, 2012).

Gray, J. K. 1977. Future gas reserve potential Western Canadian sedimentary basin. National Technical Conference.

Holditch, S. A. and Ayers, W. B. 2009. How Technology Transfer Will Expand the Development of Unconventional Gas, Worldwide. 29th Annual GCSSEPM Foundation Bob F. Perkins Research Conference, Houston, Texas, December 6-8.

Hovey, R. 2011. The Niobrara Shale. *Drillinginfo*. http://www.hartenergyconferences.com/UserFiles/File/DUO/DUO_2011/Ramona_Hovey.pdf.

Jarvie, D. M. 2012. Shale Resource Systems for Oil and Gas: Part 2—Shale-oil Resource Systems. In *Shale Reservoirs: Giant Resources for the 21st Century, AAPG Memoir 97*, ed. Breyer J. A., 89-119. AAPG.

Jarvie, D. M., Hill, R. J., Ruble, T. E. et al. 2007. Unconventional shale-gas systems: The Mississippian Barnett Shale of north-central Texas as one model for thermogenic shale-gas assessment. *AAPG Bulletin* **91** (4): 475-499. http://dx.doi.org/10.1306/12190606068

Kelly, L., Bachmann, J., Amoss, D. et al. 2012. Permian Basin Easy to Oversimplify, Hard to Overlook, Howard Weil Incorporated, New Orleans, LA (January 19, 2012).

Kennedy, R., Luo, L. X. and Kusskra, V. 2016. The Unconventional Basins and Plays - North America, the Rest of the World, and Emerging Basins. In *Unconventional Oil and Gas Resources: Exploitation and Development*, ed. Usman Ahmed and Nathan D. Meehan. Boca Raton, FL, Taylor & Francis Group.

Kieschnick, J. and Suarez-Rivera, R. Core Technology for Evaluating the Bakken - Fundamentals for Reservoir Quality Assessment and Completion Analysis http://pttc.mines.edu/casestudies/Bakken/BakkenCore.pdf.

Kuchinskiy, V., Gentry, K. and Hill, R. 2012. Source Rock Evaluation Technique: A Probabilistic Approach for Determining Hydrocarbon Generation Potential and In-Place Volume for Shale Plays. AAPG Annual Convention and Exhibition, Long Beach, California, April 22-25, 2012.

Kumar, S., Hoffman, T. and Prasad, M. 2013. Upper and Lower Bakken Shale Production Contribution to the Middle Bakken Reservoir. Unconventional Resources Technology Conference, Denver, Colorado, USA, 12-14 August. URTEC-1581459-MS.

Laherrere, J. 2006. Oil and gas: what future? Groningen Annual Energy Convention, Groningen, 21 November 2006.

Lalehrokh, F. and Bouma, J. 2014. Well Spacing Optimization in Eagle Ford. SPE/CSUR Unconventional Resources Conference – Canada, Calgary, Alberta, Canada, 30 September–2 October. SPE-171640-MS. http://dx.doi.org/10.2118/171640-MS.

LeFever, J. and Nordeng, S. 2015. Activity Update for Bakken Petroleum System, Williston Basin. *Geo News* (in press; published online July, 2015). https://www.dmr.nd.gov/ndgs/documents/newsletter/Summer 2015/Activity Update for Bakken Petroleum System, Williston Basin.pdf.

Li, G. 2011. World atlas of oil and gas basins. Pondicherry, India. *Wiley-Blackwell*.

Li, Y., Guo, Z.-Q., Liu, C. et al. 2015. A rock physics model for the characterization of organic-rich shale from elastic properties. *Petroleum Science* **12** (2): 264-272. http://dx.doi.org/10.1007/s12182-015-0029-6

Madden, B. and Vossoughi, S. 2013. US Shale Gas and Tight Oil Boom - The Opportunities and Risks for America. SPE Asia Pacific Oil and Gas Conference and Exhibition, Jakarta, Indonesia, 22-24 October. SPE-165770-MS. http://dx.doi.org/10.2118/165770-MS.

Masters, J. A. 1979. Deep Basin Gas Trap, Western Canada. *Aapg Bulletin-American Association of Petroleum Geologists* **63** (2): 152-181

Matthies, N. 2014. Understanding and Mapping the Variability of the Niobrara Formation Across Wattenberg Field, Denver Basin. Master of Science, Colorado School of Mines, Golden, CO.

McGlade, C., Speirs, J. and Sorrell, S. 2013. Methods of estimating shale gas resources – Comparison, evaluation and implications. *Energy* **59**: 116-125. http://dx.doi.org/10.1016/j.energy.2013.05.031

McGlade, C. E. 2012. A review of the uncertainties in estimates of global oil resources. *Energy* **47** (1): 262-270. http://dx.doi.org/10.1016/j.energy.2012.07.048

McGlade, C. E., Speirs, J. and Sorrell, S. 2012. A review of regional and global estimates of unconventional gas resources, The European commission (September 2012).

Menchaca, M. 2013. General Overview of Permian Strata of Delaware Basin and NW Shelf. http://info.drillinginfo.com/general-overview-of-permian-strata-of-the-delaware-basin-and-nw-shelf/ (accessed 10 February 2017).

Mendoza, E. E., Aular, J. and Sousa, L. J. 2011. Optimizing Horizontal-Well Hydraulic-Fracture Spacing in the Eagle Ford

Formation, Texas. North American Unconventional Gas Conference and Exhibition, The Woodlands, Texas, USA, 14-16 June. SPE-143681-MS. http://dx.doi.org/10.2118/143681-MS.

Modica, C. J. and Lapierre, S. G. 2012. Estimation of kerogen porosity in source rocks as a function of thermal transformation: Example from the Mowry Shale in the Powder River Basin of Wyoming. *AAPG Bulletin* **96** (1): 87-108. http://dx.doi.org/10.1306/04111110201

Mullen, J. 2010. Petrophysical Characterization of the Eagle Ford Shale in South Texas. Canadian Unconventional Resources and International Petroleum Conference, Calgary, Alberta, Canada. SPE-138145-MS. http://dx.doi.org/10.2118/138145-MS.

Murtha, J. 2001. Risk Analysis for the Oil Industry. In *Hart's E&P*. A Comprehensive Study of Risk Management.

Nutech Energy. Midland Basin - Wolfcamp: Regional Field Study, Houston, TX.

OGJ. 2013. Wolfcamp shale graduates to 'world class' play. *Oil and Gas Journal*. http://www.ogj.com/articles/uogr/print/volume1/issue3/urtecwolfcamp/wolfcampshalegraduatestoworldclassplay.html (accessed February 10 2017).

Oil and Gas Financial Journal. 2016. Unconventional Oil & Gas. *Oil and Gas Financial Journal*. http://www.ogfj.com/unconventional/niobrara-play-map.html.

Okiongbo, K. S., Aplin, A. C. and Larter, S. R. 2005. Changes in Type II Kerogen Density as a Function of Maturity: Evidence from the Kimmeridge Clay Formation. *Energy & Fuels* **19** (6): 2495-2499. http://dx.doi.org/10.1021/ef050194+

@RISK, version 7 2015. Ithaca, NY, USA, Palisade Corporation.

Peters, K. E., Curry, D. J. and Kacewicz, M. 2012. *Basin modeling : New horizons in research and applications*, AAPG Hedberg series.

Pettegrew, J., Qiu, J. and Zhan, L. 2016. Understanding Wolfcamp Well Performance – A Workflow to Describe the Relationship Between Well Spacing and EUR. Unconventional Resources Technology Conference, San Antonio, Texas, USA, 1-3 August,. URTEC-2464916-MS.

Plains and Prairies LLC. 2013. Bakken Formation and Williston Basin petroleum wells. *Flickr*. https://www.flickr.com/photos/plainsandprairielcc/9620797719/in/photolist-fEa6YK-Q4CoyW.

Pollastro, R. M., Roberts, L. N. R. and Cook, T. A. 2010. Geologic Assessment of Technically Recoverable Oil in the Devonian and Mississippian Bakken Formation. *U.S. Geological Survey*.

Rogner, H. H. 1997. An Assessment of World Hydrocarbon Resources. *Annual Review of Energy and the Environment* **22**: 217-262. http://dx.doi.org/10.1146/annurev.energy.22.1.217

Royal Dutch Shell. 2012. ROYAL DUTCH SHELL ACQUIRES LIQUIDS-RICH SHALE ACREAGE IN TEXAS http://www.shell.com/media/news-and-media-releases/2012/shell-acquires-liquids-rich-shale-acreage-in-texas-12092012.html.

Salazar, J., McVay, D. A. and Lee, W. J. 2010. Development of an Improved Methodology to Assess Potential Unconventional Gas Resources. *Natural Resources Research* **19** (4): 253-268. http://dx.doi.org/10.1007/s11053-010-9126-9

Sarg, F. J. 2012. The Bakken – An Unconventional Petroleum and Reservoir System, Colorado School of Mines, Golden, CO (March, 2012).

Schenk, C. J., Charpentier, R. R., Klett, T. R. et al. 2014a. Assessment of potential unconventional lacustrine shale-oil and shale-gas resources, Phitsanulok Basin, Thailand, 2014. http://dx.doi.org/10.3133/fs20143033

Schenk, C. J., Charpentier, R. R., Klett, T. R. et al. 2015a. Assessment of shale-oil resources of the Central Sumatra Basin, Indonesia, 2015. http://dx.doi.org/10.3133/fs20153072

Schenk, C. J., Charpentier, R. R., Klett, T. R. et al. 2015b. Assessment of undiscovered oil and gas resources of the Paris Basin, France, 2015. http://dx.doi.org/10.3133/fs20153016

Schenk, C. J., Pitman, J. K., Charpentier, R. R. et al. 2015c. Assessment of unconventional oil and gas resources in the Jurassic Sargelu Formation of Iraq, 2014. http://dx.doi.org/10.3133/fs20153006

Schenk, C. J., Pitman, J. K., Charpentier, R. R. et al. 2014b. Assessment of potential shale-oil and shale-gas resources in Silurian shales of Jordan, 2014. http://dx.doi.org/10.3133/fs20143082

Schlumberger. 2012. Channel Fracturing Increases Production by 37% for Petrohawk in the Eagle Ford Shale. In *Success in Shale Plays*. Schlumberger.

Schmoker, J. W. 1999. U.S. Geological Survey Assessment Model for Continuous (Unconventional) Oil and Gas Accumulations—The "FORSPAN" Model. *U.S. Geological Survey Bulletin 2168*

Schmoker, J. W., Crovelli, R. A. and Balay, R. H. 1995. Potential Additions to Technically Recoverable Resources for Each Continuous-Type (Unconventional) Play of the U.S Geological Survey 1995 National Assessment of United States Oil and Gas Resources -- Graphical and Tabular Presentations. Report No. 95-75E.

Scott, K. The Wolfcamp Shale: Technical Learnings to Date and Challenges Going Forward. In *Proceedings The Wolfcamp Shale: Technical Learnings to Date and Challenges Going Forward*, *Proceedings The Wolfcamp Shale: Technical Learnings to Date and Challenges Going Forward, Fort Worth, TX*.

Simenson, A. 2010. Depositional Facies And Petrophysical Analysis Of The Bakken Formation, Parshall Field, Mountrail County, North Dakota. Master of Science, Colorado School of Mines, Golden, CO.

Simenson, A., Sonnenberg, S. A. and Cluff, R. M. 2011. Depositional Facies and Petrophysical Analysis of the Bakken Formation, Parshall Field and Surrounding Area, Mountrail County, North Dakota. In *Bakken-Three Forks Petroleum System in the Williston Basin*, ed. John W. Robinson, Julie A. LeFever and Stephanie B. Gaswirth. Denver, CO, Rocky Mountain Association of Geologists.

Smith, M., Yu, G., Yang, W. et al. 2013. Shale play characteristics and correlation with anisotropic logs – a case study of Eagle Ford shale in Texas. 75th EAGE Conference & Exhibition, London, UK, 10-13 June 2013.

Sonnenberg, S. 2016. Insights into Niobrara Stratigraphic Architecture and Diagenesis, Wattenberg Field, Denver Basin, Colorado. AAPG Pacific Section and Rocky Mountain Section Joint Meeting, Las Vegas, NV, October 2-5, 2016.

Sonnenberg, S. and Taylor, J. The Niobrara Petroleum System, Rocky Mountain Region. *Colorado School of Mines: Niobrara Consortium*.

Sonnenberg, S. A. 2012. The Niobrara Petroleum System, Rocky Mountain Region. Tulsa Geological Society dinner meeting, Tulsa, OK.

SPE, AAPG, WPC et al. 2007. Petroleum Resources Management System.

Stolz, D. J. 2014. Reservoir Character of the Avalon Shale (Bone Spring Formation) of the Delaware Basin, West Texas and Southeast New Mexico: Effect of

Carbonate-rich Sediment Gravity Flows. Master of Science, The University of Kansas.

Stolz, D. J., Franseen, E. K. and Goldstein, R. H. 2015. Character of the Avalon Shale (Bone Spring Formation) of the Delaware Basin, West Texas and Southeast New Mexico: Effect of Carbonate-Rich Sediment Gravity Flows. Unconventional Resources Technology Conference, San Antonio, Texas, USA, 20-22 July. URTEC-2154681-MS. http://dx.doi.org/10.15530/URTEC-2015-2154681.

Theloy, C. and Sonnenberg, S. A. 2012. Factors Influencing Productivity in the Bakken Play, Williston Basin. AAPG Annual Convention and Exhibition, Long Beach, California, USA.

Tian, Y., Ayers, W. B. and McCain Jr., W. D. 2013. The Eagle Ford Shale Play, South Texas: Regional Variations in Fluid Types, Hydrocarbon Production and Reservoir Properties. International Petroleum Technology Conference, Beijing, China, 26-28 March. IPTC-16808-MS. http://dx.doi.org/10.2523/IPTC-16808-MS.

Tran, T., Sinurat, P. D. and Wattenbarger, B. A. 2011. Production Characteristics of the Bakken Shale Oil. SPE Annual Technical Conference and Exhibition, Denver, Colorado, USA, 30 October-2 November. SPE-145684-MS. http://dx.doi.org/10.2118/145684-MS.

United Nations. 2009. United Nations Framework Classification for Fossil Energy and Mineral Reserves and Resources 2009. New York

Geneva. *United Nations*.

USGS. Year. Assessment of Potential Shale Gas and Shale Oil Resources of the Norte Basin, Uruguay, 2011.

USGS. 2012. Potential for Technically Recoverable Unconventional Gas and Oil Resources in the Polish-Ukrainian Foredeep, Poland, 2012.

USGS. 2014. Assessment of Unconventional Oil and Gas Resources in Northeast Mexico, 2014.

USGS. 2015. Map of assessed continuous (unconventional) oil resources in the United States, 2014.

USGS. 2016. Assessment of Undiscovered Continuous Oil Resources in the Wolfcamp Shale of the Midland Basin, Permian Basin Province, Texas, 2016: National and Global Petroleum Assessment.

Vasquez, M. E. and Beggs, H. D. 1980. Correlations for Fluid Physical Property Prediction. *Journal of Petroleum Technology* (June): 968-70. SPE-6719-PA. http://dx.doi.org/10.2118/6719-PA

Velarde, J. J. 1996. Correlation of Black Oil Properties at Pressure below the Bubble Point. Master of Science, Texas A&M University, College Station, TX.

Velasco, C. A. M. 2013. Assessment of the Mexican Eagle Ford Shale Oil and Gas Resources. Master of Science, Texas A&M University, College Station, TX.

Walls, J. and Morcote-Rios, A. 2015. Quantifying Variability of Reservoir Properties From a Wolfcamp Formation Core. Unconventional Resources Technology Conference, San Antonio, Texas, USA, 20-22 July. URTEC-2154633-MS. https://doi.org/10.15530/URTEC-2015-2154633.

Walls, J. D., Diaz, E., Derzhi, N. et al. 2011. Eagle Ford Shale Reservoir Properties from Digital Rock Physics. HGS Applied Geoscience Mudrocks Conference (AGC), Woodlands, TX, 7-8, February 2011.

Waples, D. W. and Marzi, R. W. 1998. The universality of the relationship between vitrinite reflectance and transformation ratio. *Organic Geochemistry* **28** (6): 383-388

Weijermars, R., Sorek, N., Sen, D. et al. 2017. Eagle Ford Shale play economics: U.S. versus Mexico. *Journal of Natural Gas Science and Engineering* **38**: 345-372. http://dx.doi.org/10.1016/j.jngse.2016.12.009

Welker, C., Stright, L. and Anderson, T. 2013. Geologic Controls on Oil Production from the Niobrara Formation, Silo Field, Laramie County, Wyoming. Unconventional Resources Technology Conference, Denver, Colorado, 12-14 August. URTEC-1580211-MS.

Worthington, P. F. 2010. Net Pay: What is it? What does it do? How do we quantify it? How do we use it? *SPE Reservoir Evaluation &Engineering* **13** (05). SPE-123561-PA. http://dx.doi.org/10.2118/123561-PA

Worthington, P. F. and Majid, A. A. 2013. The Use of Net Pay Concepts in the Exploitation of Shale-Gas Deposits. SPE Unconventional Resources Conference and Exhibition-Asia Pacific, Brisbane, Australia. SPE-167044-MS.

Wust, R., Cui, A. and Nassichuk, B. R. 2014. Rock Characteristics of Oil-, Condensate- and Dry Gas-Producing Wells of the Unconventional Devonian Duvernay

Formation, Canada. International Petroleum Technology Confereve, Kuala Lumpur, Malaysia, 10–12 December, 2014. IPTC-18081-MS.

www.wolfcamp-shale.com. 2014. Wolfcamp Shale Overview. http://www.wolfcampshale.com/WolfcampShale/Overview.html (accessed February 10 2017).

Yesiltepe, C. 2015. Accessed Drainage Volume And Recovery Factors Of Fractured Horizontal Wells Under Transient Flow. Master of Science Thesis, Colorado School of Mines.